A NUMERICAL STUDY OF CRACK TIP BLUNTING UNDER CYCLIC LOADING

by

Per-Olof K. Boman

S.B. Luleå University of Technology (Luleå, Sweden, 1985)

SUBMITTED TO THE DEPARTMENT OF
AERONAUTICS AND ASTRONAUTICS
IN PARTIAL FULFILLMENT OF THE REQUIREMENTS
FOR THE DEGREE OF

Master of Science
at the
Massachusetts Institute of Technology

June, 1992

Signature of Author _____
Department of Aeronautics and Astronautics
May 20, 1992

Certified by _____
Boeing Assistant Professor Hugh L.N. McManus
Thesis Supervisor, Department of Aeronautics and Astronautics

Certified by _____
Professor Mårten T. Landahl
Thesis Supervisor, Department of Aeronautics and Astronautics

Accepted by _____
Professor Harold Y. Wachman
Chairman, Department Graduate Committee

A NUMERICAL STUDY OF CRACK TIP BLUNTING UNDER CYCLIC LOADING

by
Per-Olof K. Boman

Submitted to the Department of Aeronautics and Astronautics
on May 20, 1992
in partial fulfillment of the requirements for the degree of
Master of Science

Abstract

Present available and used methods to predict fatigue crack growth are essentially empirical relations. Usually they are refined and modified versions of the Paris law. Although these models in many cases show excellent performance, the fact that they have no direct coupling to the actual physics of crack growth make the model predictions unreliable and uncertain when applied to conditions much different from the ones that prevailed when the material data were determined. Prerequisites for the development of better, more general prediction methods are improved understanding of the actual physical processes involved in crack growth, and a better characterization of the "forces" that activate these processes.

This work addresses the problem of crack growth on a rather fundamental level. The principal goal is increased understanding of what happens near a crack tip, within the realm of continuum mechanics, when the crack is submitted to cyclic loading. The work is based on a detailed numerical analysis of a crack tip. No external crack growth criterion is used which implies that all extension will be due to irreversible plastic deformation. This is believed to be a good idealization for a purely ductile material. The most basic question in this work is whether or not a finite extension of the crack from cycle to cycle results from a purely continuum based analysis.

The numerical analysis was performed using the general purpose FE-program ABAQUS. A semi-circular model focused at a crack tip was used. The model consisted of 1656 elements based on a mixed formulation and 1727 nodes. The loading was applied as prescribed displacements, corresponding to the K-field, on the outer bound of the semicircular region. Non-linearities due to finite geometry changes as well as due to the material response, which was modeled as elastic-perfectly plastic, was considered. Ten loading cycles were analyzed. Due to large plastic deformations distorting the elements, the mesh had to be redefined 48 times during the analysis.

The results strongly indicate that it is in fact possible to capture crack growth using a purely continuum approach. However, for the ten cycles studied, no kind of steady-state was obtained. The crack opening displacement increased steadily from cycle to cycle. An interesting result was that the initially rounded tip tended to take a sharp cusp shape during the last cycles studied. The distribution of the deviatoric part of the stress normal to the crack face, relative the current position of the crack front, was found to remain essentially unchanged at the immediate vicinity of the crack tip during the cycles studied. The same were also found for the distribution of the mean stress, i.e. the negative of the hydrostatic pressure, if the length scale were scaled with the crack-tip-opening-displacement for each half-cycle.

Thesis Supervisors: Hugh L.N. McManus,
Boeing Assistant Professor of Aeronautics and Astronautics

Mårten T. Landahl,
Professor of Aeronautics and Astronautics

Acknowledgments

I would like to express my deepest gratitude to all the people who made this thesis possible.

First I want to thank my employer, The Aeronautical Research Institute of Sweden (FFA) for giving me this opportunity. In particular i want to thank Martin Svenzon, Anders Blom and Anders Gustavsson, who lead me into this and have supported me during this time.

Then I want to thank Professor S.N. Atluri, Professor D.M. Parks, Profesor F.A. McClintock, Professor R.M.N. Pelloux and Professor J.R. Rice for fruitful discusions in the initial stage of the program. Opinions, comments, and suggestions raised in these discussions greatly aided in setting out the main path for this research.

Special thanks to my Supervisors: Boeing Assistant Professor H.L.N. McManus and Professor M.T. Landahl, for support and guidance throughout this work. Extra thanks to Hugh McManus for his patience, help and guidance in "putting everything together" during the hectic period that preceded the first deadline, the first hard deadline, and eventually, the final-hard deadline. To his despair, as the time to the deadline(s) was extended, I started adding new "stuff"to the thesis instead of woking to finish it off.

Finally, I want to thank my family and friends back in Sweden for support and encouragement during this time.

This research was financially supported by the Swedish Research Council for Engineering Sciences (TFR) (Grant Number: 261:91-737).

Contents

List of Tables

List of Figures

Chapter 1
INTRODUCTION

For structures for which the consequences of a failure may be particularly large, in terms of huge economic loss and/or the loss of human lives, the prevailing design codes and certification procedures are largely based on fracture mechanics and the concept of damage tolerance. Typical examples of this type of structure are aircraft, nuclear power plants, ships and offshore structures.

A basic assumption in damage tolerance assessment and analysis is that flaws and crack like defects may be already present anywhere in the structure when the structure is taken into service. Based on an assumed initial flaw size, the time it takes for this initial flaw to grow and reach a critical size (when the structure/component fractures) is estimated. The initial flaw size assumed depends on a number of factors such as inspectability, likelyhood of existence of a defect, location (e.g., main load path or redundant structure), how large defects that are likely to pass inspections (in manufacturing or in in-service inspections) etc. Finally, based on the results from these predictions, inspection programs can be set up to "ensure" that cracks are detected before they reach critical size.

Consequently, a central part in analyses of this type is to be able to predict crack growth for given load histories with reasonable accuracy. The methods in use today are almost exclusively refined and modified versions of Paris' law [61]. Although these models show excellent performance in many cases, the fact that they are entirely empirical relations, with no direct visible coupling to the actual physics of crack growth, make model predictions unreliable and uncertain when applied to conditions much different from the ones that prevailed when the model parameters were determined.

In practice, crack growth predictions are often made on basis of data for conditions much different from the ones that prevailed in the situation under consideration. Due to the nature of the problem, one wants to be on the "safe side" when doing approximations and extrapolations. As a consequence, if the uncertainity is large the analyses sometimes become overly conservative. Sometimes a highly conservative design and analysis philosophy can be accepted. Structural parts that are easy to inspect and easy and cheap to repair/replace should a crack be detected can be inspected often. Alternatively, in the design phase, unacceptable inspection requirements may be avoided by chosing larger dimensions of critical sections in the structure. In other cases, however, unnecessary conservatism may lead to unrealistic inspection requirements. The structural part may not be inspectable/reparable/replaceable at all without doing a major disassembly of a larger part of the structure. In particular for the latter type of structural parts, there is obviously a strong need for better more reliable prediction tools. In addition, consistently using over conservative prediction methods in the design phase may lead to unacceptable weight penalties, in particular for weight sensitive structures such as aircrafts.

It is not likely that significantly better models can be developed before the basic mechanisms involved in crack growth are better understood. The aim of the work presented in this thesis is related to this task, and hopefully the outcome will provide some further clues toward a better understanding of the process of cyclic crack growth.

1.1 Purpose

The aim of this work is primarily to give a better understanding of the process of crack growth. The hope is to establish a link between the empirical state of the art techniques in use today for predictions of fatigue crack growth and the kinematics of the near tip deformations obtained from a continuum description. The near tip deformations are certainly more closely related to the real crack extension process than the purely empirical growth laws are, so if it is possible to establish a link between the kinematics of the crack tip and the empirical models it would be of great value both

in the development of new refined growth models and for (re)assessing existing growth models and their range of validity.

In more explicit terms, a few fundamental questions that this work aims to shred light on are:

1. Is it possible, and if it is, to what extent is it possible to capture crack growth due to cyclic loading using a continuum description ?

2. Different mechanisms have been proposed in the literature attempting to explain the growth process and striation formation in ductile materials. A continuum model is not sufficient to model these mechanisms in detail. However, is it possible that a study based on continuum analysis is sufficient to give support to one particular model in preference to the others ?

3. How important is it to have a detailed continuum model in which many characteristics of cyclic plasticity is incorporated ? Or alternatively, how large errors are introduced by using a simple elastic - perfectly plastic model ?

4. Most simplified growth models based on micro mechanics predict a power of two in a growth relation of the Paris type if they are based on plastic slip, and a power of four if they are derived based on damage mechanics. Is it possible that an exponent different (higher) than 2 can result from the cyclic-plastic properties of the material, in combination with interactions with the elastic surrounding and a detailed account of the near tip deformations, if the growth mechanism is assumed to be due to irreversible plastic deformations only ?

These questions are strongly linked, so if the answer to 1 is "no", the rest of the questions become irrelevant. It should also be clearly stated that the aim on this work is *not* to come up with a competitor to the methods in use today – the analysis performed here is much too restricted and too involved for that. Instead it is again emphasized that the aim here is to improve the understanding of the crack growth process, within the realm

of continuum mechanics. Of course, the hope is that the new information/understanding acquired through this work can be of use in the development of new, or in the refinement/reassessment of old existing growth models.

1.2 Approach

A numerical (finite element) study of a crack tip under cyclic loading is carried out. Primarily, the focus is on the kinematics at the crack tip, but the stress and strain fields are of course also of interest.

The basic approach is to perform the calculations for a few load cycles, analyze the results, and try to deduce information supporting or opposing some of the questions raised in Section 1.1.

1.3 Scope and Confinements

This work is restricted to Paris regime crack growth in ductile (FCC) metals under plane strain. The only growth mechanism considered is that due to irreversible plastic deformation near the crack tip.

The load level is assumed to be small enough for the yielding zone to be small and confined, i.e., the condition commonly referred to as small scale yielding (s.s.y.) is assumed to prevail. With reference to the real situation that are modeled, the load level is also assumed small enough not to activate the growth mechanism of void growth and coalescence.

This work does not involve any experiments. Plenty of experimental data can however be found in the literature for the material chosen as model for this work, namely aluminum 2024-T3.

The material is modeled as elastic–perfectly plastic. The load history considered is constant amplitude cyclic loading with zero minimum level; and, only a few load reversals are analyzed. Traditional crack closure, i.e., far field closure, is not included in the analyses for two reasons; firstly, present available methods are quite capable of predicting the influence of crack closure on the growth rate; secondly, the primary goal here is to concentrate on the crack extension process itself. The effect of far field closure is essentially to affect (reduce) the driving force of crack growth in a global sense, with respect to the crack tip, and it is therefore not directly coupled to the detailed growth mechanism itself. The implication of this is that the crack faces are allowed to interpenetrate each other in the analyses if the interpenetration begins sufficiently far from the crack tip. If, however, interpenetration occurs near the crack tip, the contact stresses between the crack faces will most likely affect the near tip deformations. In this case crack closure, or near tip closure, will be taken into account.

1.4 Outline of Report

The thesis is divided into seven chapters, including this chapter. Chapter 2 covers three different groups of topics and is intended to give the reader the background information needed for the following chapters. Some of the information given is not clearly related to the chapters that follow. The purpose with this kind of information is to provide the reader with a brief background for the interpretation, discussion and evaluation of the results. The group of topics are: fracture mechanics and fatigue, constitutive modeling, and phenomenological and micro mechanical aspects of crack growth. In chapter 3 the model problem is defined. The region to be modeled, the boundary conditions, and the loading to be used in the analysis are defined; and the constitutive description to be used is chosen. Chapter 4 describes the discretization of the model region. In chapter 5 the analysis methodology is described, and the analysis is discussed in general terms. The results are presented and discussed in chapter 6. Finally, the whole work is summarized in chapter 7 with emphasis on the main results.

Chapter 2
BACKGROUND

The purpose with this chapter is to give some relevant background information, and thereby serve as a base for the following chapters. Since this work is based on a continuum description of the material, the sections dealing with 'micromechanics' will not be focused on an atomistic or dislocation size scale. Instead, micro will basically mean a size scale smaller than the one usually considered in continuum analyses, with the actual micro events interpreted in an averaged smeared-out sense.

The first section briefly introduces a few basic concepts and results in fracture mechanics and fatigue and is primarily intended for readers with little of no background in the subject. For more background information in these subjects the reader is referred to standard textbooks. A recent textbook on fracture mechanics is Kanninen & Popelar[35]. Another recent textbook on fatigue, which includes a section on fracture mechanics and covers much of the present state of fatigue research, is Suresh[77].

In the second section, crack tip blunting and the notion of crack tip opening displacement (CTOD) is introduced and discussed. The third section gives a brief overview on constitutive modeling. In Section 2.4 the different regimes of crack growth are briefly discussed. Section 2.5 then takes up phenomenological growth models in use today. Micromechanical aspects of crack growth are addressed in Section 2.6, with subsection 2.6.1 focused on different proposed growth mechanisms and subsection 2.6.2 on growth laws associated with the different mechanisms. Finally, the last subsection contains a general discussion of different aspects and results presented in this chapter, and their implications on this specific work.

2.1 Basic Concepts

Linear elastic fracture mechanics (LEFM) is concerned with the analysis of mathematically sharp cracks in different geometrical configurations for linear elastic, usually isotropic, materials. A basic result in LEFM is that the stress and strain fields show a square root singularity at the crack tip. The strength of this singularity is described through the stress intensity factor, K. The complete stress or strain field at a crack tip may have three singular terms with strengths K_I, K_{II}, and K_{III}, corresponding to different loading modes. In this work only the tensile mode – mode I will be considered (the other modes are: mode II – shearing mode, and mode III – antiplane loading). Therefore, to simplify the notation, K will from now on mean K_I. The stress fields, $\tilde{\sigma}$, near a crack tip can then be written in the form (Williams[89])

$$\sigma_{\alpha\beta} = \frac{K}{\sqrt{2\pi r}} \Sigma_{\alpha\beta}(r, \theta; geometry) + \text{non-singular terms} \tag{2.1}$$

$$K = \sigma_{ref}\sqrt{a}F(a/w, ...) \tag{2.2}$$

where $\alpha, \beta = 1, 2$ refer to cartesian or polar directions, r and θ are polar coordinates with origin at the tip (in three dimensions– in a plane perpendicular to the crack front), and $\Sigma_{\alpha\beta}$ are known smooth functions (of course different depending on whether α and β refer to cartesian or polar coordinates). Equation 2.2 shows a typical form of the expression for K for a simple geometry. σ_{ref} is a reference stress representing the load level, a is the crack length, and F is a function depending on the geometry and how the loading is applied. The resulting expression for the strain field is fully analogous to Eq. (2.1), except that the smooth functions $E_{\alpha\beta}$, corresponding to $\Sigma_{\alpha\beta}$, also depend on Poisson's ratio, ν.

Clearly, sufficiently close to the crack tip the influence of the smooth non-singular terms are negligible, and the "load" on the crack tip is uniquely given by one parameter, the stress intensity factor. This means that K captures the combined effect of global loading and geometry as felt by the material near the crack tip. Note that this also implies that apart from what is implicit in K, no characteristic lengths occur in the field expressions.

The extension of the use of K to elastic-plastic materials is based on the notion of autonomy (or similitude). If the plastic zone is small compared to other relevant dimensions, and also contained within the area where the singular term dominates the elastic solution, it is reasonable to assume that K and its history uniquely determines what happens near the crack tip and in the plastic zone. This assumption is a central one upon which nearly all applications of small scale yielding fracture mechanics are based. This subject will be further discussed in Section 2.7.

Historically, the first proposed fracture criteria (for monotonic loading) was based on energy balance. Griffith [25] suggested that growth took place when the energy release rate, G, which is the loss in potential energy caused by an increase of the crack size by one unit area when the external loading is kept fixed, reached a critical value, G_c. G_c was taken to be identically the total increase in surface energy, 2γ, caused by a unit area crack extension. γ is the surface energy and the factor two arises because there are two crack faces, so increase of the crack surface by one unit area result in two unit areas new free surface. This criteria only apply to 'perfectly brittle' materials, and when applied to engineering materials it predicts failure loads several order of magnitudes too low. The extension of Griffith's theory to engineering materials was essentially due to Irwin[32] and Orowan[59]. Basically they postulated that the critical value of the energy release rate, G_c, now consisted of two terms, one term corresponding to Griffith's original theory, and the other term corresponding to the energy plastically disspated by the growth process for one unit area extension of the crack. Based on this "modified Griffith" theory some important engineering problems were solved but the major breakthrough for linear elastic fracture mechanics (LEFM) came when Irwin [33] made use of the mathematical developments of Westergaard[88] and was able to establish a relation between a *local* parameter at the crack tip, namely K–the stress intensity factor, and the energy release rate, which is a global parameter. Following this, the global energy balance approach was practically abandoned in preference for the new local crack tip characterization viewpoint, which leads to a mathematically much more convenient approach.

Linear elastic fracture mechanics works well as long as the size of the inelastic zone

near the crack tip is small compared to other relevant geometrical dimensions. Since for engineering materials inelastic usually means plastic, states when the above holds is commonly referred to as small scale yielding (SSY).

For cyclic loading the load levels are by necessity lower and the processes leading to advancement of the crack front may be entirely different from the ones that are leading to failure under monotonic loading. Nevertheless, based on arguments similar to those presented above, it is reasonable to assume an expression for the growth rate of a crack of the type

$$\frac{da}{dN} = f(K_{min}, K_{max}) \tag{2.3}$$

where $\frac{da}{dN}$ is the crack extension per load cycle, K_{min} and K_{max} define the load cycle, and f may be a function but more generally is a functional, depending not only on the instantaneous values of K_{min} and K_{max}, but on their whole past history as well. Instead of K_{min} and K_{max}, it is customary to work with the stress intensity factor range, ΔK, and a parameter defining the mean load level, R. ΔK is defined by:

$$\Delta K = \begin{cases} K_{max} - K_{min} & \text{if } K_{min} > 0 \\ K_{max} & \text{otherwise} \end{cases} \tag{2.4}$$

The reason for this subdivision is that for negative K's, the crack surfaces come into contact and the resulting stress and strain fields become nonsingular, which of course implies that $K = 0$. The other parameter, R, is defined as

$$R = \frac{K_{min}}{K_{max}} \tag{2.5}$$

That K is a very good similarity parameter for crack growth is clear and generaly accepted. However, the first time the crack growth rate was proposed to be related to the stress intensity factor, it was met with skepticism. As a matter of fact, Paris' classical paper eventually published as [61], was rejected three times by leading technical journals on the grounds that an inherently plastic process such as crack growth could not possibly be related to a purely elastic quantity such as the stress intensity factor [60].

In the above, the loading has been assumed to be of constant amplitude. In case

of variable amplitude loading, an expression similar to 2.3 applies if it is interpreted for each half-cycle and a loading/unloading flag is included in the argument list. It should also be realized that a reference state must be defined in which the crack length is defined.

2.2 Crack Tip Blunting and Crack-Tip-Opening-Displacement (CTOD)

The notion of crack-tip-opening-displacement (CTOD) is frequently used throughout this work. In this section, the CTOD as applied in this work is defined and briefly discussed.

Most studies on crack tip blunting have been performed for monotonic loading conditions. In this section, as well as throughout most of this report, the assumptions and limitations given earlier are presumed to hold if not otherwise explicitly stated. In addition, for now only monotonic loading is considered, or equally, only the first 1/2 cycle is considered.

If an initially sharp crack tip in a ductile material is progressively loaded in the tensile mode (Mode I), it will blunt. Depending on the material response different shapes of the blunted crack tip are possible. Due to the complexity of the problem, analytical solutions are only possible for strongly simplified constitutive laws. Although these solutions may have a limited value in quantitative terms, they may still provide valuable for capturing general characteristics of the blunting process. For the simplest possible constitutive law, namely for a perfectly plastic material, the governing equations become hyperbolic with non uniqueness as a consequence. In fact, by using slip-line theory McClintock[45] and Rice and Johnson[69] showed that smooth blunting profiles as well as profiles with any number of vertices were possible solutions to an initially sharp crack tip. Both types of blunting profiles have also been observed in experiments, see McClintock[45]. Crack tip blunting has been relatively extensively studied for more general material responses, such as elastic-isotropically hardening plastic materials, usually as a partial

result in studies of ductile static fracture through void growth and coalescence, eg. McMeeking[48].

The crack-tip-opening-displacement (CTOD) has neither a natural nor a unique definition, except in two "academic" cases. The first is when the blunted tip has two vertices. The second is only applicable for the Dugdale model, a strip yield model, and not for a real situation. The CTOD for these two cases are indicated in Figures A.1 (a) and (b). For all other cases, CTOD has to be more or less arbitrarily defined. The definition that seems to be the most popular and most widely used, and the one that is used in this work, is that the CTOD is taken to be the (vertical) distance between the inceptions of two lines with angles 45° to the crack plane with the two crack faces [79]. See Figure A.1 (c) for an illustration.

2.3 Constitutive Models

The modeling of the material behavior for a configuration containing a crack is in no way a trivial task, in particular when the aim is to resolve details in the blunting of the crack tip. The presence of a blunted crack implies that plastic strain levels as high as several hundred percent are encountered in the immediate vicinity of the crack tip The size of the region in which the strain[1] levels reaches 100 % or more is of the order a CTOD. The major part of the plastic region, however, has much lower strain levels. Of the order 80 % of the yielded region has plastic strain levels less than 2 %.

As a base for the discussion of constitutive modeling, small elastic strains, incompressible plastic deformation, and an associative flow rule are assumed. The constitutive relation is further assumed to be rate independent, meaning that time does not occur explicitly in the governing equations. Also, only yield conditions of J_2 type will be considered, see eg.[43, 28]. This means that the yield condition is independent of hydro-

[1]The term strain is somewhat imprecisely used in the general discussion. Often it is the plastic strain that is meant, but for the general discussion it is unimportant to distinguish between them since the elastic strain is small, typically of the order 0.5 %. Neither is it stated what measure of strain that is meant. For the purpose of this discussion, it is suggested to interpret "strain" as the logarithmic strain.

static pressure, and that the projection of the yield surface on the synoptical plane in principal stress-space is a circle. This circle may translate due to kinematic hardening and expand due to isotropic hardening. These can all be considered as good approximations for the present problem, and is furthermore the base for practically all constitutive relations developed for metal plasticity. In general, this base is sound for dense (non porous) polycrystalline materials at low homologous temperatures and moderate strain rates.

With regard to the crack-tip-opening-displacement (CTOD), it is undoubtly most important to model the material response for low plastic strain levels correctly, since this governs the bulk response of the configuration, whereas the response in the high strain range should have more to do with local characteristics of the deformation very near the tip. However, the aim here is not solely to compute the CTOD, but to try to determine actual growth increments of a crack. In order to obtain a net extension of the crack for a closed load cycle, a part of the crack surface area created[2] during the loading portion of the cycle has to be redirected into the growth direction through stretching of the crack surfaces in combination with internal plastic flow. Since these phenomena are very localized to the near tip region, it is clear that the constitutive modeling of high strain levels is important as well. In the context of the growth law based on the cyclic variation of the CTOD, Eq.(2.10)

$$\frac{da}{dN} = \beta \cdot CTOD,$$

the viewpoint presented here is that the constitutive response for low strain levels essentially determines the CTOD, whereas the response in the high strain range affects the growth rate through the factor β.

It is of course not easy to formulate a plasticity model that "accurately" describes the response for the whole strain range from zero to several hundred percent. Moreover, even if it is likely, or at least possible, that the material can sustain such high strain levels (if the flow is unconstrained) that it still makes sense to model the the material

[2] Created crack surface area means basically stretched crack surface since we are using a continuum description and no new material particles are added to the crack surface

as a continuum, the assumption of elastic isotropy is probably not a good assumption at those strain levels. Keeping in mind that the constitutive response for much smaller strain levels, say less than 5 %, determines the global characteristics of the deformation, a reasonable approach seem to be to primarily model this strain range as well as possible, and in addition require that the model does not lead to entirely unrealistic response when applied to extreme strain levels. One example of unrealistic response is if a linear kinematic hardening law is used directly, and the model is calibrated to experimental data for strains up to, say, 5 %. If this model is used to predict the response for large strains it is likely that the model will predict plastic strain increments opposing the applied stress upon unloading. Therefore, a linear kinematic hardening rule seem not to be useful as a first step if one wants to improve the constitutive modeling. In addition, a linear isotropic hardening law also leads to unrealistic behavior, since for any constant amplitude cycling, stress driven or strain driven, it ultimately leads to an entirely elastic response.

The most common refinements from the simplest elastic-perfectly plastic model, namely the linear hardening models, are therefore of no use for the present problem. Instead, the next step would be to employ some kind of non-linear kinematic hardening law, and a isotropic hardening law that saturates at large accumulated plastic strains, eg. a finite strain generalization of the model suggested by Chaboche[10].

As mentioned earlier, almost all published works where the deformations near a crack tip have been studied in detail are for monotonic loading situations. The constitutive modeling for cyclic loading is in general much more complicated. A major difference between cyclic and monotonic loading situations, if strain hardening is to be considered, is that it is important to correctly model the isotropic and the kinematic part of the hardening individually in the cyclic case. In the monotonic case, on the other hand, it is essentially the total hardening that has to be correctly modeled. This difference is rather significant since kinematic hardening is much more difficult to handle and it can usually be avoided in the monotonic case by describing the total hardening as purely isotropic. In addition, for monotonic loading a further significant simplification is often possible and usually applied if the material is hardening (non-softening). If the loading

is applied proportionally, so that the load level is given by one single parameter, the ratio between different strain components will be approximately constant at each point in the body during the entire loading. Under these conditions, the constitutive relation can be put in a total form, directly relating the total strain or plastic strain to the stress. This is nothing but the description of a non-linear elastic material, which with regard to computations is much simpler than a material with a constitutive relation in incremental form.

In this work, only the simplest possible constitutive relation will be used, namely elastic–perfectly plastic. The following discussion is included partly to give a general idea of the implications if one wants to employ a better more realistic constitutive model, and partly to give a base for later discussion of the results, and how they may depend on the simple model chosen. The purpose is therefore not to go into details giving explicit expressions etc., but to present some general ideas, results and problems related to finite deformation cyclic plasticity. In order to do that briefly, it is not possible to define and explain every "standard" terms and expressions used; however, key terms and expressions will be appropriately defined, explained or references will be given.

The following discussion will be confined to the incremental theory of plasticity, or "flow theory"; since the other type in which the stress is a direct function of the strain, representing the deformation theory of plasticity, is only suitable for monotonic loading situations (and essentially restricted to proportional loading). Furthermore, since the governing equations ultimately have to be solved numerically, the following discussion is directed with that in mind. More specifically, it is assumed that the constitutive equations eventually shall be implemented in an assumed-displacement based finite element program. This leads to "The central problem of computational plasticity", Hughes[29], and can be summarized as follows: assuming that the state at a certain time t is known, and also that the configuration (displacement) at a later time $t+\Delta t$ is given, the central problem of computational plasticity is to determine the state (stress, plastic strain and other internal variables) for the time at the end of the step, $t+\Delta t$, so that the yield condition and consistency condition are satisfied at the end of the increment.

The "solution" so obtained does not in general satisfy the equilibrium equations since the supplied driving quantity, the displacement increment between t and $t + \Delta t$, was a guess. Therefore, the constitutive response usually has to be determined several times for each timestep as part of a global Newton-Ralphson iteration scheme. This, however, is a "standard" technique not specific to the constitutive description and will therefore not be further discussed here. It will, however, be briefly discussed in the chapter treating the computations, Chapter 5.

2.3.1 Finite Strain Plasticity

Most plasticity models for finite strains are generalizations of models developed for, and that have proven successful for, infinitesimal strain levels. The basis for this generalization is a consistent description of the kinematics of the deformation with respect to a chosen reference state. The reference state can be the undeformed configuration, which corresponds to a (total) Lagrangian description, or the deformed configuration, which corresponds to an Eulerian description. Usually, however, an intermediate state is chosen as reference for the kinematic description. Since the constitutive relations are given in incremental form, the solution of a problem has to be obtained through integration of the governing equations. The constitutive part of the solution scheme is used, as already mentioned, to determine the state at a time $t + \Delta t$ when the state at a previous time t, and the displacement increment between the two states, are known. One choice of reference state that is the base for many numerical implementations is to chose the (known) state at time t as reference for the step in which the state at a later time $t + \Delta t$ shall be determined. This procedure is usually referred to as an updated Lagrangian description, since for each analysis step, the configuration in the beginning of the step is the reference.

In the integration of the constitutive relation, it is often convenient to introduce yet another reference configuration. This configuration is based on the multiplicative decomposition of the deformation gradient originally proposed by Lee[40]. The introduced new configuration is between the configuration at time t and the configuration at time

$t+\Delta t$ and is obtained by point wise elastic unloading from the state at time $t+\Delta t$. This new configuration, usually referred to as an intermediate relaxed configuration, shall be considered as a mathematical state and does not in general correspond to a physically possible state (it is a one-to-one point wise mapping and results in a configuration that does not in general satisfy the compatibility conditions). As defined above, the new configuration is only determined to within an arbitrary rigid body rotation. A popular choice which has some practical advantages is to chose the intermediate relaxed state to be isoclinic, meaning that a direction triad that defines the directions which are relevant for the constitutive description is given the same orientation for the intermediate relaxed configuration as for the reference configuration. Usually the director triad is simply taken to be fixed with respect to the material.

One of the basic equations in the constitutive description is the relation between stress and elastic strain. The elastic relation can be hyperelastic, which is based on thermodynamical considerations and in its simplest form is a linear relation between the 2nd Piola-Kirchoff stress tensor and Green's strain tensor referred to the intermediate reference configuration. It is, however, more common to use a hyperelastic relation in which the chosen stress and strain measure refer to the deformed (current) configuration, since this is computationally more efficient for most common finite element codes. A fundamental requirement on a constitutive relation is that it should be objective. This means that the constitutive response shall be independent of the location and orientation of the observer. When using stress and strain measures referring to the current configuration, an incremental relation between stress and strain are not observer invariant. Therefore, in a hypoelastic relation an objective stress rate, which is not simply the time derivative of the stress but a Lie derivative relative some intermediate configuration, is related to a consistent strain rate. The most commonly used stress rate is the Jaumann-Zaremba stress rate. This is the Lie derivative with respect to a frame that is co-rotating with the material. Therefore, the Jaumann (-Zaremba) stress rate is sometimes called the co-rotational rate. If the plastic spin is given its own evolution equation, it is irrelevant which stress rate is used since the differences between different stress rates can be accommodated through the evolution equation. Hyperelasticity has a sound physical basis in that it is defined based on established thermodynamical

concepts. Hypoelasticity, however, does not have such a basis. As a matter of fact is has some undesirable features such as that it may dissipate energy during a closed purely "elastic" strain cycle. However, when the elastic strains are small and there is also plastic flow present, which is the case for the present problem, it is a very good model of the actual response.

The evolution equation for the tensorial state variable, the back stress, representing the kinematic hardening, is the one that is most difficult to generalize from small deformation to finite deformation theory. Attempts to directly generalize Melan-Prager linear kinematic hardening to finite deformations, by posing the relation in terms of the Jaumann rate of the back stress as a linear function of the symmetric part of the velocity gradient tensor, results in oscillations in the response to simple shear at large deformation levels. This anomalous behavior was first observed by Nagtegaal & De Jong[54], and has since then been extensively investigated. Some researchers found that this problem did not occur when using other stress rates, eg. Johnson & Bammann[34] using the Green-Naghdi stress rate. This stress rate is the Lie derivative with respect to the triad representing the principal deformation directions.

Although some researchers blamed the oscillatory shear response on the stress rate used and suggested that other stress rates be used, a more consistent treatment of the "oscillation problem" seem to be the inclusion of the plastic spin as a variable in the constitutive relation. This approach was pioneered by Dafalias[12] and has since then been followed by numerous researchers. The inclusion of the plastic spin in the constitutive description can also be related to the definition of the intermediate relaxed configuration frequently employed in the multiplicative decomposition of the deformation gradient. At present, however, these new theories essentially exist only as theoretical frameworks, and very few applications of the theories have been attempted. The main problem is that the plastic spin has its own evolution equation, which, together and simultaneously with the "usual" evolution equations, has to be determined on the basis of experimental data. This, of course, adds a lot to the already complex problem of extracting information from experimental data which is invariably limited, by economical and practical considerations. Specific constitutive relations based on the use of plastic spin have, how-

ever, been constructed (postulated) guided by certain imposed invariance requirements (Wang[82]).

2.3.2 Cyclic Plasticity

Constitutive relations for cyclic plasticity may be of two different types.

Internal Variable Theories: The state of the material is at any instant of time uniquely defined by the present values of observable variables and a set of internal variables. The observable variables in this case are stress and total strain, and the internal variables are variables describing the plastic state of the material. A fairly general model of this type has three internal variables. The first one is a second order tensor and is the plastic strain; the second is a scalar, the deformation resistance, and represents the isotropic hardening; and the third is a 2nd order tensorial variable, usually referred to as the back-stress, representing the kinematic hardening. Each internal variable has its own evolution equation (rate form). The isotropic deformation resistance and the back stress is sometimes given a micro mechanical interpretation in that the former is related to the dislocation density, and the latter to the dislocation structure.

Most theories in use today are of this type.

Hereditary Theories: In hereditary theories only real observable variables occur. The description of the state of the material does here takes a functional form, meaning that the state depends both on the present values and the history of a set of observable variables.

An interesting theory of the latter type is the "endochronic" theory, originally proposed by Valanis[80] for visco-plasticity. The endochronic theory was then expanded to elastic-plastic materials, Valanis[81] and Watanabe & Atluri[86], and later by Im & Atluri[31] to account for finite deformations. Im & Atluri also showed that this theory, with regard to computer implementation, can be put on a form similar to the one that arises for

internal variable theories. One interpretation of this is that the evolution equations for an internal variable theory were derived on basis of the endochronic theory. Since it therefore is possible, at least with regard to computations, to treat this theory as an internal variable theory, only internal variable theories will be considered in the following.

The central parts of an internal variable plasticity theory are the yield function and the associated flow rule, which defines the evolution equation for plastic strain; the relation between stress and elastic strain; and the evolution equations for the other internal variables.

The difference between monotonic plasticity and cyclic plasticity, and the motivation for distinguishing between them, is not that they use different theories. The two cases emphasize different characteristics of the actual behavior that the model should be able to capture. As indicated in the earlier discussion, the principal difference between these cases is that it in the cyclic case it is important to correctly model the kinematic and isotropic parts of the hardening individually. In the monotonic case it is essentially the total effect of the hardening that matters. For cyclic loading the kinematic part of the hardening is generally considered to be more important to model than the isotropic part. As discussed above, the kinematic part is also the one that is more difficult to model, in particular if finite deformations shall be considered. Therefore, the main emphasis in the discipline of cyclic plasticity has for a long time been focused on how to describe the evolution of kinematic hardening accurately.

At present three different types of models can be identified that are able to model many of the important features of cyclic plasticity. The first type is the endochronic theory cited above. The second type is models using two or more "yield" surfaces, eg. Dafalias[13] and Mroz[53]. In the third type, the evolution (differential)equations are postulated directly. In particular, a non-linear evolution equation for the kinematic hardening is used, eg. Chaboche[10].

The above mentioned models have essentially been developed for, and proved useful for, small plastic strains. Although a direct tensorial formalistic generalization to finite strains is possible, it is only a mathematically "consistent" generalization. It has not yet been investigated how well such generalized models perform. The problems encountered for the monotonic case certainly suggest that much more research is needed before useful quantitative models for large strain cyclic loading can be expected. However, this does not imply that direct tensorial generalizations are of no use. They may even be useful in quantitative terms under certain conditions (for example, under essentially uniaxial or biaxial loading when the rotations are small). They may also be useful if they are able to model the essentials of response qualitatively correctly, for the type of problem addressed here where a small region of large strains is contained within a large region with small plastic strains.

2.4 Regimes of crack growth

Fatigue crack growth is traditionally divided into three different stages. An illustration of the different stages of crack growth is shown in Figure A.2. In Figure A.3, the different stages of crack growth are indicated in a schematic representation of typical crack growth data.

1. **Short crack regime:** Here the crack size is of the order microstructural dimensions or smaller, and/or of the same order as the plastic zone size. The growth in this regime typically occurs on primary slip systems, which in a uniaxially loaded polycrystal (FCC–many available slip systems) means that the growth will take place in a direction approximately 45° to the tensile axis where the resolved shear stress is highest. Crack growth in this regime is highly dependent on the microstructure of the material. This regime is the most important regime in design with regard to the economical life of the structure.

2. **Paris regime, or power-law regime:** The crack size in this regime is large compared to microstructural dimensions, but still small compared to typical dimension

of the structure or specimen itself. The growth rate in this regime is essentially independent on the material's microstructure, and the direction of growth is perpendicular to the direction of the maximum principal stress. This regime is the most important one regarding structural safety and integrity, in the design phase as well as later in setting up and revising inspection programs.

3. **Static regime:** In this regime, the crack size or the plastic zone size may be of the same order as the smallest structural dimensions, or the load level high enough, so that additional growth mechanisms come into play, e.g., cleavage, or void growth and coalescence - so called static fracture modes. This regime essentially contributes to a crack growth prediction by determining the failure criteria. Very little time is usually spent in this regime, due to the high growth-rate.

In the following, attention will be focused on the Paris regime of crack growth.

2.5 Phenomenological Growth Models

Present available and used methods for predicting fatigue crack growth, i.e., the growth of a crack under time dependent loading, are almost exclusively based on Paris law [61].

$$\frac{da}{dN} = C\Delta K^m \tag{2.6}$$

C and m are constants with m usually in the range 2–4. This kind of laws are in essence empirical relations between some stress intensity factor range and the crack growth rate, typically expressed in terms of crack growth increment per load cycle. The refined growth laws typically involve an effective stress intensity factor, ΔK_{eff}, instead of just the applied stress intensity factor range, ΔK_{app}. Effects of different mean load levels (R-values) and different closure opening loads can then be incorporated through the definition of ΔK_{eff}. The closure opening load, K_{op}, corresponds to the load at which the crack opens. In the definition of ΔK in 2.4 it was "assumed" that the crack closes at zero load. In practice, however, the crack may close at a different (usually higher)

load level due to residual stresses in front of the crack, residual plastic deformation left in the wake of the tip, oxidation of the crack surfaces and non compatible crack surfaces due to roughness. Based on the crack closure approach, the effective stress intensity factor range can be defined as[3]

$$\Delta K = K_{max} - K_{op} \tag{2.7}$$

Of the above mentioned closure mechanisms, plasticity induced crack closure [17], seems to dominate in the Paris regime. This is closure due to contact stresses caused by residual plastic deformation left in the wake of the crack tip. It should be mentioned that many of these refined models are derived for, and in a strict sense are only useful for, constant amplitude loading. An example of a widely used "refined" growth law for constant amplitude loading is Forman et al.[18]:

$$\frac{da}{dN} = Const \frac{\Delta K^{m_F}}{(1-R)K_c - \Delta K} \tag{2.8}$$

where K_c is the static fracture toughness, and m_F like m in (2.6) a dimensionless constant usually between 2 and 4. In addition to modeling the dependency of R in the Paris regime, the model also accounts for the asymptotically rising growth rate as K_{max} approaches the static fracture toughness. Some proposed models even attempt to capture all three growth regimes in one closed form expression, e.g., Saxena et al.[73].

The models that are based on crack closure implicitly account for the dependency on R for constant amplitude loading. Elber[17] derived the relation, $K_{op}/K_{max} = 0.5+0.1R+0.4R^2$ for a particular geometry and testing conditions (plane stress). Similar expressions can be empirically determined for any given geometry and testing conditions. The models explicitly based on crack closure are the ones that have shown the best ability to model general variable amplitude loading. For these models, the closure opening load has to be computed throughout the whole load history. In doing this, methods based on the Dugdale model have proven particularly effective for plasticity induced crack closure [21, 20, 19, 14, 15, 9, 58, 83]. Clearly, the growth laws of the form discussed here are direct functions of the load and not functionals as suggested in

[3] In this simplified discussion the opening load and the closure load is assumed to be the same. In practice this is not entirely true due to reversed plasticity.

Eq. (2.3). However, by the introduction of variables such as the closure load, with their own evolution equations, the history dependency is condensed into these variables. This is fully analogous to hereditary theories versus internal variable theories in the theory of plasticity; therefore variables such as the closure load can be thought of as global internal variables.

These state of the art models allow relatively reliable predictions for variable amplitude loading as long as the time history is not too irregular. Some sequence effects, in particular effects of single/multiple over/under loads to an otherwise constant amplitude loading, have also been successfully modeled, see e.g., Ward-Close et al.[85]. It must be remembered, though, that these models are empirical in nature and they have no direct relation to the actual crack extension process. Therefore, using a model with parameters derived for a certain load spectrum and load level to predict crack growth for a different load spectrum and/or load level, may lead to large errors if the two load spectra are not sufficiently similar in some integral sense, since what is actually being done is an extrapolation of an empirical relation.

2.6 Micromechanics of Crack Growth

Attention is here restricted to Paris regime crack growth, and further, to materials of FCC structure (eg. aluminum alloys), in which the predominant growth mechanism is irreversible plastic deformation. Under these conditions, the crack growth often leaves trench marks on the fracture surface; one trench corresponding to one load cycle. The opposite, that each load cycle give rise to one trench mark, is not necessarily true. These trench marks are usually referred to as striations, and typically they appear on 40% of the fracture surface. Broek [8] found striations over as much as 90-95% of the fracture surface by tilting the replica of the fracture surface with respect to the electron beam in the microscope to different angles, thereby searching for the angle that gave best contrast of the features of interest. Broek's results suggest that a much larger part of the fracture surface may have striations than what is observed in a fixed setup. However, no matter whether 40% or 90% better represent the typical situation, it is still clear

that the growth mechanism that give rise to striations[4] is of outmost importance for this kind of materials. Growth due to irreversible plastic deformation is usually a significant contributor to the total growth rate for other materials as well, e.g., BCC, HCP; but for these materials other growth mechanisms, such as cleavage and intergranular separation, may also be significant contributors to the total growth rate.

For the materials under consideration here, two different types of striations have been observed: brittle/cleavage striations, and ductile striations. For the microstructure under consideration, FCC, cleavage is not a likely fracture mechanism since too many slip systems are available so that slip occurs before stresses high enough to cause cleavage have built up. Garret & Knott [22] showed that these brittle/cleavage striations, in FCC metals, in fact resulted from plastic slip. It is therefore grossly misleading to refer to theses striations as brittle/cleavage striations since, although their appearance are akin to true cleavage striations, they in fact originates from the same micromechanical event as which is the source in the formation of ductile striations, namely plastic slip.

The reason for the interest in striations and how they are formed is that they are the only strong feature of the fracture surface. It should be noted that it is not possible to do direct experimental observations of the near tip deformations and the growth process for plane strain since the surfaces of a test specimen, which are the observable parts, always are under a state of plane stress. Adopting the viewpoint that striations are formed by the growth process itself, or by a separate process strongly coupled to the growth process, studies of striations and their appearance under different load levels and environmental conditions can give much valuable information about the actual growth mechanism.

There are substantial differences between the mechanisms of crack growth taking place in air and in vacuum. Crack growth in vacuum, particularly in the low Paris regime, shows a much lower growth rate than in air. In the low Paris regime, the difference in growth rate may be up to an order of magnitude, whereas in the upper Paris

[4] Rice[68] pointed out that although it is unlikely, it is possible that the process giving rise to striations is uncoupled from the process governing the actual growth of the crack

regime the difference is much smaller. It is usually not possible to detect any striation pattern on fracture surfaces from tests in vacuum. At present no generally accepted explanation of these effects has been offered. However, there is evidence that crack growth in vacuum, like crack growth in air, is a continuos process that occurs cycle by cycle [51, 64, 84, 38]. Due to the large differences between the two environments, some researchers have proposed that different growth mechanisms operate in the two environments [51, 64]. Here the viewpoint by Ritter & Wei[71] will be adopted, namely that the growth mechanism in the two cases is the same but that the striations become flattened and smeared out in vacuum, so that they become difficult or impossible to observe. In the paper cited above, Ritter & Wei examined fracture surfaces for a titanium alloy, Ti-6Al-4V, and adopted the same "tilting technique" as used by Broek, to show that a clear striation pattern also occurred on specimens that had been tested in vacuum. So at least for some alloys, in this case a titanium alloy, and certain testing conditions, striations do form in vacuum. Moreover, even if it is not possible to identify a striation pattern under any tilt angle, this does not necessarily imply that the mechanism associated with striation formation is absent. It is equally possible that the "striations" formed are so flattened and smooth so that they are not distinguishable from other features/irregularities on the fracture surface. Regarding the growth rate, most researchers seem to have accepted the following explanation given by Pelloux[65]: On a small scale, plastic deformation consist of slip along discrete slip planes. These deformations are in principle reversible. However, near a free surface (here the crack faces/tip) the presence of air causes the newly exposed surfaces to oxidize which makes the slip largely irreversible, which in turn results in an increase in the macroscopic growth rate.

In conclusion, on the basis of the above discussion, the following viewpoint is taken in this work:

- The entire growth increment is due to the same micro event, namely, plastic slip.
- Crack growth in vacuum is, like in air, a continuous process occurring cycle to cycle.

- The growth process in vacuum is assumed to be the same as in air even if no visible striations occur on the fracture surface.

Since it is not possible to incorporate the effect of "increased irreversibility" near a free surface in a continuum model, at least in a direct way, the work presented in this thesis should be thought of as an attempt to capture crack growth in vacuum.

2.6.1 Growth Mechanisms

A number of different growth mechanisms have been proposed during the last 30 years for explaining fatigue crack propagation and striation formation. The goal has been to find a mechanism upon which a realistic growth law can be based, and also which can explain how the different types of observed striation morphologies are created. Laird[37] has identified four different morphologies, which are schematically shown in Figure A.4 (a)-(d). (a) shows the most commonly observed striation pattern for ductile materials with juxtaposed depressions, or trenches, on the surfaces. (b) is also frequently observed. The features of the surfaces are here in antiregister to each other, and the small fissures undercutting the ridges are most likely to be found in brittle materials. (c) and (d) are basically the same patterns as in (a) and (b), respectively, but as they turn out at a lower load level. What is important to note is that striation patterns usually have rather distinct trenches, and that the surface between the trenches are fairly flat, see e.g., [65, 84, 52].

The models that exist for explaining crack growth and striation formation can be grouped into two different classes. The first is based on the alternating shear rupture mechanism originally proposed by Orowan[59] for ductile fracture. This approach has been used by Pelloux [66], McMillan & Pelloux (including a written discussion by Schijve)[50], Neumann [56], Bowles & Broek[7] and Kuo & Liu [36] to explain fatigue crack propagation and striation formation. They all describe essentially the same mechanism and are based on a series of discrete slip events. Here the model/description by Neumann[56] is chosen for illustration, see Figure A.5. During the first loading, slip

occur on plane 1 until hardening or increased constraints imposed from the surrounding material elevates the stresses so that slip on an other plane, 2, is activated. (a) corresponds to the state when slip system 2 is activated and (b) is at maximum load. In the unloading phase, reversed slip must first take place on plane 1, and then on plane 2 in order to produce a growth increment. In their paper they discuss this model in terms of "the most unfavorable case of completely reversible coarse slip", but the requirement on a certain slip sequence order seem to be easiest to motivate by irreversibility, presumably through oxidation, which prevents surfaces that have "slipped off" the free surface to reenter the interior of the material. Nevertheless, when the "correct" order of slip events is chosen, the growth process is simply repetitions of the described first cycle, successively activating slip on new slip systems. This model is sometimes referred to as "the alternating shear process", Pelloux[66]; or "the unzipping model", Kuo & Liu[36].

The other main class does not rely on plastic deformation confined to discrete slip planes. There are two models belonging to this class that both are widely accepted. One model is the "plastic bunting process" by Laird[37]. The other one is the model proposed by Tomkins & Biggs[78]. In general terms the two models are very similar, the main difference being that the latter model has an additional brittle-type growth mechanism in addition to the plastic blunting process. Laird's model adopts a purely continuum approach, whereas Tomkins & Biggs describe their model based on the plastic deformation essentially taking place on discrete slip planes. In contrast to models of the first type, however, the growth increment of the crack is not as directly a consequence of the very slip events, but more a consequence of the overall kinematics of the near tip deformation.

Laird's model is shown in Figure A.6. (a) to (c) represents loading from zero to maximum load; (c) to (e) unloading back to zero; and (f) indicates the beginning of next cycle with an extended crack and one more striation compared to (b). The double notched Y-shaped tip is motivated by the fact that newly created crack surface is forced into the plane of the crack and partly folded by buckling. McEvily[46] et al. have made direct observations of the growth process occurring for polymers (PMMA, PC and PE), which largely support the mechanism suggested by Laird. It should be remembered,

however, that on a micro scale the deformation mechanism in polymers and metals are entirely different so it is dangerous to draw too strong conclusions from McEvily's experiment.

The other model, the one proposed by Tomkins & Biggs, is shown in Figure A.7. In contrast to Laird's model, which depicted the plastic flow as continuously distributed, the basic deformation mechanism is assumed to occur on a few discrete slip planes. Figure A.7 (a) shows the initial crack at minimum load. In (b) a small load has been applied and as the load increases, the stresses increases as well due to strain hardening and at some point "fracture" occurs at the tip as indicated in (c). The sharp notch formed by this fracture now acts as a strain concentrator and activates slip on new slip planes from this notch as indicated in (d). As the load is further increased, the fracture process depicted in (c) may be repeated several times before the maximum load is reached, resulting in (e). (f) shows the schematic shape of the crack after unloading. The last of the figures, Figure A.7 (g), shows the situation when the load is reversed at (c) before more slip systems have been activated.

The models of the first class always predict a sawtooth shaped striation profile which is not in accord with experimental observations for polycrystalline materials. Nevertheless, they have found relatively strong support from experiments performed on mono-crystals, see eg. Neumann[56, 57]. In a polycrystalline material it is likely that the combined effect of strain hardening and constraints from surrounding grains "smooths out" the plastic deformation so that the deformation is rather to be considered as a continuous process than as a finite number of discrete slip events. Both Laird's model and the model by Tomkins & Biggs are able to at least conceptually explain the most commonly observed striation morphologies.

The models discussed above should all be interpreted as simplified conceptual models, aiming to explain the essential characteristics of the real process of fatigue crack growth. The real process may consist of several cooperatively or competitively coexisting mechanisms and "fracture" processes. It is therefore not to be expected that one specific model should be "better" than the others under all circumstances. Models of

the first type discussed above are likely better than models of the second type to explain the deformations and the growth process for single crystals. Here, however, when the material is polycrystalline, models of the second type seem more appropriate.

As Laird pointed out in [38], it is unclear what causes the "fracture" in the Tomkins & Biggs model in a purely ductile material. Laird's model may also seem more attractive here since it is based on a purely continuum approach. For both models, however, one may wonder how realistic the shape of the very tip are, at least as depicted in their sketches. As shown in Figures A.6 and A.7, the Tomkins & Biggs model predicts a concave shape of the tip, while in Laird's model, the shape changes from being convex at maximum load to become concave at minimum load. For Laird's model, the unfolding/buckling of the crack-face may also seem a bit suspicious. However, all this criticism only concerns details and are at least for now irrelevant. Finally, the two models cited above also have been used in attempts to explain the growth process in more detail. However, since the models are only conceptual, these "explanations" are very discursive and rely largely on subjective interpretations of the model as well as the actual growth mechanism(s). An example is the discussion concerning whether the trenches form during the loading stroke or the unloading stroke of a cycle. Wanhill[84] claims that they form during the tensile stroke based on his interpretation of experimental results. Based on his interpretation and a following discussion he supports the Tomkins & Biggs model and "disqualify" Laird's model. Laird & De La Veaux[38], however, arrive at the opposite conclusion, partly based on an interpretation of the same experimental results as Wanhill used.

2.6.2 Growth Laws

Growth laws based on micromechanical or other physical arguments are essentially of two types:

The first type is the laws derived based on simplified plasticity models, discrete slip events and slip-line theory. Based on geometrical and physical arguments it is assumed

that the growth increment for one load cycle is a linear function of the cyclic variation of CTOD, $\Delta\delta$,

$$\Delta\delta = \alpha\frac{(\Delta K)^2}{\sigma_f E} \tag{2.9}$$

$$\frac{da}{dN} = \beta\alpha\frac{(\Delta K)^2}{\sigma_f E} \tag{2.10}$$

where σ_f is a representative flow stress, typically corresponding to a cyclically saturated state, E is Young's modulus, and $\frac{da}{dN}$ is the growth increment per cycle. α and β are both dimensionless factors, α typically slightly less than 0.5. The "transition", or "efficiency" factor, β, corresponding to the fraction of $\Delta\delta$ that is transformed into an actual growth increment, is sometimes as a first approximation assumed to be a constant about 0.5. Comparing Eq. (2.10) with the Paris law, Eq. (2.6) it is clear that this approach corresponds to an exponent $m = 2$ in the Paris law. This type of relation has been suggested and used by numerous researchers, see eg. Laird[37] and the written discussion by McClintock in the same paper, Pelloux[65], and Rice[68].

The other type of laws are laws based on damage arguments. A typical viewpoint in this case is to assume that growth takes place when a critical accumulated strain level has been achieved, not locally but over a certain characteristic volume. The characteristic volume may for instance be correlated to the average inter particle/void spacing. A growth law can then be formulated based of Manson-Coffin's law[5] for low cycle fatigue, see e.g., McClintock[44], or for a summary of several growth laws Rice[68]. These laws result in an exponent $m = 4$ in Paris law. Liu[42] arrived at the same result by using the hysteresis energy as a measure of damage.

I should be mentioned that laws with other "exponents" when compared to Paris law have been proposed. For example, Head[26] derived a growth relation based on strongly simplified physical assumptions and obtained an exponent $m = 3$ in a Paris type expression. However, these laws have, in general, a weaker physical base than the laws discussed above, and therefore will not be further discussed here.

[5] Manson-Coffin's Law is a strain based approach to life predictions with its main application in "low cycle fatigue", i.e., fatigue under high strain amplitudes. A description of the law can be found in any standard textbook in the subject, e.g., Suresh[77]

Purely dimensional considerations, see eg. Liu[41] and Rice[68], requires $m = 2$ as long as the crack length, which occurs implicitly through K, is the only characteristic length for the problem. Therefore, in order to obtain an exponent different than two, one or more additional characteristic lengths, or combinations of other parameters that provide the dimension length, must be added to the argument list. Since stage 2 crack growth is essentially independent of microstructure, it seem unlikely that a measurable micro structural dimension such as the grain size should provide a relevant characteristic length. It is, however, possible that a "new" parameter that provides the dimension length by itself, or by combination with the other parameters, is derivable from the cyclic-plastic properties of the material. Another possibility, as discussed by Rice in the paper cited above, is that the surface energy, or some other "bond breaking" measure, enters as a parameter. The dimension of these measures is work per area, so combined with eg. the yield stress or the Young's modulus, a quantity with the dimension length is obtained.

Consequently, growth laws of the first type are dimensionally consistent, but those of the second type are not. In addition, at least for ductile materials, laws of the first type have a sounder physical base in that the growth increment is directly related to the variation CTOD. Garret & Knott[23] actually showed that the growth increment per cycle was directly related to the variation in CTOD in experiments performed on an aluminum-copper alloy, Al-3Cu (akin to 2024, Al-4Cu). They further discarded damage based growth laws on the grounds that these would lead to a gradual change in the growth rate when the load amplitude was suddenly changed, which would be in contradiction with experimental results. Finally, it should be noted that (2.10) can be interpreted in more general terms by simply viewing it as a relation between the growth rate and the CTOD, with the CTOD not necessarily given by (2.10) which was derived based on several simplifying assumptions.

2.7 Growth Models – General Discussion

The whole discussion has so far been based on small-scale-yielding, so that K alone provides the relevant similarity parameter. This is, however, not necessarily true. If normal stresses parallel to the crack faces (T-stresses) are present, they have a rather large influence on the shape of the plastic zone, and are therefore likely to have a pronounced influence on the growth mechanism(s) as well. The maximum extension of the plastic zone, however, is only weakly dependent on the T-stress, so the criterion for small scale yielding is essentially independent of the T-stress. T-stresses may be imposed through biaxial loading, or induced internally by internal constraints that depend on the geometry of the cracked configuration, see Larsson & Carlsson[39]. These T-stresses are at present the focus of relatively extensive research aiming to develop new improved (static) two-parameter fracture criteria for large scale yielding, see eg. Betegón & Hancock[5] and Parks[63]. For fatigue problems, introduction of the T-stress as a second similarity parameter may enable a consistent treatment of biaxial loading situations, and also for addressing the problem of "configuration dependency", i.e., different growth rates obtained under globally uniaxial loading for test specimens of different geometries but with everything else kept the same.

In many engineering problems of practical interest, the load levels are such that the cyclic-plastic zone size reasonably well comply with the small-scale-yielding (SSY) assumption. The monotonic zone size, which is roughly four times the cyclic zone size for $R = 0$, often becomes too large for SSY to be a justifiable assumption. In engineering practice, whether or not SSY prevails is usually assessed based on the cyclic plastic zone size only. This can nevertheless be justified by the fact that the crack growth rate, which is the focus of our interest, is much more sensitive to variations in the loading than to the mean load level, and the main effect of the "monotonic plastic zone" is essentially to offset the load locally by inducing residual stresses in front of the crack. However, the accuracy of crack growth predictions using present state of the art techniques is probably near the point when this kind of phenomena has to be considered and dealt with before further significant improvements of prediction models can be expected. It

should be kept in mind that ultimately it is the actual growth process and scatter in experimental data that sets the limit for the accuracy, and that dictates how far it is meaningful to go in refining the analysis tools.

Neither of the the above discussed phenomena will be specifically addressed in this analysis. Analysis of the same kind as the one performed here may however be useful for addressing these phenomena as well, in particular by doing relative comparisons between different "extreme" cases.

Now, returning the attention to the "micro mechanical" growth laws, it is seen that the dimensional consistent growth relation, Eq. (2.10), predicts an inverse dependency on the flow stress. This is generally not in accord with experimental observations, as noted by eg. Beevers et al.[4]. One possible explanation to this is that the flow stress is often taken to be simply the yield stress. For materials that are essentially the same, but with different yield stresses, there seems to be a tendency for material with a high yield stress to soften and for material with a low yield stress to harden, see e.g., Dugdale[16], Schijve[74], Coffin[11]. Therefore, the difference in flow stress between the two materials gets less as the accumulated plastic strain increases. This is not anomalous or unexpected behavior but can be perfectly well explained by micro mechanics and dislocation theory. The saturated flow stress as obtained through micro mechanics is essentially a constant fraction (for a given material) of the elastic modulus. The resulting growth relation then becomes proportional to E^{-2}.

Parks in [62] provides an entirely different explanation for the lack of inverse dependency on the yield stress. He argues that since the growth rate for a rigid plastic material is zero[6], but nonzero for an elastic-plastic material, the "constant" β in Eq. (2.10) could be considered to be a function of $\frac{\sigma_y}{E}$, with $\beta(0) = 0$. Further, assuming that this function is analytic at $\frac{\sigma_y}{E} = 0$, and only using the first term in the Taylor (McLauren) expansion of β, he arrives at the result that the growth rate is independent of the flow stress. As for the micro mechanical approach, the growth rate is proportional to E^{-2}.

[6]This is only one possible solution.

An interesting observation was made by Bates & Clark[2]. They plotted the growth rate as function of $\frac{\Delta K}{E}$ (log-log) and showed that the curves for several entirely different materials, including different steels, aluminum alloys and titanium, fell within a surprisingly narrow "scatter" band. This kind of result greatly supports the idea that stage 2 crack growth is independent of microstructure, and also suggests that the inverse dependency on the yield stress in (2.10) is unreal. It should be mentioned that in the above mentioned investigation, all materials had an exponent close to two.

An other important experimental observation, which more of less have been presumed in the above discussion, is that there is essentially a one-one correspondence between macroscopic growth rates and striation spacing. See e.g., McMillan & Pelloux[50] and Hertzberg & Paris[27].

Chapter 3
MODEL PROBLEM

3.1 Material and Constitutive Model

As was discussed in section 2.3 it is a huge step between using the simplest elastic-perfectly plastic model and the improved more complete constitutive models. Also, the author has not been able to find anything in the literature closely related this work apart from one report, Parks[62]. Therefore, it seem unreasonable to employ a complicated constitutive model before the problem for the simplest constitutive model has been better investigated and understood. Consequently, the simplest possible material model is employed in this work, namely a (homogeneous, isotropic,) linearly elastic–perfectly plastic material with only three material parameters: the yield stress–σ_y, Young's modulus–E, and Poisson's ratio–ν. Since these three parameters uniquely defines the material response in the analysis, it is in principle not necessary to define a material in more detail.

However, a particular material has been chosen as model for this work, namely the aluminum alloy 2024-T3. There are three reasons for this. First, a huge number of experiments have been performed and published for this material; second, 2024-T3 is a typical material for which crack growth is predominantly due to irreversible plastic deformation; and third, if there will be a continuation of this work, e.g. involving more complete constitutive models, it is advantageous to have a specific real material as a base.

Even though a specific material has been chosen, the material constants is far from uniquely defined. In particular the yield stress can vary significantly; but the variations in E and ν is also relatively large. Here the data are chosen based on cyclically saturated

and monotonic stress vs. strain curves in [6]. The chosen parameters are:

$$\sigma_y = 360MPa \quad ; \quad E = 73.8GPa \quad ; \quad \nu = 0.3 \tag{3.1}$$

3.2 Model Geometry and Loading

The loading in the analysis is defined by $R = 0 \Rightarrow K_{min} = 0$, and

$$K_{max} = \Delta K = 630MPa\sqrt{mm} \tag{3.2}$$

which is a load level typical for stage 2 crack growth. Based on this and the material data given in section 3.1 it is possible to obtain an approximation of the size of the plastic zone and the CTOD at maximum load,

$$r_p \approx \frac{1}{3\pi}\left(\frac{K_{max}}{\sigma_y}\right)^2 \tag{3.3}$$

$$\delta = \alpha\frac{K_{max}^2}{E\sigma_y} = \alpha'\frac{(1-\nu^2)K_{max}^2}{E\sigma_y} \tag{3.4}$$

for plane strain. r_p is here the 'size' of the plastic zone, or better, its extension ahead of the crack in the crack plane; δ is the crack tip opening displacement, CTOD ; and the parameter α is a dimensionless constant of the order 1. In the literature, the expression involving α' is more common since it relates δ to the J-integral, which is the analogue to the stress intensity factor under general yielding conditions, and under small scale yielding leads to the second expression in (3.4). The extension of the plastic zone in the direction perpendicular to the crack surface is roughly four times r_p for plane strain. (Eqn's (3.3) and (3.4) are standard approximations and can be found in any textbook in the subject).

For cyclic loading, the active plastic zone size, r_{pc}, and the variation in δ, $\Delta\delta$ are given by the same expression if $2\sigma_y$ is substituted for σ_y and ΔK for K_{max} (eg. Rice[68]). Consequently, the cyclic plastic zone size is roughly one fourth of the monotonic size for $R = 0$, and the cyclic variation of the CTOD is approximately half of the monotonic

CTOD.

The geometry for the problem is defined by a crack in a plane with the outer boundary sufficiently far from the crack tip such that the K–field applied on the outer boundary gives an accurate description of the loading. This approach is sometimes referred to as a boundary layer solution. Since in this case both the loading and the geometry are symmetric with respect to the crack plane, only half of the geometry has to be modeled[1]. In defining the physical dimensions to model, it is expedient to express all length measures in a non-dimensional form. Here δ according to Eq. (3.4) with $\alpha = 1$ is used as reference length:

$$l_{ref} = \frac{K_{max}^2}{E\sigma_y} \approx 1.4939 \cdot 10^{-2} mm \tag{3.5}$$

In the following, a " ˆ " over a variable name will indicate its non-dimensionalized form. With $\sigma_y/E = 4.878 \cdot 10^{-3}$, the nondimensional form of (3.3) and (3.4) become:

$$\hat{r}_p \approx 21.75 \tag{3.6}$$

$$\hat{\delta} = \alpha \tag{3.7}$$

The crack was not modeled as a crack, but as a thin slit with a finite radius equal to half the width of the slit at the tip. (Trial runs were made for a mathematically sharp crack, using 4-noded isoparametric elements with two of the nodes initially coincident, but the results were not promising). The notch radius, r_n, corresponding to half the thickness of the slit, was chosen as

$$\hat{r_n} = 0.0251 \tag{3.8}$$

Considering a typical value of $\alpha = 0.66$ [70] then would mean that $\hat{\delta} \approx 0.66 \approx 13 \cdot (2\hat{r}_n)$, i.e., that the crack opening due to the first half cycle is approximately 13

[1]This is not entirely true. The solution(s) may have branch points where some solution paths correspond to non-symmetrical deformation modes introduced by instability. Here, these modes are excluded since consideration of them would require a full model and also a strategy for the treatment/identification of bifurcation points; and by that, add considerably to the size as well as to the complexity of the problem.

times the initial width of the slit, so the initial slit and tip radius can in be considered as relatively sharp.

The outer border of the model region was chosen to be semicircular, with a radius much larger than both the plastic zone size and the total crack growth to be considered. The radius chosen was:

$$\hat{R}_{outer} \approx 3445 \tag{3.9}$$

which approximately correspond to 40 times the maximum extension of the plastic zone. This may seem unnecessarily large, and it probably is. However, regarding the total number of degrees of freedom in the model, the difference between choosing the outer bound 6 or 40 times the plastic zone size is marginal since the mesh is extremely focused to the tip region. Nevertheless, by choosing the outer bound much larger than the plastic zone size, the conditions for small scale yielding will be satisfied; and also, the position of the crack front can be considered as fixed with regard to the the applied loading, i.e. the loading applied does not have to be adjusted as the crack grows.

Chapter 4
FINITE ELEMENT MODEL

A problem that occurs in this kind of analysis, and which is much more acute than under monotonic loading situations, is that some elements soon become severely distorted due to large plastic deformations. Therefore, the mesh has to be changed several times during the analysis in order to maintain a reasonable accuracy. The remeshing is also necessary to obtain convergence of the Newton-Ralphson iterations which is part of the solution process.

Since the region within which the elements become so distorted that remodeling is necessary is relatively small, the region was divided into two parts: an outer part which was kept fixed[1] and an inner part which was remodeled several times per cycle. Figure A.8 shows the finite element mesh (not the initial), with (b) fitted into (a) constituting the outer part, and (c) the inner part. As can be seen, the mesh is extremely graded in order to keep down the number of degrees of freedom, and at the same time resolve the near tip region in detail. This means that the mesh will be rather coarse at the elastic–plastic border so it will not be possible to study the advancement of the plastic zone in detail from cycle to cycle.

Apart from the frequent remeshing of the inner region, the topology of the mesh was changed one time. This change occurred early in the analysis and consisted of adding elements to the inner region, and removing a few of the outermost element layers. These changes will however not be further discussed here. All plots and data for the mesh is for the "final" version. In this "final" version the mesh had 1656 elements and 1727 nodes. The ratio between the largest and smallest element side length in the model was $\approx 5 \cdot 10^5$

[1] This is not entirely true. In the sixth cycle (analysis step 51) the outer part was slightly adjusted: the outer bound was kept fixed and the inner bound, connecting to the inner region, was somewhat translated in the growth direction.

for the first analysis step, but then more typically $\approx$ 5000. No numerical difficulties were detected due to the the large variation in element size, nor were they expected. The grading of the mesh is progressive so the situation that may cause problem, that very small elements couple to very large ones, did not occur in the model. Trial runs were also made in which the ratio between the largest and smallest element was of the order $10 \cdot 7$. Neither in that case were any numerical difficulties detectable.

4.1 Boundary Conditions and Loading

Symmetry conditions, i.e., restraint of displacements normal to the crack plane ($u_y = 0$) are applied to all nodes on the crack plane ahead of and including the node at the crack tip.

The loading is applied as prescribed displacements corresponding to the K–field on the nodes on the outer semicircular boundary (plane strain):

$$u_x = \frac{K(1+\nu)}{4E}\sqrt{\frac{2r}{\pi}}\left[(5-8\nu)\cos(\frac{\theta}{2}) - \cos(\frac{3\theta}{2})\right] \tag{4.1}$$

$$u_y = \frac{K(1+\nu)}{4E}\sqrt{\frac{2r}{\pi}}\left[(7-8\nu)\sin(\frac{\theta}{2}) - \sin(\frac{3\theta}{2})\right] \tag{4.2}$$

$$K = \hat{P}K_{max}, \tag{4.3}$$

where r and θ are the nodes' polar coordinates. The load level is described through the dimensionless parameter $\hat{P}$. $\hat{P} = 0$ corresponds to no load and $\hat{P} = 1$ to maximum load, which is $K_{max} = 630MPa\sqrt{mm}$; so the cyclic loading ($R = 0$) corresponds to variation of $\hat{P}$ between 0 and 1.

4.2 Preprocessor

In order to facilitate the remeshing operations, a simple mesh generator was developed. The region was first subdivided into six subregions numbered I–VI, with the curves defining the edges of the subregions numbered 1–17, see Figure A.9.

The bounding curves are of three different types:

1. **Fixed boundaries :** The curves 1,2,3,4 and 11 attach to the outer fixed region, so nodes on these curves are fixed.

2. **Given geometry :** Curve 7,14,15,16, and 17 are of this type. The shape of these curves are given, but the placement of the nodes along each curve is free. Curves 15,16 and 17 are simple lines with $y = 0$ since they define the symmetry plane. The shape of the other two curves, 7 and 14, are given from the previous analysis step. The shape of these curves are described as piecewise cubic parametric splines, where the parameter is chosen so that it approximately corresponds to an arc length coordinate, which makes mapping of new nodes onto the curve easy.

3. **Auxiliary (internal) curves:** The remaining curves:5, 6, 8, 9, 10, 12, and 13 are auxiliary curves for which only the end points are fixed.

The meshing is now controlled by data[2] supplied through a data file in combination with interactive input. The following mesh controlling parameters/features are available:

- The placement of node 4415 (N4415) on the spline(s) describing curve 7 and 14 can be arbitrarily chosen.

- The relative location of P_2 and P_1 between N4415 and N15; and the relative location of P_3 and P_4 between N4459 and N59 are free with the obvious limitations that the relative location for P_2 and P_3 are less than P_1 and P_4, respectively, and $0 <$ relative location < 1.

- The nodes on any curve can be biased to one of the ends or to the middle. The biasing is controlled by two parameters, one being the ratio between the smallest and largest element length, and the other controlling the speed of the transition from small to large..

[2]Only minor changes, if any, of the data are usually required between different analysis steps

- The shape of curves 12 and 13 can be slightly controlled. Choosing curve 12 for illustration, a local coordinate system,(x', y') with origin on the x-axis with the x-coordinate as P_1 is defined. Then define R1 as the difference in x between P_4 and P_1 and R_2 as the y-coordinate for P_1. Then the shape of the curve is defined as,

$$\begin{aligned} x' &= R_1 \cos^p \phi \\ y' &= R_2 \sin^p \phi \end{aligned}$$

where the parameter p may be used to control the shape. Clearly $p = 1$ corresponds to a quarter elliptical shape. (Note, ϕ is only a parameter used in defining the geometry. The mapping of nodes onto the curve(s) is done in arc-length coordinates and has nothing to do with ϕ.)

Chapter 5
COMPUTATIONS

5.1 Numerical Methods

The general purpose FE-code ABAQUS was used for the computations. Is is, as most finite element codes for structural analysis and solid mechanics are, based on an assumed displacement field and a weak formulation of the equilibrium equation, which usually leads to the principle of virtual work.

Non-linear problems are in general treated by first dividing the load history in a number of discrete steps. The problem is then solved successively step by step. In the present case, when finite deformations have to be taken into account, the configuration at the end of one step is used as reference configuration for the subsequent step. This approach is usually referred to as an "updated-Lagrangian procedure". The implementation in ABAQUS is essentially a discretized version of the formulation given by McMeeking & Rice[49], which included some appropriate simplifications for metal plasticity when the dilatation is small (a consequence of small elastic strains and incompressible plastic deformation).

The finite element solution process can briefly be summarized by considering one step in the solution process. The state at the beginning of the step, corresponding to $i = 0$ below, is then presumed to be an equilibrium state. In the following square brackets represent square matrices, and curly brackets row vectors, of order $N \times N$ and N respectively, where N is the total number of degree of freedoms. The step is defined/driven by an incremental change of the external load, $\{\Delta R\}^s$; and the solution

process can be summarized as follows:

$$[K]_i^s\{\Delta D\}_{i+1}^s = \{\Delta R\}^s - \{\Delta f\}_i^s \tag{5.1}$$

$$\{D\}_{i+1}^s = \{D\}_i^s + \{\Delta D\}_{i+1}^s \tag{5.2}$$

where $[K]_i^s$ is the tangent stiffness matrix of the system, $\{D\}_i^s$ the global dispacement vector and $\{\Delta D\}_i^s$ is the incremental displacement. $\{\Delta f\}_i^s$ represents the increment in the internal load vector relative the internal load vector at the beginning of the step, and is a functional of the deformation. The superscript, s, refers to the step under consideration, and the subscript, i, is the iteration number. First, Eq. 5.1 with $i = 0$ is solved for $\{\Delta D\}_1^s$, and it is understood that $\{\Delta f\}_0^s = 0$. $\{D\}_1^s$ is then computed using Eq. 5.2, and based on this "updated" dispacement vector the tangent stiffness matrix and the internal load vector is updated. The updated tangent stiffness matrix and incremental load vector are now used in Eq. 5.1, with the second term on the right hand side now non-zero, to determine a new "correction" to the displacement vector, which then is used to update the displacement vector according to 5.2. This procedure is repeated until a predefined convergence criterion is satisfied. The above described procedure is nothing but a full, global Newton-Ralphson (N-R) iteration scheme. In ABAQUS, the convergence criterion is given in terms of an absolute measure of the maximum allowable unbalance force, P_{max}, at any node in the entire model. In this work $P_{max} = 0.0001N$ (per unit thickness) was used, which corresponds to the order $8 \cdot 10^{-4}$· [(smallest element side-length)·(yield stress)].

Determination of $[K]_i^s$ and $\{\Delta f\}_i^s$ is based on a discrete variational formulation of the equilibrium equation and involves integration in space as well as in time. The nonlinearity due to the constitutive response enters the analysis implicitly in these integrations. The spatial integrations are performed using Gaussian quadrature, which means that the constitutive response only have to be evaluated at the integration (Gauss) points. Remembering that the solution process is displacement driven, the configuration at the start and at the end of the time interval for the global iteration step under consideration is known. In order to integrate the relations with respect to time to obtain the stress, plastic strain and other internal variables at the end of the time increment, a deformation path must be assumed within the interval. Based on the assumed defor-

mation path, discrete integration algorithms can be formulated. An important point to consider then is that the algorithms shall be objective, or more precisely incrementally objective, meaning that the results shall be observer invariant. ABAQUS uses the original algorithm by Huges & Winget[30], although more refined algorithms now are available, e.g., Rubinstein & Atluri [72], Reed & Atluri [67] and Weber et al. [87]. The algorithms are, like in ABAQUS, usually based on the unconditionally stable backward Euler scheme. In the integration, yield and consistency conditions are enforced at the end of the increment which leads to a return-mapping procedure, see eg. Hughes [29], which in turn involve Newton-Ralphson iterations on this sub-level of the analysis. The determination of $[K]_i^g$ has one term that corresponds to the initial stress stiffness, see eg. ABAQUS theory manual [1], and one term that arise from the material response. The latter term is basically the discrete Jacobian, or the consistent tangent modulus, see eg. Simo & Taylor [75] for the constitutive relation. It should be noted that an accurately determined $[K]_i^g$ is not strictly necessary for the accuracy of the analysis, but it is important for the convergence properties of the algorithm.

It should be mentioned that ABAQUS provides a user interface, UMAT, that allows the user to implement his own constitutive laws. For more general and complex constitutive formulations it is not always possible to determine the "consistent tangent modulus" in closed form. One then has to do approximations/simplifications which means that the global iterative solution process will no longer be a true Newton-Ralphson procedure. It may then be efficient to use a simplified updating procedure for the tangent stiffness matrix, eg. the BFGS method, see eg. [3, 24], which is also available in ABAQUS.

Abaqus also has a built in option for remeshing (Rezoning), which automatically maps solution variables (plastic strain) from a previous analysis step to a new mesh to be used in the subsequent step. This option is however only available for linear elements at present. The procedures as implemented at present does not allow for rezoning of only parts of a model, which would have been desirable for the problem at hand. There are two disadvantageous by doing the mapping/remapping also for the parts of the model that are kept fixed. First, it is a waste of computer time. Second, it leads to pollution of plastic strain meaning that nonzero plastic strain is spread into regions which have

not been plasticized. This, however, is not likely to affect the results noticeable since the plastic strain levels in theses regions are very small; but, it makes it more difficult to identify where the boundary between plasticized and non-plasticized material. Within the scope of the present work it is however not possible to develop and implement new rezoning routines and procedures.

The element that was chosen was ABAQUS element CPE4H, which is a four noded isoparametric quadrilateral (linear) element that employs a mixed formulation in the determination of the element stiffness and the internal load vector. The mixed formulation basically means that the hydrostatic pressure is introduced as an independent variable in addition to the displacement field. Therefore, the variational formulation upon which the tangent stiffness matrix and the internal load vector are derived does not correspond identically to the principle of virtual work, but to an augmented formulation that is a suitable linear combination between the functional corresponding to the principle of virtual work, and a functional in which the dilatational part and the distortional part are separated and coupled through Lagrange multipliers. Apart from divider checks in the program, this approach is able to handle entirely incompressible deformations. However, the standard four noded plane strain element in ABAQUS, CPE4, also allow for nearly incompressible deformations, essentially by splitting the deformation into a deviatoric part and a dilatational part and integrating the dilatational (pressure) response using a lower order of quadrature, meaning in this case that the pressure is constant in each element (only one integration point per element for the dilatation). This procedure, the B-bar method, was originally proposed by Nagtegaal, Parks and Rice[55].

Trial runs made for the two element types showed that the computational cost was only marginally higher for the mixed element (for the present problem). An admittedly subjective inspection and comparison of the results favored the mixed element. On parts of the crack surface, weak tendencies towards a sawtooth shape were observed. This was also what Parks[62] obtained using the same element type. The overall deformation pattern was reminiscent of the zero energy modes that can occur when under-integration for the entire field is used. Therefore it was concluded that the sawtooth tendencies

were an artifact of the element/integration used, and not a real physical phenomenon. When using the mixed element, no such tendencies were observed.

5.2 Numerical Procedure

The mesh had 1727 nodes. With two translational degrees of freedom, and the pressure treated as an independent variable, each node had three degrees of freedom. Subtracting boundary restraints lead to a total number of degrees of freedom (dof) for the model of 5110.

A total of ten load cycles were analyzed. Each half cycle was divided into three to six "global" analysis steps. "Global" is here used only to distinguish these externally used steps from the term "steps" used within ABAQUS. The whole ten cycle load history consisted of 85 global steps. Tables A.1 and A.2 shows the meaning of these 85 steps in terms of load history. The information given in the columns "Restart from", and "Results in" is essentially a log of the analysis and are not of direct interest here. However, if the figure in the column "step" under "Results in" is 1, the step is a "rezoning" step, meaning that state variables from the previous step have been mapped onto a new mesh for this step. The whole analysis involved approximately 550 increments, typically with between 5 and 6 Newton-Ralphson iterations in each increment. This means that the full equation system, of 5110 dof's, was solved about 3000 times.

Rezoning, or remeshing, was done 48 times during the analysis. It turned out that this was a very expensive operation. For a typical step which included rezoning, the cost (cpu-time) for the rezoning operation was nearly twice the cost for the actual analysis. Despite the fact that the rezoning operation involves several partial mapping procedures and solutions of non-linear equation systems, it is not reasonable that the cost should be that high, in particular since the topologically simplest element type was used. One possible explanation may be that the rezoning routines are very rough (this is a new utility in ABAQUS), and are not optimized for the computer that was used, a CRAY XMP4-64.

Figure A.10 illustrates the analysis process for the first half cycle, step 1 to step 6, in which rezonings were done between every step. Note that the scaling of the figures for the different steps are different. As can be seen in the figure, the meshes were designed attempting to anticipate the expected deformation in that elements were made elongated in directions perpendicular to the direction where the maximum stretch was expected, and vice versa. However, as also can be seen, the elements in the fourth layer from the crack surface for step one were given an unmotivated large aspect ratio[1]. In addition, during the first steps the transition between "fine" and "coarse" meshes was rather abrupt. Neither this abrupt transition from fine to coarse, nor the extreme aspect ratio used during the first step, is likely to affect the overall accuracy of the analysis. The elements with the extreme aspect ratios are otherwise well shaped, meaning that all interior angles are close to 90°, and the rapid transition from fine to coarse occur in the "wake" of the tip were the gradients of the field variables are moderate.

Figure A.11 shows the corresponding picture for a later stage in the analysis. Here it is seen that only four rezonings were made for a full cycle. And also, only six global steps were used here for a full cycle–the same number of steps used in the first half cycle. It should be noted that the number of global steps per (half) cycle has nothing to do with the accuracy. Instead, the global steps were used as "break points" in the analysis for deciding whether or not rezoning was necessary, and to define points in the analysis where output of results was desired. It should also be noted that the configuration coresponding to maximum and minimum load are not shown in the figure (minimum load for the considered cycle occur between step 67 and step 68, and maximum load between step 70 and 71). In contrast to the figure showing the first cycle, all partial figures here have the same scale.

If it is not obvious from these figures, the necessity of redefining or rezoning the mesh should be clear from figures A.12 and A.13. These figures show the initial meshes, i.e., for steps 1 and 67, respectively, convected onto the deformed configuration at maximum load corresponding to the end of steps 6 and 70, respectively.

[1]The aspect ratio in this discussion is defined as the ratio between the length of the element side which is closest aligned to the "radial" direction to the side length closest to the "tangential" direction.

Chapter 6
RESULTS AND DISCUSSION

The outline of this chapter is as follows: The first section introduces some basic notation and definitions used in the presentation of results. In the second section the analysis is "verified" by comparison with published results. The third section presents the primary and global results of the work, with only minor discussion. In the fourth section secondary results are presented. These are typically contour plots for a few selected stress/strain components and are included partly as a reference to the following discussion, and partly to give the reader a chance to make his own interpretation. Here as in the previous section, the discussion is kept brief, essentially confining to comments on direct observations and leaving the more interpretative discussions to the last section. Finally, in the last section, everything is put together and discussed in more detail.

6.1 Definitions and Notation

In figure A.14 four different near-tip regions are defined for easy reference in the presentation of the results and the subsequent discussion. All results are presented in non-dimensionalized, or normalized, forms. For length quantities the non-dimensionalization procedure was introduced in chapter 3. Analogous to that a " ˆ " over a variable will be used to denote the non-dimensional form. For stress quantities, the yield stress is chosen the as reference stress. Although strains are non-dimensional as they are, they have also been normalized by the elastic yield strain, ε_{ref}, defined below.

The reference measures used are:

$$l_{ref} = \frac{K_{max}^2}{\sigma_y E} = 1.4939 \cdot 10^{-2}\,\text{mm} \tag{6.1}$$

$$\sigma_{ref} = \sigma_y = 360\,\text{MPa} \tag{6.2}$$

$$\varepsilon_{ref} = \frac{\sigma_y}{E} = 4.878 \cdot 10^{-3} \tag{6.3}$$

for length, stress and strain respectively.

The stress measure used is the Cauchy (true) stress. The strain measure used is the integral of the rate of deformation tensor, see eg. the ABAQUS theory manual[1], and has in general no simple physical interpretation. However, in the special case that the principal deformation directions remain fixed throughout the deformation history, the strain measure corresponds to the logarithmic strain.

For practical reasons, two alterative notations are used to denote the field variables considered. In the text we will use σ_{ij} to denote the stress components, ε_{ij} to denote the strain components, with the superscripts e or p appended to specify only the elastic or plastic part, respectively. The mean stress is, in this notation, denoted by $\frac{1}{3}\sigma_{kk}$ where the usual summation rule for repeated indices is implied (i.e., $\sigma_{kk} = \sigma_{11} + \sigma_{22} + \sigma_{33}$). The deviatoric part of the tensors are denoted by appending a " $'$ " to the name of the field variable, e.g., σ'_{22} denotes the deviatoric part of σ_{22}. The other notation, which occurs on some of the plots, uses Sij to denote the stress, PEij to denote plastic strain components, and PRESS to denote the hydrostatic pressure, which is equal the negative of the mean stress.

6.2 Verification

It is a non trivial task to verify numerical computations of the kind as the one performed here. No analytical solutions are possible, nor are there many published results for similar problems to compare with. What is possible and reasonable to do is to compare results for the first half cycle, which correspond to monotonic increasing load, with published results. The model is rezoned five times during the first half cycle. Thus the most "tricky" part of the analysis chain is at least partly verified.

Step	$\hat{P}^2$	α'	α
1	0.144	0.684	0.622
2	0.292	0.672	0.612
3	0.436	0.669	0.609
4	0.640	0.669	0.609
5	0.828	0.669	0.609
6	1.000	0.668	0.607

Table 6.1: Table showing α and α' values obtained for the steps defining the first half cycle.

Although it was not explicitly stated, the expressions given earlier for the crack tip opening displacement, e.g. Eq. (3.4), assumed a mathematically sharp crack. In numerical analysis of cracks modeled as slits with a finite radius at the tip, it is customary to "back extrapolate" the crack opening profile to zero slit width/root radius. Strictly, the initial shape should be subtracted from the deformed configuration in Lagrangian space, which for a rigid-perfectly plastic material represents a mathematically correct relation between a rounded slit and a sharp crack, see Rice and Johnson[69]; and therefore should be the best justified procedure also for an elastic-plastic material. With regard to the crack tip opening displacement, it is often justifiable simply to subtract the initial slit width from the obtained CTOD, which is what has been done here. Consequently,

$$\delta^{>} = \delta - 2r_n, \tag{6.4}$$

have been used, where $\delta^{>}$ represents the back extrapolated CTOD for a sharp crack, δ the CTOD obtained for the initially rounded slit and $2r_n$ represents the width of the slit. When $\delta^{>}$ has been determined, the proportionality factors α and α' defined through Eq. 3.4 can be determined. α' is chosen here as the base for the comparison with published results.

In the present analysis, $\sigma_y/E \approx 4.878 \cdot 10^{-3} \approx 1/205$. McMeeking[47] obtained $\alpha' = 0.58$ for $\sigma_y/E = 1/300$ and $\alpha' = 0.65$ for $\sigma_y/E = 1/100$; and Sorensen[76] $\alpha' = 0.66$ for $\sigma_y/E = 1/1000$. The agreement with the values in table 6.1 is good. That the values for the present analysis are slightly larger than the published results is likely due to the use of more degrees of freedom and a mixed formulation in the present study, which

both tend to "soften" the material response, and therefore should lead to slightly higher values of α compared to a purely assumed displacement approach.

Apart from this, the only checks/validation of the numerical results have been to check that the stresses near the outer boundary of the model are in accord with the applied K–field, and to look for peculiarities in the results.

6.3 Primary and Global results

In this section results related to the kinematics of the crack tip and the development of the plastic zone during the considered load history are presented.

The shape of the crack front at maximum and minimum load are shown in Figures A.15 and A.16, respectively. The most obvious observation is that a net extension of the crack was actually obtained for each of the cycles studied. This result is not as obvious as it may seem since no fracture, or material de-cohesion, criteria were used. Of these two figures, Figure A.16 can be considered of more interest since the unloaded state is a more natural reference state. Both figures, however, clearly show a rather significant shape change of the crack front for the cycles studied. In the figure for maximum load, the shape is in the beginning clearly convex, but then tends to develop a corner and otherwise obtain a relatively straight shape, and in the last cycles, even a weak tendency to a concave shape is seen. For the unloaded state, these tendencies come out clearly. At the end of the first three cycles, the shape is clearly convex. Then there are a few transition cycles where the profile essentially can be described by two fairly straight line segments connected by a "corner" with relatively small radius. For the last cycles, the shape of the crack tip clearly takes a concave shape. The overall crack front shape at maximum load show concave tendencies, but small portions of the front remain convex. In contrast, the shape at minimum load is also locally concave. Strong tendencies to form sharp corners at the top and bottom of the crack face, and a cusp shape at the center of the crack face, are clearly seen in the figure.

The advance of the crack front cycle by cycle is shown in figure A.17. It seems as if the growth increment per cycle approaches a constant "steady state" value, which is expected. However, it one cannot draw any definite conclusions here, in particular in quantitative terms, since the shape change of the crack front was so large during the cycles studied.

That no kind of steady state[1] has been obtained is clear from the figures A.15 and A.16 discussed above, in that the total crack tip opening is monotonically increasing during these ten cycles. This is illustrated in a more direct form in figure A.18 which shows the (half) variation of the crack tip opening displacement for each half cycle. The achievement of a steady state would imply that the variation of the CTOD during a loading half-cycle and an unloading half-cycle be the same, which would correspond to a horizontal line in figure A.18. In the figure A.18 no definite trend towards steady state can be observed. In the only related work that the author has been able to find, Parks[62] obtained a gradual increase in the CTOD for the three cycles he studied. However, the crack opening $\hat{y}$ for a given position (spatial) does not increase from cycle to cycle, but remains seemingly constant for all comparable cycles, which includes all cycles studied if $\hat{x} < 0.05$ is chosen, see Figure A.16.

The development of the CTOD from step to step is shown in the Figures A.19, at two different scales, for all steps involved in the analysis. The figures are somewhat difficult to interpret but one can note that the first loading half cycle is linear. The second and the last cycle are plotted with thicker lines to aid in distinguishing them from the others. For both of these it is seen that the relation between $\hat{\delta}/2$ and $\hat{P}^2$ for the loading part is still fairly linear, although not to the same degree as for the first half cycle. As expected, the slope is approximately half of the slope for the first half cycle (see the discussion in Section 3.2 about the use of $2\sigma_y$ in place of σ_y for cyclic loading). For the unloading half cycles, the relation is clearly strongly non linear.

[1] The term "steady-state " (S-S) is used in a weak sense, not necessarily meaning a true S-S which can not be expected until the crack has extended on the order a few plastic zone sizes, but rather referring to a state when changes in field variables and shape, relative the moving tip, are negligible over a few cycles.

The material flow occurring during the two last cycles is illustrated in figure A.20. This is of primary interest since no fracture criterion is used in this study, and therefore, the extension of the crack must be entirely due to material transport caused by plastic deformation. The figure does not identically represent the two last cycles between fully unloaded states, but instead between states with the relative load level $\hat{P} = 0.2$. The reason why the fully unloaded states were not used was purely practical; namely, the fully unloaded states do not have their own meshes to be used as references since they are not rezoning steps. Nevertheless, the two configurations define two complete cycles. The flow is easiest seen on the crack surface where the strain level is highest, and the material flows to the right in the figure. The "back flow" in the left direction occurs over a larger, lower strained region. It is possible to see a small shift to the left in the upper parts of the region shown when the lower figure is compared to the upper one.

The plastic zone shapes are shown in Figures A.21 and A.22 at maximum and minimum load level for four cycles. Both the active plastic zone and the boundary between plasticized and non-plasticized material are shown. The active plastic zone is obtained by plotting contours of the von Mises stress for stress levels equal to the yield stress $+/-$ a small tolerance, and the boundary between plasticized and non-plasticized material is analogously obtained from contour curves for the accumulated plastic strain for strain levels near zero. At the first maximum load, both these zones should be identically the same, which is not what is obtained in the top figure in Figure A.21. However, this is neither alarming, nor unexpected. First, the mesh is very coarse where the discrepancy occurs, see and compare to the mesh in figure A.14. Second, due to pollution from the rezoning process, the boundary between plasticized and non-plasticized material becomes smeared out (extended) and more difficult to identify. Due to the coarseness of the mesh in the outer regions, the boundary between plasticized and non-plasticized material looks essentially the same throughout the whole history studied. The reversed active plastic zone, i.e., the active zone during unloading, also looks essentially the same throughout the history, but since this zone is smaller and therefore has its boundary in finer discretized regions, it is possible to resolve that the zone moves with the tip.

The active plastic zone at maximum load shows a bit more interesting, although in no way unexpected, features. It is seen that the upper part of the active zone continuously reduces in size, whereas the lower part seems to tend towards a stable bulged concentrical shape. The upper and lower parts are connected by a gradually thinning strip. It should, however, not be concluded that this strip would vanish identically after more cycles. At least a strip width of the same order as the growth increment for one cycle should result for any maximum load in the load history[2], even when (if) a true steady-state has been achieved. It is also seen that there is a small essentially semicircular inactive zone in front of the crack tip. The center of the inactive region is on the crack plane (read symmetry plane), and is located a few (≈ 8) CTOD's in front of the current position of the crack tip. Consequently, the inactive region moves with the crack tip, and it is also clear that its shape and size remain essentially constant during the cycles studied. At maximum load, the front of the boundary between plasticized and non-plasticized material, and the front of the boundary of the active plastic zone should largely coincide. This is not exactly in accord with the figures. However, as was discussed for the first cycle, this is most likely due to pollution from the rezoning procedure in combination with a relatively coarse mesh used in these parts of the model. In addition, the differences between the two bounding curves are of the order one element length. Therefore, the discrepancy between the two bounding curves is nothing to be concerned with.

6.4 Secondary Results

The results presented in this section are not as clearly linked, or coupled, to the actual extension of the crack as most of the results in the previous section were. This does not imply that these results are less important than the results of the previous section. Unfortunately, however, the results presented here are in general more difficult to evaluate and interpret.

[2] Constant amplitude loading is here presumed. Of course, for general amplitude loading, or a sudden drop in the amplitude, the active plastic zone may be entirely confined within previously plasticized material.

The purpose of this section is to present a general picture of the stress and stain fields near the crack-tip. This is done by plotting the distributions of selected field variables. Of particular interest is how these distributions change during the cycles studied. As in the previous section, the discussion is essentially confined to comments on direct observations, leaving more speculative interpretations to the last section. The field variables chosen as a base for the presentation are the normal stress normal to the crack surface, σ_{22}, the hydrostatic pressure, $-\frac{1}{3}\sigma_{kk}$, and the plastic strain components, ε_{11}^p and ε_{22}^p. First, contour plots of these stresses and strains are shown and discussed. Then the distribution of σ_{22} in front of the crack tip is shown and discussed. After that, the hydrostatic and deviatoric part of σ_{22} are treated. Finally, the plastic strain distribution in front of the crack is presented and discussed.

The four Figures A.23 – A.26 show contour plots at two different scales. The left column showing the region GL2 has the larger scale, and the right column showing the region GL1 has the smaller scale. For easy comparison, the sub-figures are arranged in groups of four, so that sub-figures showing results for the last cycle are located below the corresponding figures for the first cycle. The vertical lines that go through all the sub-figures are reference lines, fixed in space, representing the initial position of the crack front.

From Figures A.23 and A.24, it is seen that the magnitude of σ_{22} reaches nearly three times the yield stress. This is, however, fully in accord with what is obtained from simple slip line solutions, eg. [69]. For a mathematically sharp crack, maximum/minimum of σ_{22} and hydrostatic pressure occur at the tip of the crack. For a blunted crack tip, this is not the case, since high hydrostatic pressure cannot be sustained near a free surface. Instead, the extreme of the hydrostatic pressure is obtained a small distance ahead of the tip. Essentially, this distance scales with the crack-tip-opening-displacement and is of the order a few CTOD's. This is clearly seen in the Figures A.23 and A.24, for minimum load as well as for maximum load, and likewise, for the first cycle as well as for the last cycle. When comparing the results for the last cycle with those for the first cycle, it is seen that the maximum attained magnitude of σ_{22} at maximum load decreases, while the maximum value attained at minimum load increases.

The Figures A.25 and A.26 showing plastic strain components are, in some sense, of more direct interest since the plastic strain better represents the state of the material. It is seen that the difference in the strain fields between maximum and minimum load is relatively small for the last cycle. The same is true for all cycles apart from the very first, for which the maximum load is obtained from virgin material. This does not imply that the fields do not change, but that they change slowly so that the variation in the fields within a cycle, or from one cycle to the next, is small. It is also noted that the two plastic strain components shown are of similar magnitude and opposite sign. This may be expected from standard arguments assuming that the elastic strains are small compared to the plastic ones. Under these conditions, plane strain implies that the plastic strain in the thickness direction is negligible, and the incompressibility condition becomes $\varepsilon_{22}^p \approx -\varepsilon_{11}^p$, which holds for any proper strain measure at moderate strain levels. The assumption that the elastic strains are small compared to the plastic strains may be violated due to the high hydrostatic pressure near the crack tip. However, it was found that the elastic strain in the thickness direction (which is the only elastic strain component that affects the incompressibility condition for the in-plane plastic strain components) was typically of the order 1/10 or less of the in-plane plastic strain levels, in the regions considered.

Based on the above discussion, it is clear that most of the information regarding the plastic strains, at least for relatively high strain levels, are contained in one single group of figures. Here, and for later reference, the last group (the last four sub-figures in Figure A.26) is chosen as reference. This particular group is chosen partly because ε_{22}^p is in the more interesting direction–the direction normal to the crack surface, and partly because minimum load is a more natural reference state than maximum load. To simplify notation, "plastic strain" will be used with the meaning ε_{22}^p in the following discussion.

Comparing ε_{22}^p at the end of the first cycle, step 11, with that obtained at the end of the last cycle, step 85, shows that a relatively small region with compressive plastic strains are left in the wake of the crack tip. It is also seen that a larger region, farther away from the crack plane, with positive plastic strains also is left in the wake of the

crack tip. The larger region with positive plastic strains consists of residuals from the previous "monotonic" plastic zones, and the smaller region with compressive plastic deformations consists of residuals from the previous reversed plastic zones.

In the next group of figures, the stress distribution of σ_{22}, i.e., the stress component normal to the crack plane, is studied. This distribution is shown in Figures A.27–A.30, of which the three Figures A.28–A.30 are all partial magnifications of Figure A.27. These figures are therefore discussed collectively. Is is clearly seen in the first three of these figures that the stress distribution not only translates corresponding to the movement of the crack tip, but changes shape as well. In the region between the positive maximum of stress and $\hat{x} \approx 20$, the initially fairly straight down slope attains a sine-like shape. This can be seen in both Figures A.27 and A.28.

Another region where a change in shape occurs is on a much smaller scale. This is best shown in the top part of Figure A.29, corresponding to maximum load. Very near the current tip position, i.e., the beginning of each curve, it is clearly seen that the initial gradient gets sharper as the crack grows, and also that the early part of the curve tends to bulge. For the last step shown, this bulging has developed into a local maximum for the stress. In the lower part of the figure, corresponding to minimum load, this tendency is also clearly seen. For the third step shown, a local minimum has developed and the overall shape is very similar to the one for the last cycle at maximum load. For the last step, however, the shape is no longer smooth.

Figure A.30 shows a magnification of the above discussed region. The mean stress (the negative hydrostatic pressure) is also shown in the same figure. Some of the features are obviously on the limit of what is resolvable with the discretization used. The wave length of these apparent irregularities are of the order a few element widths. Nevertheless, the seemingly anomalous behavior very near the tip is real and expected. In the previous section we noted that the crack front obtained a cusp shape at the end of the last cycles. On a very small scale, this cusp corresponds to a mathematically sharp crack, implying that high hydrostatic stresses can be sustained at the very tip, and that normal stresses of the order $3\sigma_y$ can be expected there. Here, however, we have

a discrete model and the term "mathematically sharp" has a only a vague meaning. In addition, as already mentioned, this behavior is observed on a scale that is on the limit of what the model can resolve. It is therefore not advisable to focus on details on this fine scale, but it is still possible that the the entire curve, even the "switch backs" in the early part, represents true characteristics of the solution to the mathematical problem posed. That the stress first increases, then decreases, then increases again to eventually decrease towards the global minimum is not unrealistic. Many parts of this behavior are observable in the smooth curves for the earlier steps plotted, and introducing a sharp near tip field corresponding to the cusp would, in general terms, explain the entire shape.

The mean stress part is clearly is a major contributor to the total stress. It may therefore be useful to divide the stress into the deviatoric part and the hydrostatic part. Figure A.31 shows the deviatoric part of σ_{22}, σ'_{22}, plotted on the same scale as Figure A.28. The figure shows the stress distributions for four steps corresponding to maximum load, and four steps corresponding to minimum load. The curves are shifted to the left so that the origin correspond to the current position of the crack front. Consequently, the abscissa represents the distance from the current crack front position. It is seen that, apart from for the first loading (which is obtained from a virgin state), the curves essentially coincide for distances[3] less than 6 from the crack front. The most noticeable features in these curves are the bulges a short distance ahead of the tip.

The distance to the bulges is larger for maximum load than for minimum load. This can be taken as an indication that this distance scales with the CTOD, which is the only characteristic length in the problem (apart from what is implicit in the stress intensity factor). When the same data as shown in Figure A.31 was plotted with the distance scaled by the CTOD, the coincidence of the the curves representing minimum load was improved for distances less than the distance to the extreme point of the bump. However, for all other parts of theses curves, and for the entire curves corresponding to maximum load, the scaling was detrimental with regard to coincidence.

[3] Distances here are nondimensionalized according to Eq.6.1

The near tip distributions of the mean stress did not coincide when plotted in the same fashion as that used in Figure A.31. However, in this case, scaling the distances by the CTOD (for the current step) made the curves largely coincide up to the global extreme point. Figure A.32 shows these curves for the steps corresponding to minimum load. The region shown corresponds to $\hat{x} - \hat{x}_0$ between 0 and 2.9 for step 11, and 0 and 5.2 for step 85.

The next two figures, Figure A.33 and A.34, show the plastic strain ε_{22}^p. In the first of the figures, the strain is plotted as function of the position ahead of the crack tip. It is seen that the regions with strain levels larger that 100, i.e., 100 times the reference yield strain, are very small. It is also seen the shape of the distributions changes markedly, in particular between the first cycle and the fourth cycle, but also between the last two cycles shown, cycles seven and ten. The next figure, Figure A.34, shows the same data plotted on logarithmic scales. There the "inactive" region, identified and discussed in the previous section, is clearly seen. All curves coincide in this region. An inactive zone, at a given instance, is defined as a region in which the plastic state has not changed during the last cycle. It can be seen that the strain distribution within the current inactive zone changes rather markedly during the cycles studied. In the beginning, the strain level decreases monotonically with increasing distance from the crack tip. As the crack grows, the strain in the trailing "edge" of the inactive region decreases, which can be seen in Figure A.34 in that the curves, from the high strain near tip region, join with the static part, representing the inactive region, at progressively lower strain levels. At the other end of the inactive region, the strain level in the newly defined parts increases. Therefore, a "knee" occurs in the strain distribution. The point originally defining the leading position of the inactive zone corresponds to the "knee point" and represents a minimum of the strain distribution within the inactive zone.

6.5 Discussion

The main results of this analysis are:

- A net extension of the crack actually occurred for each of the cycles studied.
- The change in shape of the crack front was significant during the ten cycles studied.
- No quasi steady-state was achieved in the cycles studied. The CTOD increased monotonically, and other studied variables and features changed as well for the cycles studied.

The first result, that crack growth actually occurred, is a clear and explicit result and will not as such be further discussed. The results in the second and third item essentially tell us that no kind of quasi-stable situation was achieved for the cycles studied. This is an important point since it is strongly coupled to the interpretation and relevancy of the first listed result. The shape change may nevertheless be of interest by itself. In particular, studies of the shape change that occurs within one cycle, or between maximum and minimum load, may provide a useful overall picture of the deformations to be used in the interpretation of the growth process. Again, however, the relevancy of this kind of studies is somewhat undermined by the fact that no quasi-stable situation has been achieved, and the change in shape from one cycle to the next is relatively large. Therefore, the following discussion will largely be focused on why a quasi-stable situation was not achieved, and when or if it can be expected.

The discussion that follows is divided into two parts. The first part briefly covers whether all features of the shape changes represent "real" features for the model, and not are artifacts from the discretization or the numerical treatment. The second part, consequently, addresses the main problem in detail.

All observed features are believed to represent true features for the model used, and not features introduced by the discretization or numerical treatment. This belief is based on the fact that all changes took place gradually. This is seen in the Figures A.15 and Figures A.16, which show the development of the shape cycle by cycle. The gradual change was also confirmed by studying the change in shape within each cycle.

The formation of the cusp may cause problems when only one element is connected to the tip node. The problem that arises is that this element becomes badly shaped, with one of its interior angles approaching 180° for a true cusp. Only at two occasions in the whole analysis was the shape of the "tip-element" bad enough to cause concern. That was in the last increment of the steps 79 and 85. However, possible errors due to the two occasions when this element became badly shaped should be of minor importance. The shapes obtained were not entirely "catastrophic"; and in any case, possible errors would be localized to the vicinity of the tip. The cusp shape, or strong indications of a cusp shape, can be seen on a larger scale involving many well shaped elements. The possibility that the entire development of the cusp is a numerical artifact exists, but is not deemed likely. The step in which the cusp formed, and the step preceding it in the last cycle were re analyzed using an alternate mesh. No noticeable difference occurred.

No detailed qualitative explanation of the change in shape will be attempted here. The main cause is to be found in changes in the state of the material ahead of the crack tip. The actual processes causing the shape change takes place in the interior of the material where all field variables are intimately coupled. It is therefore difficult to separate causes from effects (which easily results that attempts to explain complicated phenomena becoming circular).

We have already seen and discussed several strong indications that a stabilized, or steady, state has not yet been achieved in the ten cycles studied. In this section, we will discuss why a stabilized state has not been achieved, and to try to identify key events that would lead towards a more stabilized state. In this context, we will assign a characteristic length for each identified event that is indicative of how much the crack must grow before the effects of the related phenomena reaches a steady state. First, however, the meaning of steady-state, both for crack problems in general, but more specifically, as used in this discussion, is discussed and defined.

Steady-state (S-S), is here used in a weak sense. In the context of cracks under SSY, the natural definition of S-S is a state in which all relevant variables and parameters remain constant in time for a fixed position relative the moving crack tip. Such a defi-

nition can never be exactly satisfied for an elastic-plastic material, since the plasticized material in the wake of the crack tip is essentially fixed in space, but the fields ahead of the crack moves essentially with the crack-tip. In practice S-S is usually used in a vague sense, simply referring to a state that does not change noticeable, in a specific region, with time. The actual meaning depends largely on what we mean by "not change" and what our time frame is. When crack closure is present/considered, it may take 100000 cycles or more before a reasonably steady state has been reached. If closure is not considered, 100–200 cycles may be enough to reach a state that does not change noticeable over periods of thousands of subsequent cycles. In this work, we are not interested in that high degree of steady state. Since this investigation is focused on the crack extension process, and the emphasis is qualitative and not quantitative, it may suffice to reach a state that does not change appreciable over, say, ten cycles. We will use the terms "quasi stable" or "quasi steady-state" to emphasize a weakened meaning of S-S.

A possible explanation of the monotonically increasing CTOD can be found by considering the plastic zone above, and left in the wake of, the crack tip. The discussion uses the figures showing $\hat{\varepsilon}^p_{22}$, in Figure A.26, as reference. From these figures, it is clear that a band of material along the crack face, plastically compressed in the 2 direction, is left behind the tip as the tip moves. The width of this band, i.e., its extension above the crack face, is of the order[4] 6. Assume for the purpose of simplifying the following discussion that the only plastic strain component is ε^p_{22}, and that it is constant in the entire band. Then the increase of the CTOD obtained in the analysis can be explained as follows. If the band were isolated from the rest of the structure, or equally, if the band were long compared to its width, it would contract or expand fully in accord with the plastic strain in the band (the elastic strain in this direction is small since the crack face is traction free). However, when the band is connected to the structure, the ends of the band are constrained which affects the deformations in the regions near the ends. In the present case, the extension of the band in the growth direction is small, so the constraint imposed from the surrounding material prevents the band from contracting as much as it would if the band were longer. Consequently, the more the crack grows,

[4]Distances are here as before nondimensionalized according to Eq.6.1

the longer the band becomes, and hence the CTOD should increase. When the length of the band becomes comparable to the height, the imposed constraints from the trailing end of the zone should have only minor influence on the CTOD and the deformations near the tip. This means that, with regard to this phenomenon, a stabilization can be expected after a crack extension of the order 6. Assuming a growth rate of 0.1 per cycle, see Figure A.17, then implies that the order of 60 cycles be required for the effect of this compressive zone to be stabilized.

Based on the same figure, Figure A.26, another effect on a larger "time" scale can be expected. That is when the larger zone, with $\hat{\varepsilon}_{22} > 0$ and partly located above the previously discussed compressive zone, is left sufficiently far behind the tip. For the purpose of the following discussion, we use "zone" to refer to the upper parts of the region that has normalized plastic strain levels between 1 and 3 (the contour curves 4 and 5, respectively). The left edge of this region remains essentially unchanged for the cycles studied, which can be seen in Figures A.25 and A.26. Hence, this edge is left behind the crack tip as the crack extends. It should be mentioned that an analogous zone for lower strain levels becomes much larger. It is clear from the figures that this zone initially had its center ahead of the tip. Therefore, to become "sufficiently" left behind the tip, the crack must first grow a distance comparable to the zone's initial location ahead of the tip. Then, as before, it is reasonable to assume that the crack has to leave the zone a distance behind the tip of the same order as the distance from the crack to a characteristic center of the zone, before a stabilized condition can be expected. Thus, on basis of the figures, it seems reasonable to chose 15-20 as a characteristic crack extension required for the effects of this zone, to become stabilized. In terms of cycles, this would mean 150-200 cycles. The same result is obtained if we simply require that the whole initial plastic zone be left in the wake of the tip, compare Figure A.21.

The zones discussed above can also be interpreted as the sources of closure. Obviously, the zones counteract. The compressive zone, which dominates during the first cycles, tends to open the crack. After more cycles, the influence of the larger zone progressively comes into play, resulting in the net effect that the crack closes. From the figures, it is seen that the strain levels in the compressive zone are higher than they are

in the expansive zone. However, the expansive zone is much larger, so that the integrated effect in terms of displacements in the opening direction becomes larger. This has been confirmed by rough strain-space integration based on strain data taken from contour plots. In the context of closure, it should be mention that at no time during the analysis did the crack face reach the symmetry plane, or even enter the space occupied by the initial slit.

Other phenomena which may relate to quasi-stabilization are to be found ahead the crack. These are not believed to be of primary importance for the CTOD, but may be important for the shape of the crack front. No discussion based on physical arguments, as the ones above, is attempted here. Instead, two events are identified, both related to the inactive zone. The first event, when some kind of stabilization can be expected, is when the crack extends to the trailing edge of the original (first cycle) inactive region. The second event is when the crack extends to the center of the original inactive region. These two events correspond to the characteristic distances 2.5 and 5, respectively; and in terms of cycles, 25 and 50, respectively.

For the purpose of studying growth mechanisms, a very weak definition of S-S may be sufficient. The variations of the conditions near the crack tip are unlikely to be greatly affected by the expansive plastic zone as it is located comparatively far above the crack tip and the strain levels are comparatively small. Therefore, the quasi-steady state near the crack tip will be reached much earlier than the 150–200 cycles needed for this plastic zone to reach a quasi-steady state. On basis of the above estimates, only 25–60 cycles would be needed.

Chapter 7

CONCLUSIONS AND RECOMMENDATIONS

This chapter consists of two short sections. In the first section the questions posed in the beginning of the work, see section 1.1, are recapitulated and discussed one the basis of the results obtained. In the second section, some suggestions for further research are given.

7.1 The Basic Questions

- The first fundamental question: Is it possible to capture crack growth using a purely continuum approach ?

  The answer to this question must, on basis of the results presented in this thesis, definitely be yes. A finite growth increment of the crack was clearly obtained for each of the cycles studied. No kind of steady state was obtained, but, it seems highly unlikely that the crack would entirely stop growing after more cycles.

- The second fundamental question: Do these results support any in particular of the growth mechanism discussed in Section 2.6 ?

  As was concluded in the presentation and discussion of different proposed growth mechanisms in section 2.6, Laird's model and the Tomkins & Biggs model seem to be most suitable for the present situation. That is, however, not surprising since they are the models that are most closely related to a continuum description,

which is what this study is based on. It is possible to find features in the results that are characteristic of each of the two models. The overall deformation pattern definitely supports Laird's model. However, actual buckling of the crack surfaces, as Laird suggested, was not observed. On the other hand, the development of the "corner" and the concave shape of the crack face are certainly related features. A characteristic of the Tomkins & Biggs model is the sharp small crack in the center of the main crack's front. In this analysis, the cusp shape obtained at the end of the last cycles corresponds locally to a sharp small crack. In the model the sharp crack was explained as arising from a brittle fracture mechanism. Here, in the analysis the cause is presumably plastic instability.

- The third fundamental question: Is it important to model the constitutive response in detail, eg. with hardening ?

  It is of course not possible to give a direct and explicit answer to this question since only one constitutive model was used. On basis of the results, it does not seem necessary to use more refined constitutive relations to capture the main characteristics of the process considered. Use of more involved constitutive models is unmotivated until the potential of the simples model has been better explored.

- The fourth fundamental question: Is it possible to explain an exponent different than two in a Paris-type growth relation ?

  This analysis did not address this problem specifically. We saw in section 2.6.2 that an exponent 2 is dictated by dimensional considerations for a sharp crack in an elastic-plastic material. In this analysis, this dimensional restraint is relived since the crack is modeled as a slit of finite width, which introduces a new characteristic length. For a rigid-plastic material, the slit width appears as an additive term in the expression for the CTOD, which was shown analytically by Rice & Johnson[69]. On basis of these facts, it is believed that an exponent different than two is unlikely as long as the material is modeled as elastic-perfectly plastic. However, analyses for different load levels would provide a more definite answer to this question. Because only one load level was used, it is not possible to confirm the exponent 2.

The first question, which was the main focus of this work, was answered in the affirmative. The second question was also answered partially, considering that the growth mechanisms proposed are only conceptual. The last two questions would have required comparative analyses for different constitutive models and for different load levels as a base for their assessment. Such analysis were outside the scope of this program as performed.

To what extent a link has been established between the kinematics of the near tip deformations, and empirical growth laws, is yet another diffuse question to which a definite answer is not possible. It is, nevertheless, the author's opinion that the fact that crack growth actually was obtained using a purely continuum approach, as such, constitutes a link between the near tip kinematics and the empirical growth laws.

The fact that a continuous, from cycle to cycle, extension of the crack was obtained must be considered as the main result of this work. This result should motivate further exploration of the approach used in this work.

7.2 Suggestions for Further Research

The most obvious continuation would be to perform an analysis, or to continue this analysis, to a few more cycles. It may suffice with of the order 10 more cycles to get a better picture regarding the changing shape of the crack front.

More extended analyses than of the above mentioned order are not recommended before some other aspects have been investigated. Some of these aspects are:

- Dependency of initial slit width.
- Dependency of load level.
- Mesh dependency/sensitivity.

which are easily addressed by making a few comparative analyses.

If ABAQUS is to be used, alternative rezoning methods should be considered. Since only a part of the model is re-meshed, it is unnecessary to perform the extrapolations and mapping operations involved in the rezoning on the whole mesh. Local rezoning would also eliminate the pollution problem, although this is more an annoyance than a problem, if the rezoned region is confined within the plastic zone. The rezoning option, as currently implemented in ABAQUS, does not allow selective rezoning at present. In addition, the rezoning operations were seemingly unrealistically expensive in terms of required CPU-time. For the analysis steps that involved rezoning, the rezoning took twice as long as the actual solution. Therefore, independently of what code that shall be used, it is essential to develop and implement efficient rezoning algorithms if they are not already present.

Bibliography

[1] ABAQUS. *Reference Manuals.* Hibbit, Karlsson and Sorensen Inc., 100 Medway Street,Providence,RI 02906-4402.

[2] R.C. Bates and W.G. Clark. Fractography and fracture mechanics. *Transactions of the American Society for Metals*, 62:380–389, 1969.

[3] K.J. Bathe and A.P. Cimento. Some practical procedures for the solution of nonlinear finite element equations. *Computer Methods in Applied Mechanics and Engineering*, 22:59–85, 1980.

[4] C.J. Beevers, R.J. Cooke, J.F. Knott, and R.O. Ritchie. Some considerations of the influence of sub-critical cleavage growth during fatigue-crack propagation in steel. *Metal Science*, 9:119, 1975.

[5] C. Betegón and J.W. Hancock. Two parameter characterization of elastic-plastic crack tip fields. *ASME: Journal of Applied Mechanics*, 58(1):104–110, March 1991.

[6] C.H.R. Boller and T. Seeger. *Materials Data for Cyclic Loading: Part D: Aluminium and Titanium Alloys.* Elsevier, 1987. (Materials Science Monographs, 42D).

[7] C.Q. Bowles and D. Broek. On the formation on fatigue striations. *International Journal of Fracture Mechanics*, 8(1):75–85, 1972.

[8] D. Broek. A critical note on electron fractography. *Engineering Fracture Mechanics*, 1:691–695, 1970.

[9] B. Budiansky and J.W. Hutchinson. Analysis of closure in fatigue crack growth. *ASME: Journal of Applied Mechanics*, 45:267–276, September 1978.

[10] J.L. Chaboche. Time-dependent constitutive theories for cyclic plasticity. *International Journal of Plasticity*, 2(2):149–189, 1986.

[11] L.F. Coffin, Jr. and J.F. Tavernelli. The cyclic straining and fatigue of metals. *Transactions of the Metallurgical Society of AIME*, 215:794–807, October 1959.

[12] Y.F. Dafalias. The plastic spin. *ASME: Journal of Applied Mechanics*, 52:865–871, 1985.

[13] Y.F. Dafalias and E.P. Popov. Plastic internal variables formalism of cyclic plasticity. *ASME: Journal of Applied Mechanics*, 98:645–651, 1976.

[14] A.U. De Koning and G. Liefting. Criteria for determination of significant load cycles in variable amplitude load sequences. In *International Symposium on Fatigue Crack Closure*, Charlestown, May 1986. ASTM.

[15] H.D. Dill and C.R. Saff. Spectrum crack growth prediction method based on crack surface displacement and contact analysis. In *ASTM STP 595*, pages 306–319, 1976.

[16] D.S. Dugdale. Stress-strain cycles of large amplitude. *Journal of the Mechanics and Physics of Solids*, 7:135–142, 1958.

[17] W. Elber. The significance of crack closure. In *ASTM STP 486*, pages 230–242, 1971.

[18] R.G. Forman, V.E. Kearney, and R.M. Engle. Numerical analysis of crack propagation in cyclic-loaded structures. *Journal of Basic Engineering*, 89:459–464, 1967.

[19] H. Führing. Practical application of a model for fatigue damage with irregular cyclic loading. In *Proceedings of the 5th International Conference on Fracture, ICF5*, volume 4, pages 1823–1832, Cannes, 1981.

[20] H. Führing and T. Seeger. Dugdale crack closure analysis of fatigue cracks under constant amplitude loading. *Engineering Fracture Mechanics*, 11:99–122, 1979.

[21] H. Führing and T. Seeger. Structural memory of cracked components under irregular loading. In *ASTM STP 677*, pages 144–167, 1979.

[22] G.G. Garret and J.F. Knott. Crystallographic fatue crack growth in aluminium alloys. *Acta Metallurgica*, 23:841–848, July 1975.

[23] G.G. Garret and J.F. Knott. On the influence of cyclic hardening and crack opening displacement (cod) on crack advance during fatigue. *Metallurgical Transactions*, 7A:884–887, June 1976.

[24] Gelin.J.C. and P. Picart. Use of quasi-newton methods for large strain elastic-plastic finite element computations. *Communications in Applied Numerical Methods*, 4:457–469, 1988.

[25] A.A. Griffth. The phenomenon of rupture and flow in solids. *Philosophical Transactions of the Royal Society of London, series.A*, A221:163–197, 1921.

[26] A.K. Head. The propagation of fatigue cracks. *ASME: Journal of Applied Mechanics*, 23:407–, September 1956.

[27] P.C. Hertzberg, R.W. & Paris. Application of electron fractography and fracture mechanics to fatigue crack propagation. In *Proceedings of the First International Conference on Fracture, ICF1*, volume 1, pages 459–479, Japan, 1965.

[28] R. Hill. *The Mathematical Theory of Plasticity.* Oxford University Press, London, 1950.

[29] T.J.R. Hughes. Numerical implementation of constitutive models: Rate-independent deviatoric plasticity. In S. Nemat-Nasser, R.J. Asaro, et al., editors, *Theoretical Foundation for Large Scale Computations for Non Linear Material Behavior*, pages 29–63. Martinus Nijhoff Pubishers, 1984.

[30] T.J.R. Hughes and J. Winget. Finite rotation effects in numerical integration of rate constitutive equations arising in large deformation analysis. *International Journal for Numerical Methods in Engineering*, 15:1862–1867, 1980.

[31] S. Im and S.N. Atluri. A study of two finite strain plasticity models: An internal time theory using mandel's director concept, and a general isotropic/kinematic-hardening theory. *International Journal of Plasticity*, 3:163–191, 1987.

[32] G.R. Irwin. Fracture dynamics. In *Fracturing of Metals: ASM-29th National Metal Congress and Exposition, Chicago*, pages 147–166, 1948.

[33] G.R. Irwin. Analysis of stess and strain near the end of crack traversing a plate. *ASME: Journal of Applied Mechanics*, 24:361–364, 1957.

[34] G.C. Johnson and D.J. Bammann. A discussion of stress rates in finite deformation problems. Technical Report SAND-82-8821, Sandia National Laboratories, Alburquerque, Mexico, 1982.

[35] M.L. Kanninen and C.H. Popelar. *Advanced Fracture Mechanics.* Oxford University Press, New York, 1985.

[36] A.S. Kuo and H.W. Liu. An analysis of unzipping model for fatigue crack growth. *Scripta Metallurgica*, 10:723–728, 1976.

[37] C. Laird. The influence of metallurgical structure on the mechanisms of fatigue crack propagation. In *ASTM STP 415*, pages 131–168, Philadelphia, 1967.

[38] C. Laird and R. De La Veaux. Additional evidence for the plastic blunting process of fatigue crack propagation. *Metallurgical Transactions A*, 8A:657–664, April 1977.

[39] S.G. Larsson and A.J. Carlsson. Influence of non-singular stress terms and specimen geometry on small-scale yielding at crack tips in elastic-plastic material. *Journal of the Mechanics and Physics of Solids*, 21:263–278, 1973.

[40] E.H. Lee. Elastic-plastic deformation at finite strain. *ASME: Journal of Applied Mechanics*, 36:1–6, 1969.

[41] H.W. Liu. Crack propagation in thin metal sheet under repeated loading. *ASME: Journal of Basic Engineering*, 83(1):23–31, 1961.

[42] H.W. Liu. Fatigue crack propagation and applied stress range–an energy approach. *ASME: Journal of Basic Engineering*, 85(1):116–122, 1963.

[43] J. Lubliner. *Plasticity Theory.* Macmillian Publishing Company, New York, 1990.

[44] F.A. McClintock. *On the Plasticity of the Growth of Fatigue Cracks.* John Wiley & Sons Inc., New York, 1963.

[45] F.A. McClintock. Plasticity aspects of fracture. In *Fracture: An Advanced Treatise*, volume 3, pages 47–225. Academic Press, New York, 1971.

[46] A.J. McEvily, Jr., R.C. Boettner, and T.L. Johnston. On the formation and growth of fatigue cracks in polymers. In *Fatigue-An Interdiciplinary Approach; Proceedings of the 10th Sagamore Army Materials Research Conference,New York,1963*, pages 95–103. Syracuse University Press, 1964.

[47] R.M. Mcmeeking. Finite deformation analysis of crack-tip opening in elastic-plastic materials and implications for fracture. *Journal of the Mechanics and Physics of Solids*, 25:357–381, 1977.

[48] R.M. McMeeking. Numerical calculation for problems of ductile fracture. In *International Conference Advances in Fracture Research: Proceedings of the 7th International Conference on Fracture, ICF7*, volume 3, pages 1971–1999, Houston, Texas, 1989.

[49] R.M. McMeeking and J.R. Rice. Finite-element formulations for problems of large elastic-plastic deformation. *International Journal for Solids and Structures*, 11:601–617, 1975.

[50] J.C. McMillan and R.M.N. Pelloux. Fatigue crack propagation under program and random loads. In *ASTM STP 415*, pages 505–532, 1967.

[51] D.A. Meyn. The nature of fatigue-crack propagation in air and vacuum for 2024 aluminum. *Transactions of the American Society for Metals*, 61:52–61, 1968.

[52] D.A. Meyn. Observations on micromechanisms of fatigue-crack propagation in 2024 aluminum. *Transactions of the American Society for Metals*, 61:42–51, 1968.

[53] Z. Mroz. On the description of anisotropic work-hardening. *Journal of the Mechanics and Physics of Solids*, 15:163–, 1967.

[54] J.C. Nagtegaal and J.E. De Jong. Some aspects of non-isotropic workhardening in finite strain plasticity. In *Proceedings of the Workshop on Plasticity of Metals at Finite Strain: Theory, Experiment and Computation*, Stanford University, Stanford, California, 1981.

[55] J.C. Nagtegaal, D.M. Parks, and J.R. Rice. On numerically accurate finite element solutions in the fully plastic range. *Computer Methods in Applied Mechanics and Engineering*, 4:153–177, 1974.

[56] P. Neumann. Course slip model of fatigue. *Acta Metallurgica*, 17:1219–1225, September 1969.

[57] P. Neumann. Modelling of changes in dislocation structure in cyclically deformed crystals. In *Constitutive Equations in Plasticity*, pages 251–326, Cambridge, Massachusetts, 1974. MIT Press.

[58] J.C. Newman, Jr. Prediction of fatigue crack growth under variable amplitude and spectrum loading using a closure model. In *ASTM STP 761*, pages 255–277, 1982.

[59] E. Orowan. Fracture and strength of solids. volume XII, pages 185–232. The Royal Society, London, 1949.

[60] P.C. Paris. Twenty years of reflection on questions involving fatigue crack growth. part i: historical observations and perspectives. In J. Bäcklund, A.F. Blom, and C.J. Beevers, editors, *Fatigue Thresholds*, volume 1, pages 3–10, Stockholm, 1982.

[61] P.C. Paris, M. Gomez, and W.E. Anderson. A rational analytic theory of fatigue. *Trend in Engineering*, 13(1):1219–1225, September 1961.

[62] D.M. Parks. Elastic-plastic continuum mechanics of fatigue crack growth. Technical Report AFOSR-77-3424, Department of Engineering and Applied Science, Yale University, 1978.

[63] D.M. Parks. In *European Group on Fracture: Proceedings from a symposium held in Freiburg, October,1989 (Not yet Published)*, 1992 ?

[64] R.M.N. Pelloux. Corrosion-fatigue crack propagation. In *Fracture 1969: Proceedings of the Second International Conference on Fracture,Brighton, April,1969*, pages 731–745. Chapman and Hall LTD, London, 1969.

[65] R.M.N. Pelloux. Mechanisms of formation of ductile fatigue striations. *Transactions of the American Society for Metals*, 62:281–285, 1969.

[66] R.M.N. Pelloux. Crack extension by alternating shear. *Engineering Fracture Mechanics*, 1:697–704, 1970.

[67] K.W. Reed and S.N. Atluri. Constitutive modeling and computational implementation for finite strain plasticity. *International Journal of Plasticity*, 1:63–87, 1985.

[68] J.R. Rice. Mechanics of crack tip deformation and extension by fatigue. In *ASTM STP 415*, pages 247–311, Philadelphia, 1967.

[69] J.R. Rice and M.A. Johnson. The role of large crack tip geometry changes in plane strain fracture. In *Inelastic Behavior of Solids*, pages 641–672, New York, 1970. McGraw-Hill.

[70] J.R. Rice and E.P. Sorensen. Continuing crack-tip deformation and fracture for plane-strain crack growth in elastic plastic solids. *Journal of the Mechanics and Physics of Solids*, 26:163–186, June 1978.

[71] D.L. Ritter and R.P. Wei. Fractographic observarions of ti-6al-4v alloy fatigued in vacuum. *Metallurgical Transactions*, 2:3229–3230, November 1971.

[72] R. Rubenstein and S.N. Atluri. Objectivity of incremental constitutive relations over finite time steps in computational finite deformation analysis. *Computer Methods in Applied Mechanics and Engineering*, 36:277–290, 1983.

[73] A. Saxena, S.J. Hudak, Jr., and G.M. Jouris. A three component model for representing wide range fatigue crack growth data. *Engineering Fracture Mechanics*, 12:103–115, 1979.

[74] J. Schijve. Analysis of the fatigue phenomenon in aluminum alloys. Technical Report NLR-TR-M2122, National Aero and Astronautical Research Institute, Amsterdam, April 1964.

[75] J.C. Simo and R.L. Taylor. Consistent tangent operators for rate-independent elastoplasticity. *Computer Methods in Applied Mechanics and Engineering*, 48:101–118, 1985.

[76] E.P. Sorensen. A numerical investigation of plane strain stable crack growth under small-scale yielding conditions. In *Elastic-Plastic Fracture, ASTM STP 668*, pages 151–174, 1977.

[77] S. Suresh. *Fatigue of materials.* Cambridge University Press, New York, 1991.

[78] B. Tomkins and W.D. Biggs. Low endurance fatigue in metals and polymers. Part 3: The mechanisms of failure. *Journal of Materials Science*, 4(6):544–553, 1969.

[79] D.M. Tracey. Finite element solutions for crack-tip behavior in small scale yielding. *Journal of Engineering Materials and Technology*, 98:146–151, April 1976.

[80] K.C. Valanis. A theory of viscoplasticity without a yieldsurface. part 1: General theory. *Archives of Mechanics*, 23:517–533, 1971.

[81] K.C. Valanis. Fundamental consequences of a new intrinsic time measure plasticity as a limit of the endochronic theory. *Archives of Mechanics*, 32:171–191, 1980.

[82] Wang. A new representation theorem for isotropic functions: An answer to professor g.f. smith's criticism of my papers on representations for isotropic functions. *Arch. Rational Mech. Anal.*, 36:167–223, 1970.

[83] G.S. Wang and A.F. Blom. A strip model for fatigue crack growth predictions under general load conditions. *Engineering Fracture Mechanics*, 40:507–533, 1991.

[84] R.J.H. Wanhill. Fractography of fatigue crack propagation in 2024-t3 and 7075-t6 aluminum alloys in air and vacuum. *Metallurgical Transactions A*, 6A:1587–1596, August 1975.

[85] C.M. Ward-Close, A.F. Blom, and R.O. Ritchie. Mechanisms associated with transient fatigue crack growth under variable amplitude loading: An experimental and numerical study. *Engineering Fracture Mechanics*, 32(4):613–638, 1989.

[86] O. Watanabe and S.N. Atluri. A new endochronic approach to computational elasto-plasticity: Example of a cyclically loaded cracked plate. *ASME Journal of Applied Mechanics*, 52:857–864, 1985.

[87] G.G. Weber, A.M. Lush, A. Zavalianglos, and L. Anand. An objective time-integration procedure for isotropic rate-independent and rate-dependent elastic-plastic constitutive equations. *International Journal of Plasticity*, 6:701–744, 1990.

[88] H.M. Westgaard. Bearing pressure and cracks. *ASME: Journal of Applied Mechanics*, 61:A49–A53, 1939.

[89] M.L. Williams. On the stress distribution at the base of a stationary crack. *ASME: Journal of Applied Mechanics*, 24:109–114, 1957.

Tables

Analysis history

Cycle number	*Global step*	*Rel. load range*	*Restart from*		*Results in*		*comments*
			step	*inc.*	*step*	*inc.*	
1	1	0.00 – 0.38	–	–	1	27	Start with virgin mtrl.
1	2	0.38 – 0.54	1	27	1	12	
1	3	0.54 – 0.66	1	12	1	9	
1	4	0.66 – 0.80	1	9	1	9	
1	5	0.80 – 0.91	1	9	1	8	
1	6	0.91 – 1.00	1	8	1	6	Model modified. Fully loaded
1	7	1.00 – 0.85	1	6	1	6	
1	8	0.85 – 0.66	1	6	1	6	
1	9	0.66 – 0.33	1	6	1	6	
1	10	0.33 – 0.15	1	6	1	6	
1	11	0.15 – 0.00	1	6	1	6	Unloaded.
2	12	0.00 – 0.15	1	6	2	6	No rezoning
2	13	0.15 – 0.33	2	6	1	6	
2	14	0.33 – 0.75	1	6	1	14	
2	15	0.75 – 1.00	1	14	1	12	Fully loaded
2	16	1.00 – 0.75	1	12	2	6	No rezoning
2	17	0.75 – 0.33	2	6	1	6	
2	18	0.33 – 0.20	1	6	2	6	No rezoning
2	19	0.20 – 0.00	2	6	1	8	Unloaded
3	20	0.00 – 0.20	1	8	2	6	No rezoning
3	21	0.20 – 0.50	2	6	3	6	No rezoning
3	22	0.50 – 0.80	3	6	1	6	
3	23	0.80 – 1.00	1	6	1	8	Fully loaded
3	24	1.00 – 0.80	1	8	2	6	No rezoning
3	25	0.80 – 0.50	2	6	1	6	
3	26	0.50 – 0.30	1	6	2	6	No rezoning
3	27	0.30 – 0.15	2	6	1	4	
3	28	0.15 – 0.00	1	4	1	4	Unloaded
4	29	0.00 – 0.15	1	4	2	6	No rezoning
4	30	0.15 – 0.30	2	6	3	4	No rezoning
4	31	0.30 – 0.50	3	4	4	4	No rezoning
4	32	0.50 – 0.80	4	4	1	7	
4	33	0.80 – 1.00	1	7	1	4	Fully loaded
4	34	1.00 – 0.80	1	4	2	4	No rezoning
4	35	0.80 – 0.40	2	4	1	4	
4	36	0.40 – 0.20	1	4	2	4	No rezoning
4	37	0.20 – 0.00	2	4	1	4	Unloaded
4	38	0.00 – 0.20	1	4	2	4	No rezoning
5	39	0.20 – 0.40	2	4	3	4	No rezoning
5	40	0.40 – 0.60	3	4	4	4	No rezoning
5	41	0.60 – 0.85	4	4	1	7	
5	42	0.85 – 1.00	1	7	1	4	Fully loaded

Table A.1: Table showing a brief analysis history: Analysis step 1–42

Cycle number	*Global step*	*Rel. load range*	*Restart from*		*Results in*		*comments*
			step	*inc.*	*step*	*inc.*	
5	43	1.00 – 0.85	1	4	2	4	No rezoning
5	44	0.85 – 0.60	2	4	3	4	No rezoning
5	45	0.60 – 0.40	3	4	1	4	
5	46	0.40 – 0.20	1	4	2	4	No rezoning
5	47	0.20 – 0.00	2	4	1	4	Unloaded
6	48	0.00 – 0.20	1	4	2	4	No rezoning
6	49	0.20 – 0.40	2	4	3	4	No rezoning
6	50	0.40 – 0.60	3	4	4	4	No rezoning
6	51	0.60 – 0.85	4	4	1	9	
6	52	0.85 – 1.00	1	9	1	4	Fully loaded
6	53	1.00 – 0.85	1	4	2	4	No rezoning
6	54	0.85 – 0.60	2	4	3	4	No rezoning
6	55	0.60 – 0.40	3	4	1	4	
6	56	0.40 – 0.20	1	4	2	4	No rezoning
6	57	0.20 – 0.00	2	4	1	5	Unloaded
7	58	0.00 – 0.20	1	5	2	4	No rezoning
7	59	0.20 – 0.40	2	4	3	4	No rezoning
7	60	0.40 – 0.60	3	4	4	5	No rezoning
7	61	0.60 – 0.85	4	5	1	10	
7	62	0.85 – 1.00	1	10	1	5	Fully loaded
7	63	1.00 – 0.85	1	5	2	4	No rezoning
7	64	0.85 – 0.60	2	4	3	4	No rezoning
7	65	0.60 – 0.40	3	4	1	4	
7	66	0.40 – 0.20	1	4	2	4	No rezoning
7	67	0.20 – 0.00	2	4	1	5	Unloaded
8	68	0.00 – 0.60	1	5	2	11	No rezoning
8	69	0.60 – 0.85	2	11	1	7	
8	70	0.85 – 1.00	1	7	1	4	Fully loaded
8	71	1.00 – 0.60	1	4	2	6	No rezoning
8	72	0.60 – 0.20	2	6	1	5	
8	73	0.20 – 0.00	1	5	1	5	Unloaded
9	74	0.00 – 0.60	1	5	2	12	No rezoning
9	75	0.60 – 0.85	2	12	1	7	
9	76	0.85 – 1.00	1	7	1	5	Fully loaded
9	77	1.00 – 0.60	1	5	2	6	No rezoning
9	78	0.60 – 0.20	2	6	1	7	
9	79	0.20 – 0.00	1	7	1	4	Unloaded
10	80	0.00 – 0.60	1	4	2	9	No rezoning
10	81	0.60 – 0.85	2	9	1	7	
10	82	0.85 – 1.00	1	7	1	7	Fully loaded
10	83	1.00 – 0.60	1	7	2	4	No rezoning
10	84	0.60 – 0.20	2	4	1	7	
10	85	0.20 – 0.00	1	7	1	5	Unloaded

Table A.2: Table showing a brief analysis history: Analysis step 42–85

Figures

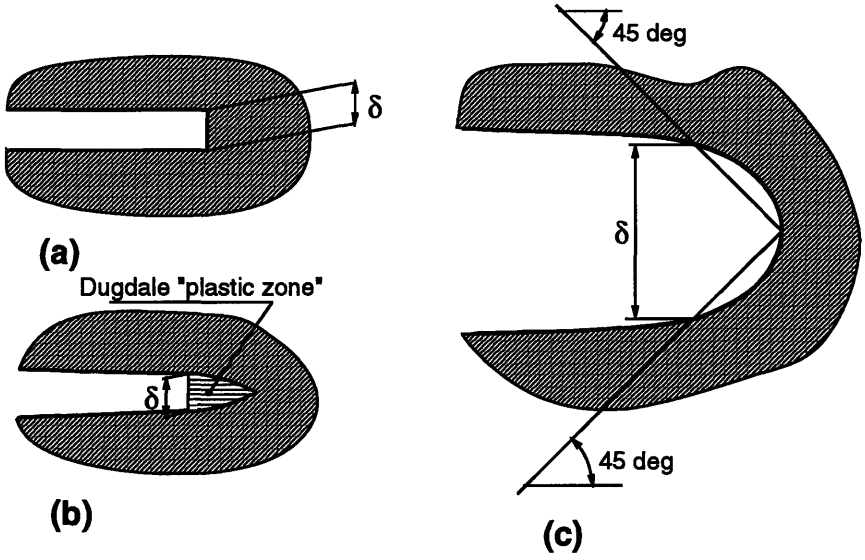

Figure A.1: Definiton of crack-tip-opening-displacement (CTOD): (a)–For crack tip with two corners; (b)–for the Dugdale model; and (c), the definition that is used in this work

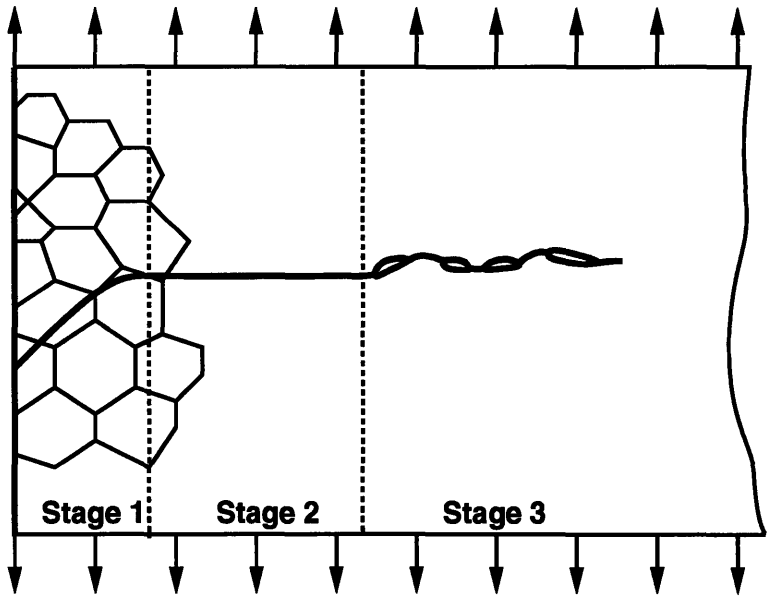

Figure A.2: Schematic representation of the three regimes of crack growth.

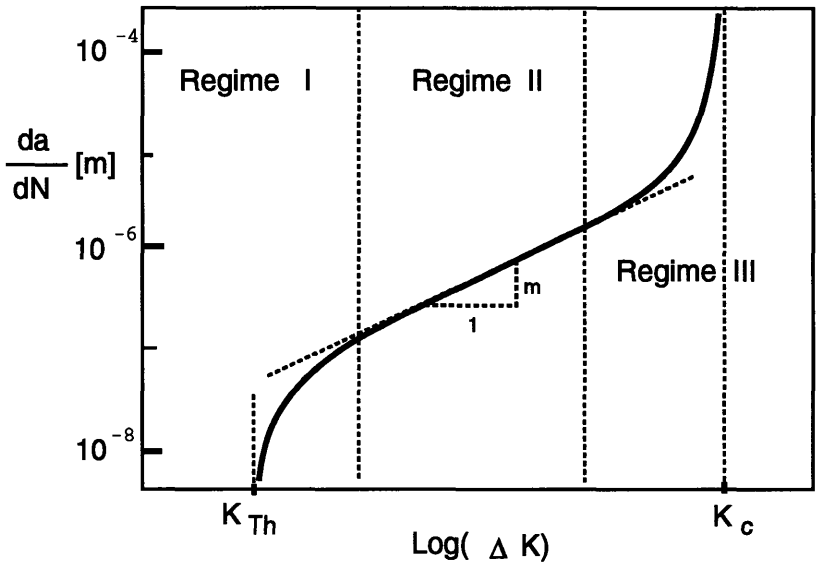

Figure A.3: Schematic $\frac{da}{dN}$ v.s. ΔK curve [4]. The curve shows the typical sigmodial shape. K_{th} is the threshold stress intensity factor below which no growth occur, and K_c is the critical stress intensity factor corresponding to static fracture.

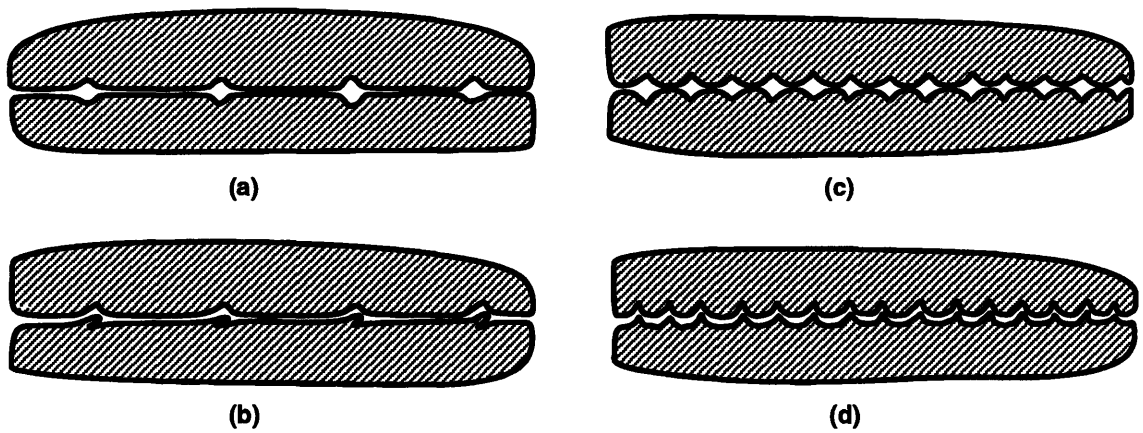

Figure A.4: Four principally different striation morphologies, Laird [37]

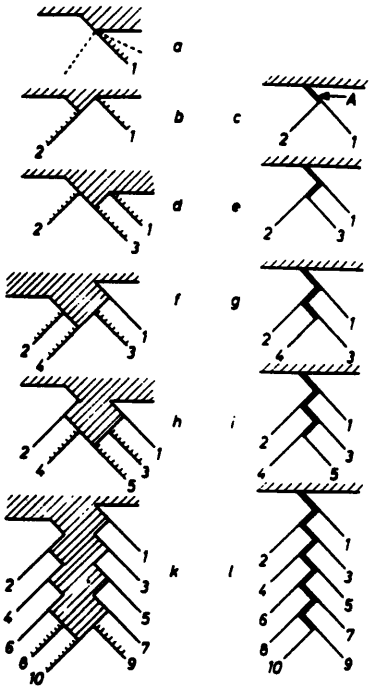

Figure A.5: The coarse slip model[56] (Unzipping model)

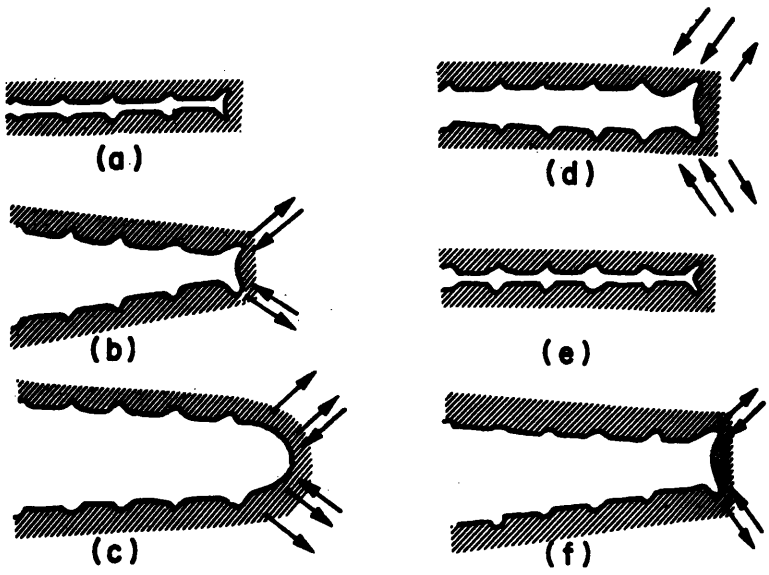

Figure A.6: The plastic blunting process (PBP) model[37]

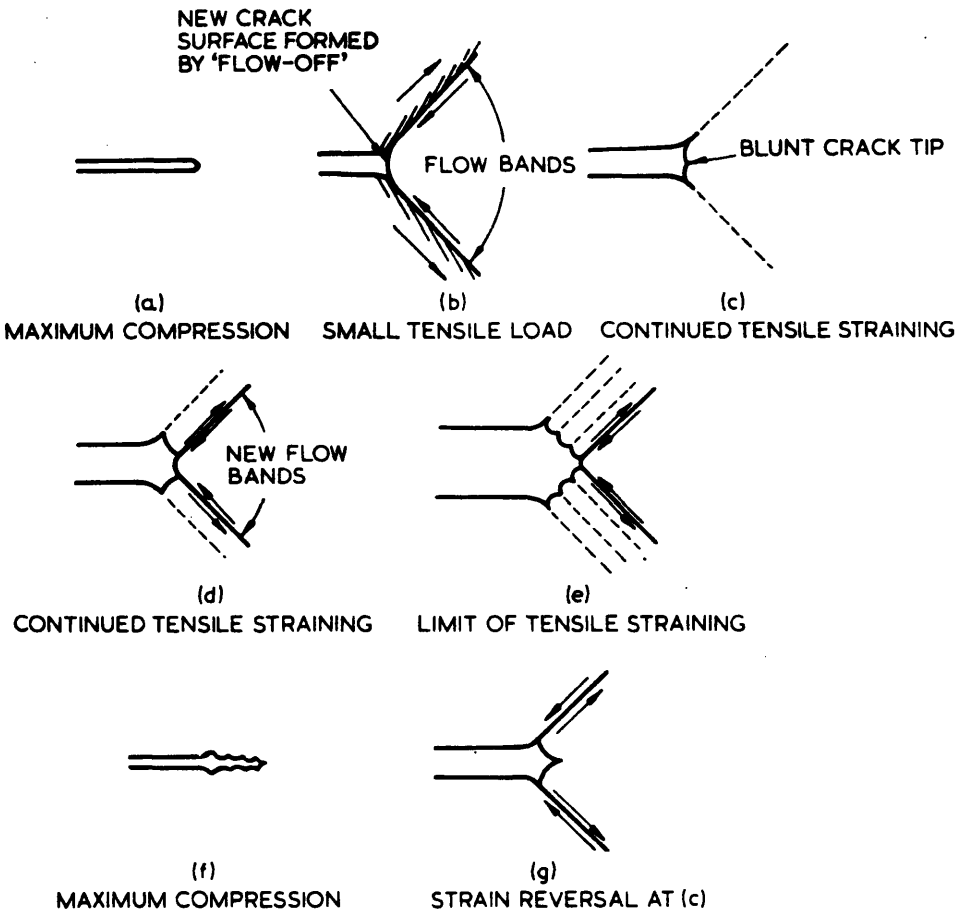

Figure A.7: The model by Tomkins & Biggs[78]

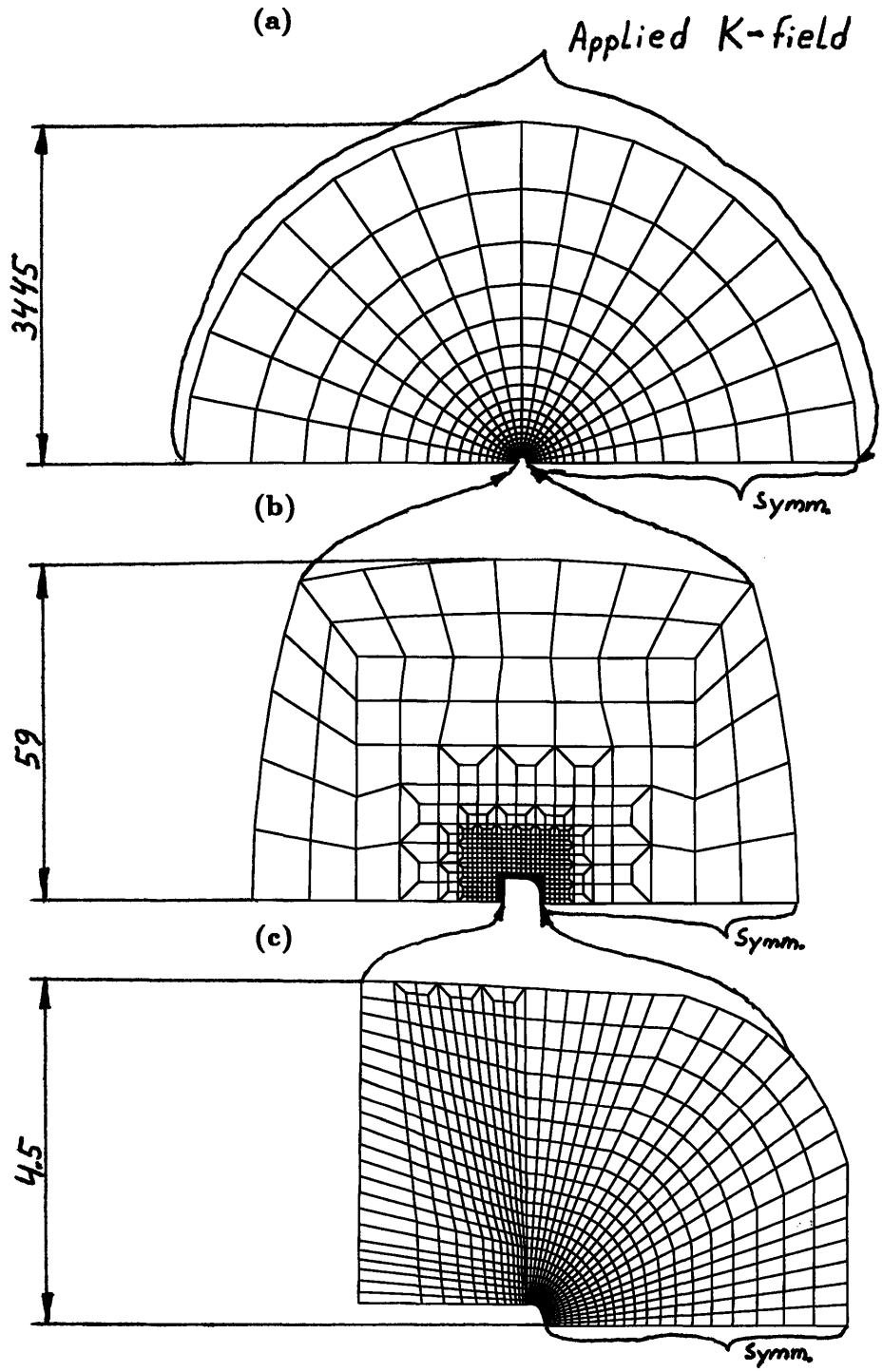

Figure A.8: Discretization,loads and boundary conditions: (a) and (b) – outer, fixed region; (c) inner region from preprocessor; The indicated dimensions are non dimensionalized by division by $\frac{K^2}{E\sigma_y}$, where for comparison $\frac{1}{2}\delta_{max.load} \approx \frac{1}{3}$ and the inital half width of the slit 0.0251. The K-field is imposed through prescribed displacements according to Eqs. 4.1 and 4.2, and the indicated symmetry condition is given by u_y=0.

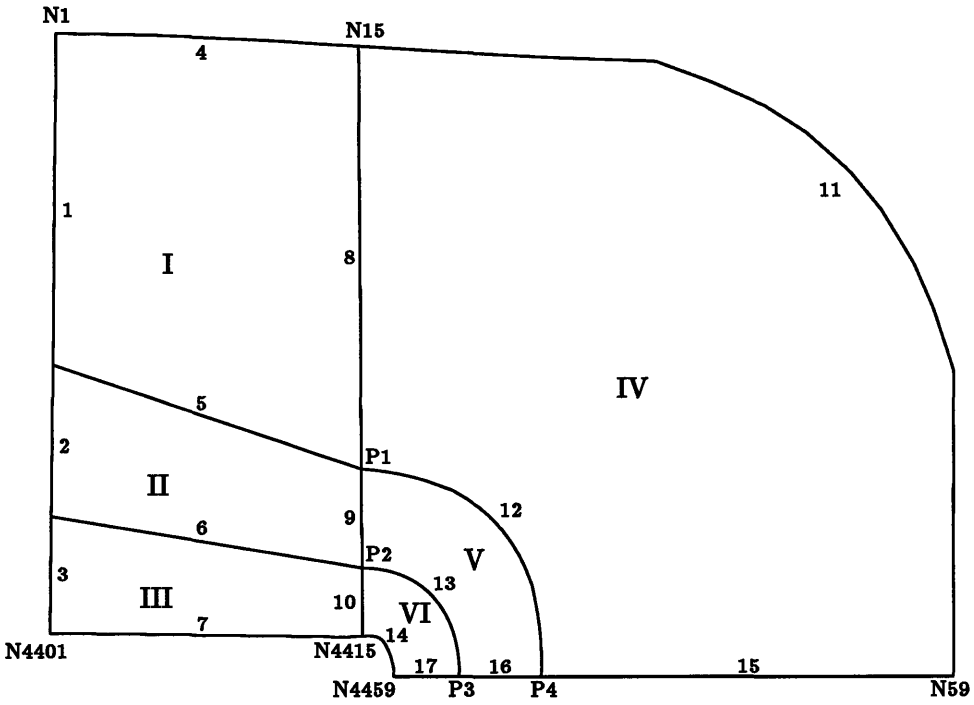

Figure A.9: Inner region: Subregions I-VI, contol curves 1-17

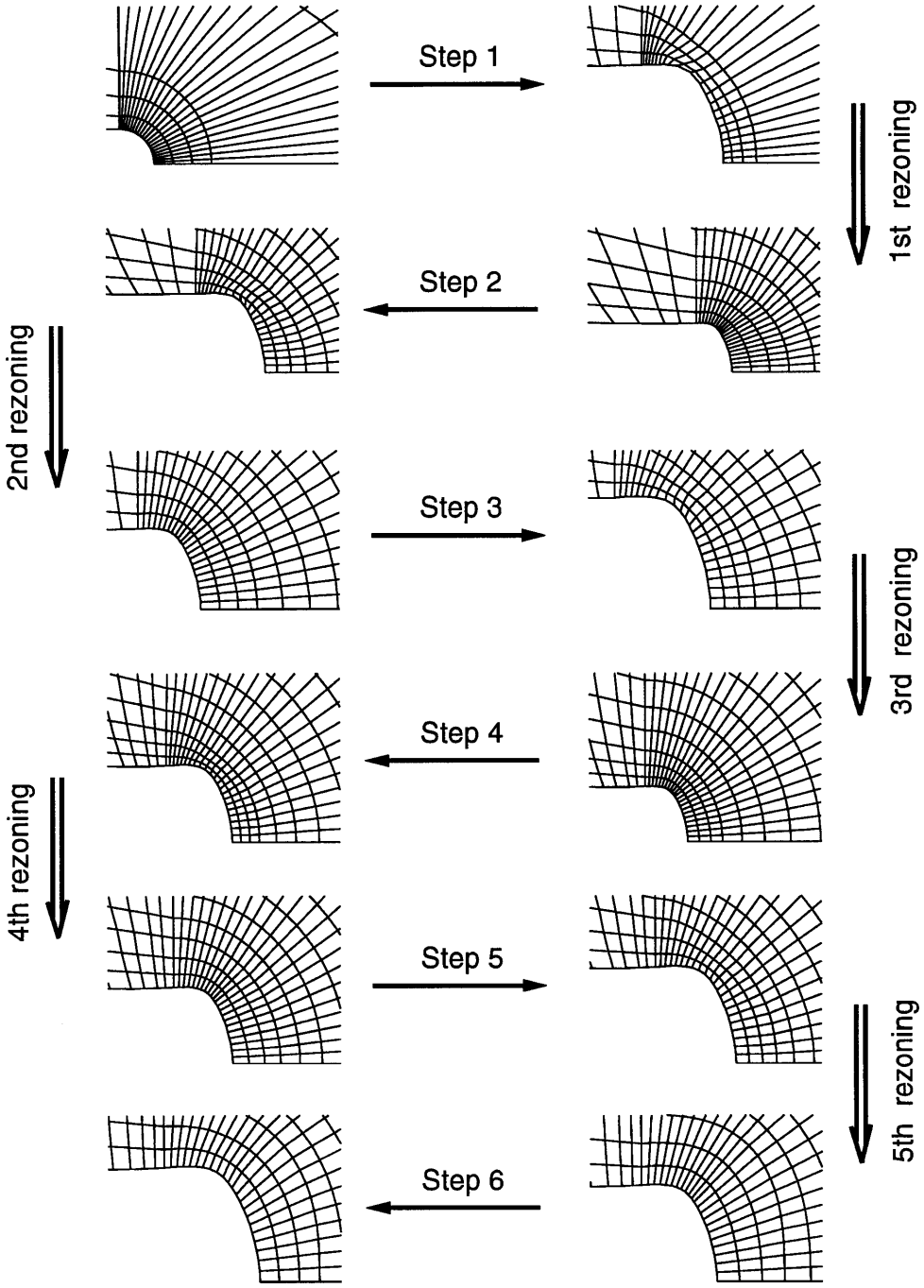

Figure A.10: Figure showing the mesh at the begining and end of each step during the first half cycle. As is indicated, rezoning was done after each step. The shape of the crack tip is the same at both ends of a rezoning arrow, but the scaling differs between the steps.

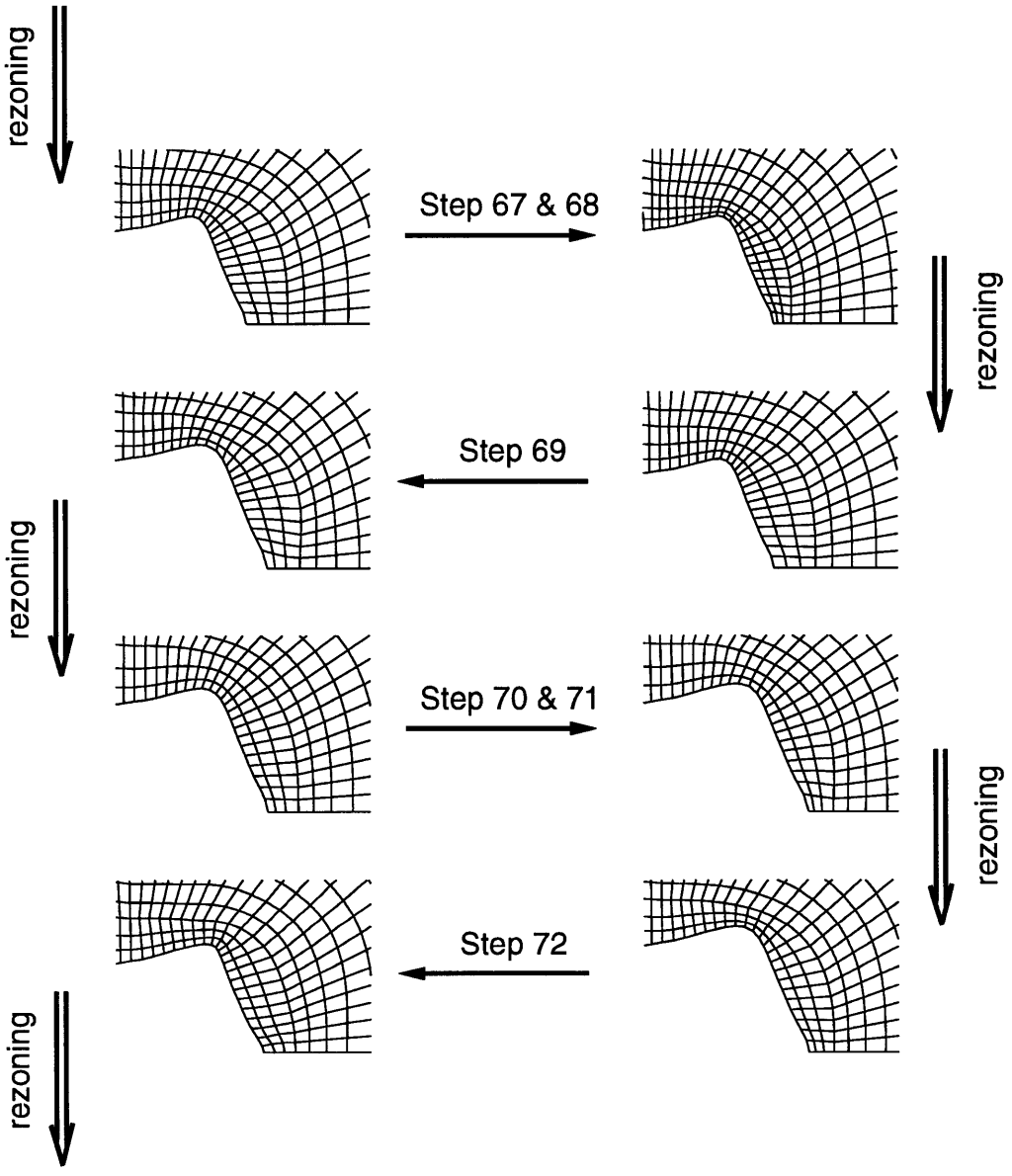

Figure A.11: Figure showing the rezoning steps for a typical cycle. The cycle starts at the relative load $\hat{P} = 0.2$ with dropping load, step 67, and closes with step 72.

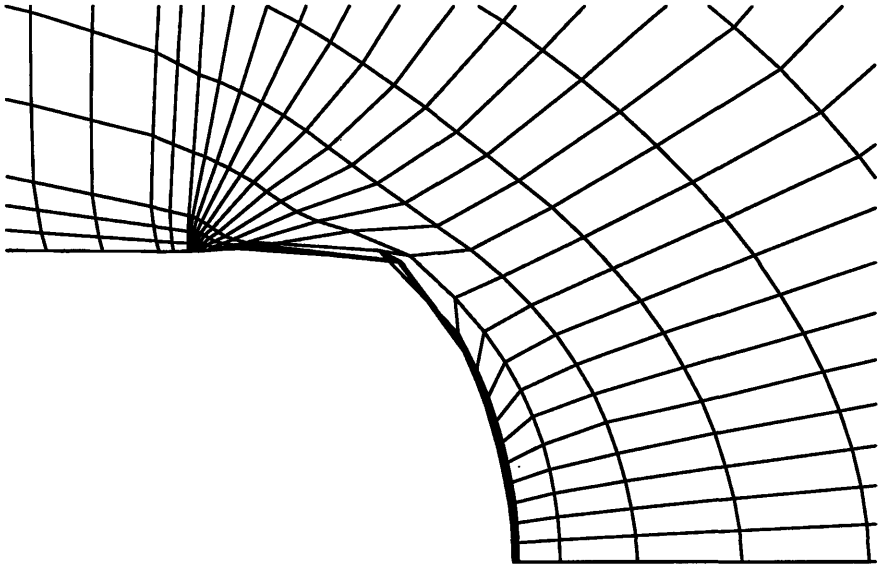

Figure A.12: The original mesh, see first figure in Figure A.10, as it would have looked on the deformed configuration at the end of the first half cycle if rezoning had not been done.

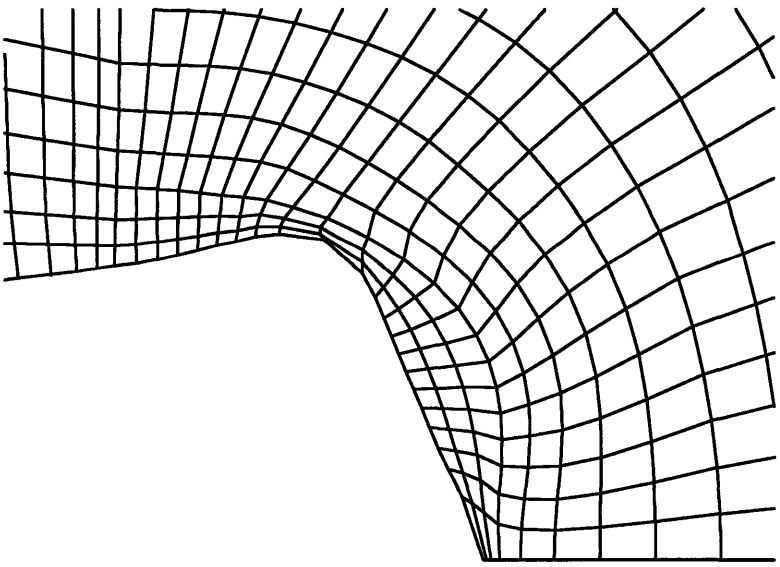

Figure A.13: The initial mesh used for step 70, see first figure in Figure A.11, as it would have looked at maximum load (approx. a half cycle from step 70) if rezoning had not been done

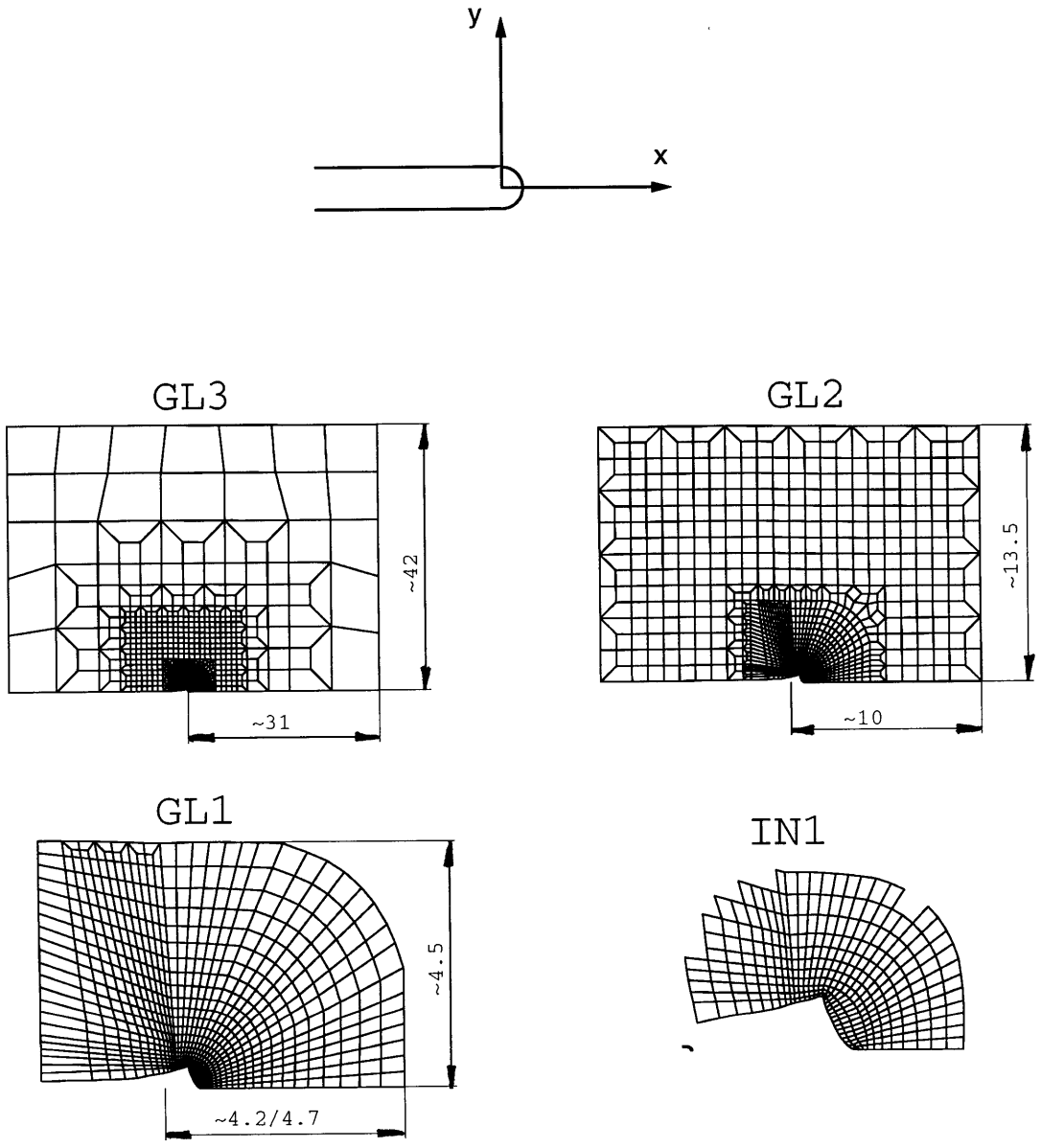

Figure A.14: Coordinate system and denotation of four different near tip regions. The indicated distances are normalized with l_{ref} according to Eq. (3.5), and the "mid point" corresponds to the locus of the initial tip radius. In the figure defining GL1, two horizontal lengths are indicated. The first is for step 1-50, and the other one, due to modification of the whole mesh, for step 51-85. The other indicated lengths in the same direction is also affected, but for the purpose here, the difference is neglible. The black "dot" in the figure IN1 is the near tip elements for the original mesh/configuration.

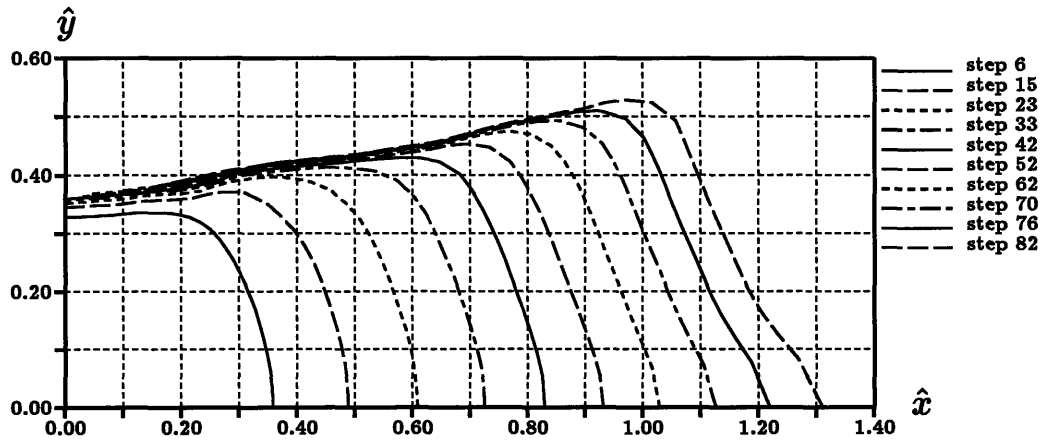

Figure A.15: Shape and location of crackfront for the steps that correspond to maximum load. $\hat{y}$ and $\hat{x}$ are normalized with l_{ref} according to Eq. (3.5)

.

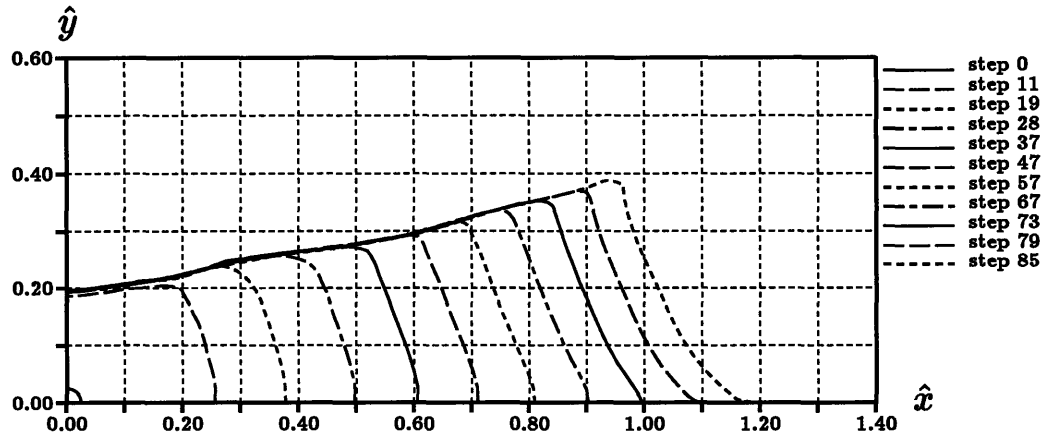

Figure A.16: Shape and location of crackfront for the steps that correspond to minimum load. $\hat{y}$ and $\hat{x}$ are normalized with l_{ref} according to Eq. (3.5)

.

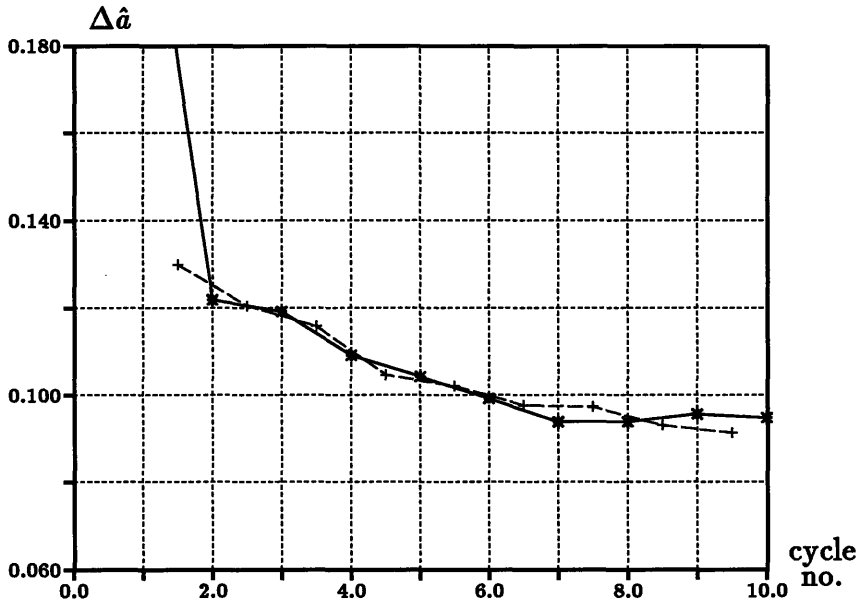

Figure A.17: Advancement of crack front cycle by cycle. The thicker solid line represents the "real" advancement refered to the unloaded state, and the thinner dashed line to the advancement refered to the maximum loaded state. The growth increment during the first initial cycle was 0.2313.

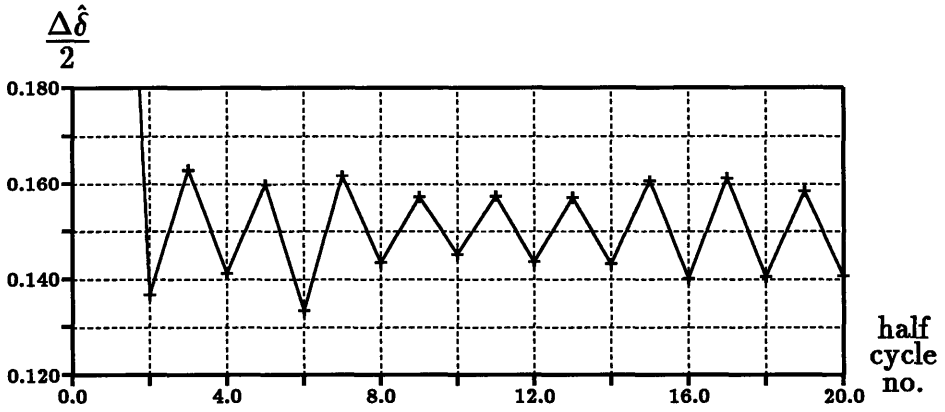

Figure A.18: Variation of half the crack-tip-opening-displacement for each half cycle. $\Delta\hat{\delta}$ is defined by $\Delta\hat{\delta}_i = |\hat{\delta}_i - \hat{\delta}_{i-1}|$, where i is the half cycle number, with $i = 0$ corresponding to the initial configuration.

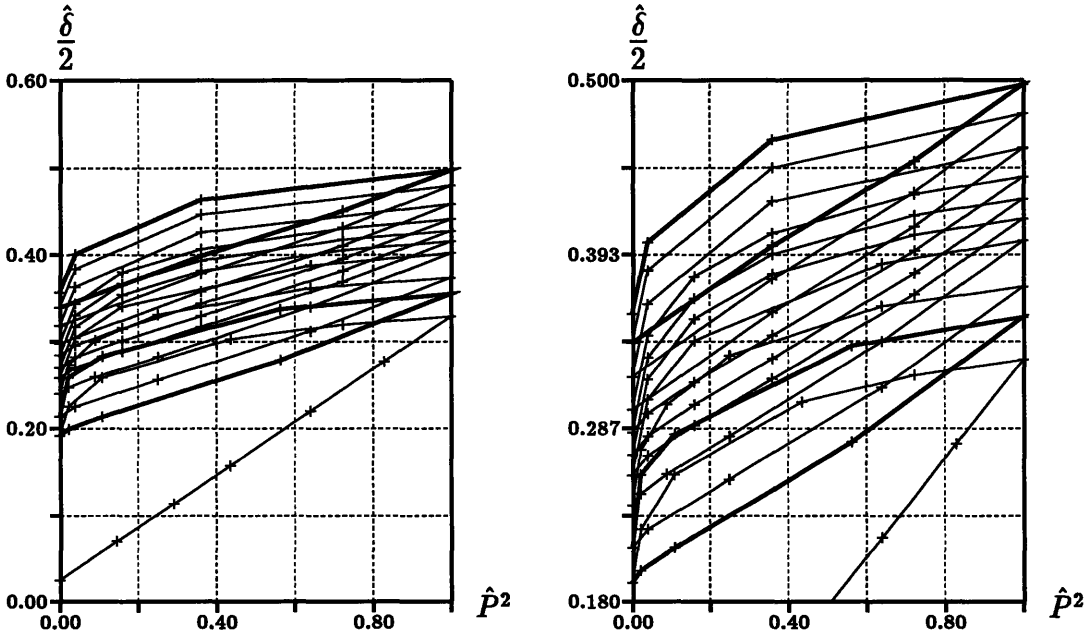

Figure A.19: Time history of the half crack-tip-opening-displacement. The "+" indicate analysis steps. The 2nd and last cycle are indicated with the thicker line type.

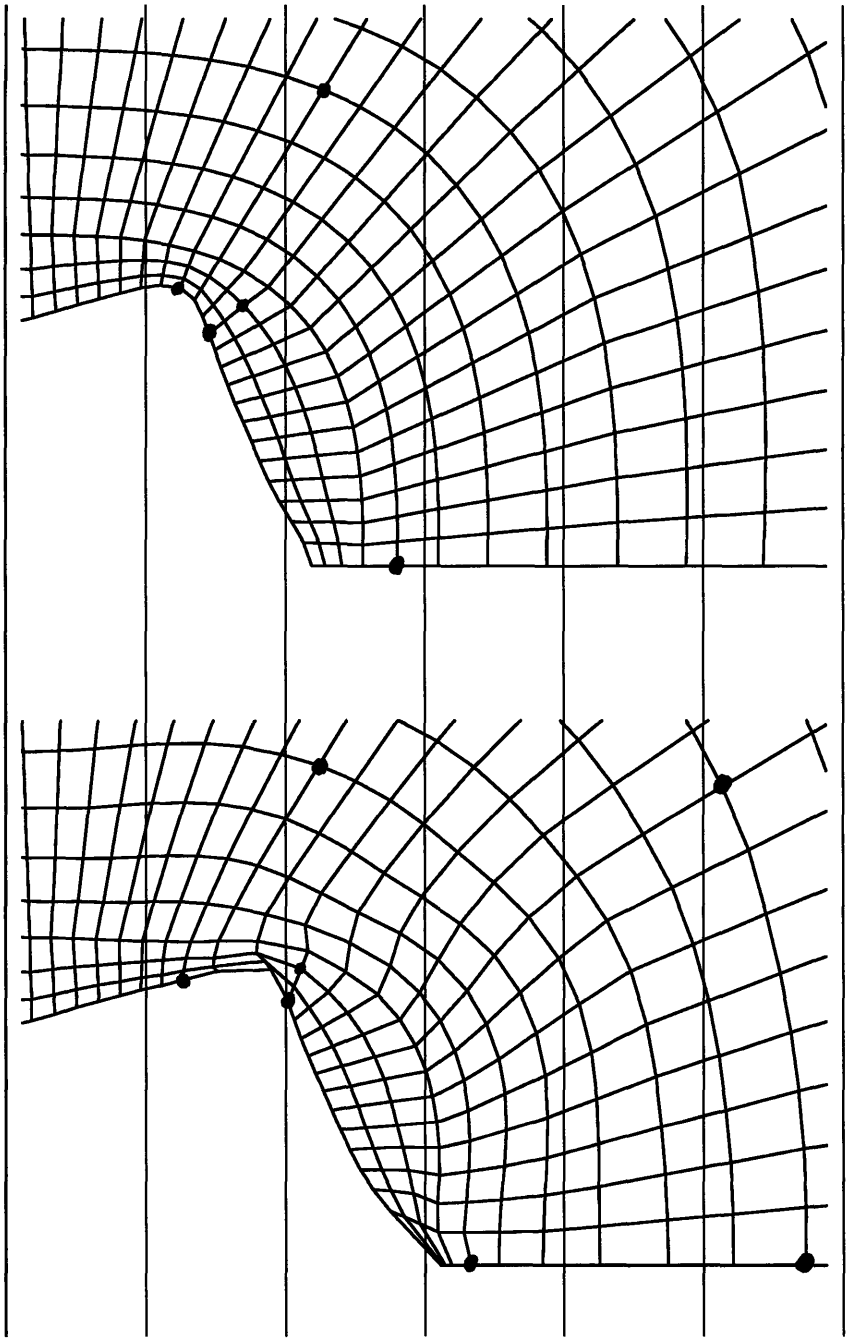

Figure A.20: Illustration of the material flow occuring during the last two cycles. The top figure is the initial mesh for step 67. The bottom figure is the same mesh mapped onto the same material points at the end of step 84. The vertical thinner lines and the black dots are only for reference. The dots in both figures are for the same material points. (The plots do not correspond to the unloaded state, but to $\hat{P} = 0.2$).

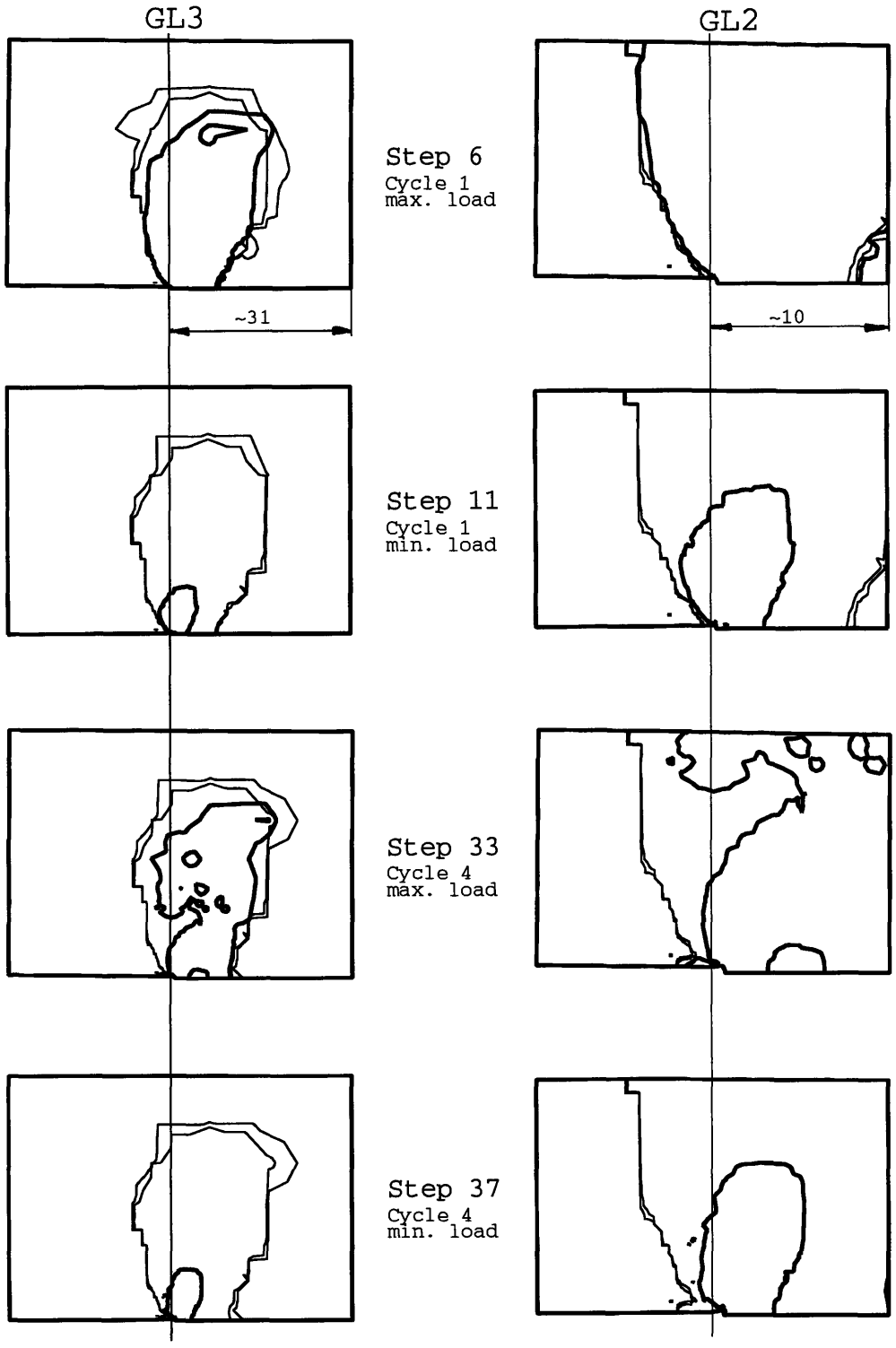

Figure A.21: Plastic zone shapes. The thicker lines represent the active plastic zone and the thinner lines the boundary between plasticized and non-plasticized material

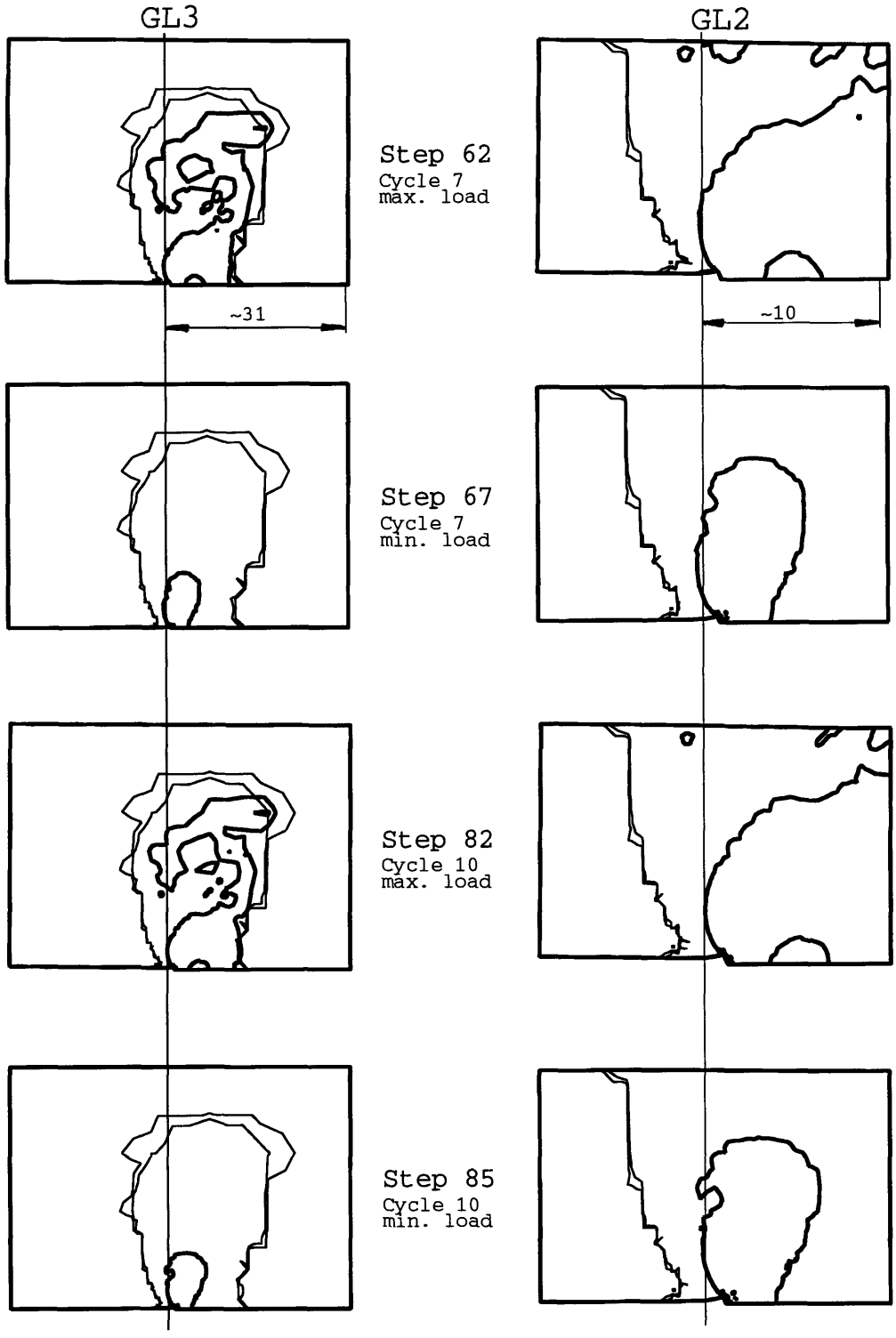

Figure A.22: Plastic zone shapes. The thicker lines represent the active plastic zone and the thinner lines the boundary between plasticized and non-plasticized material

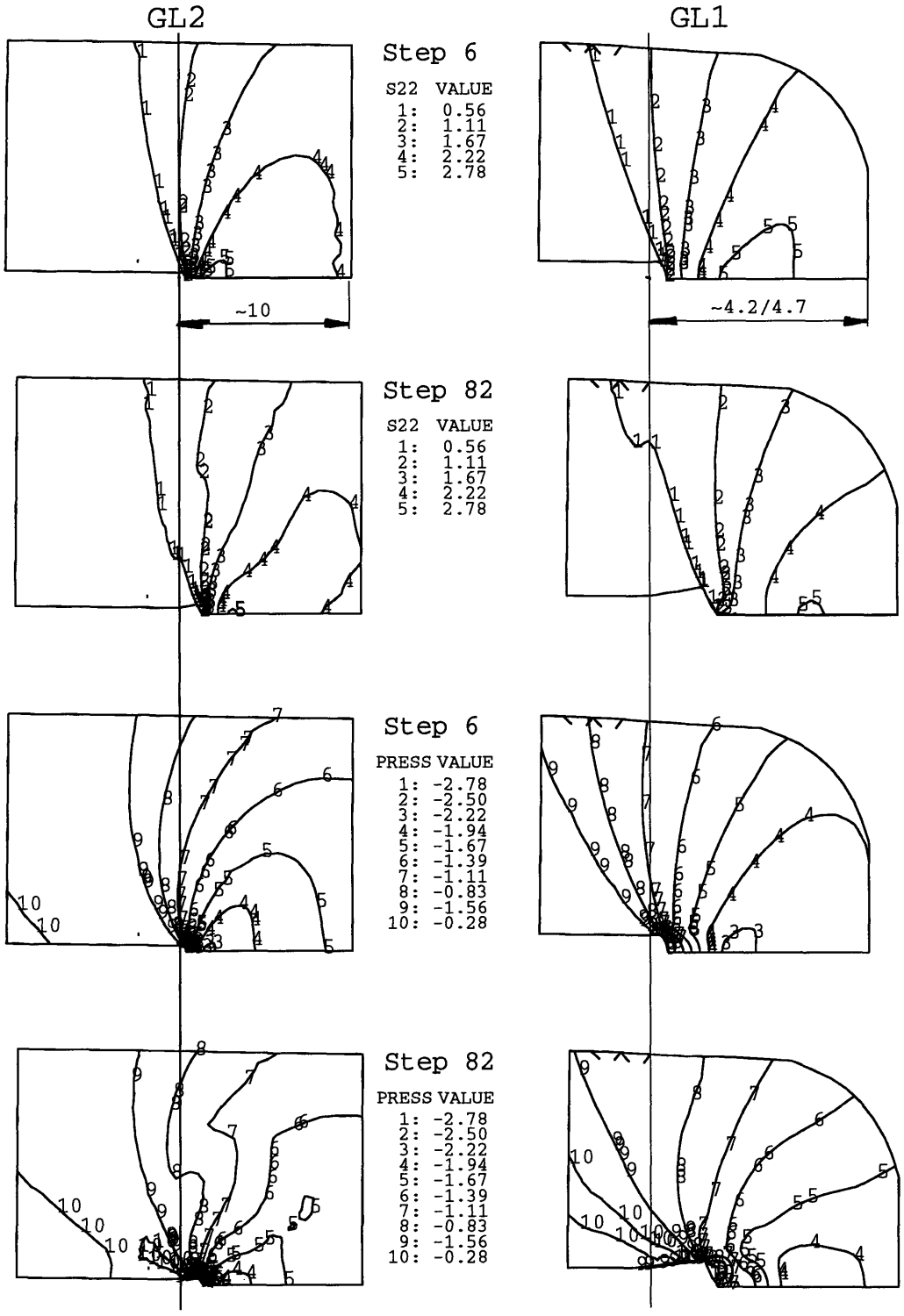

Figure A.23: Contour curves showing $\hat{\sigma}_{22}$ (S22) and the hydrostatic pressure $-\frac{1}{3}\hat{\sigma}_{kk}$ (PRESS) for *maximum* load in cycle 1 (step 6) and cycle 10 (step 82).

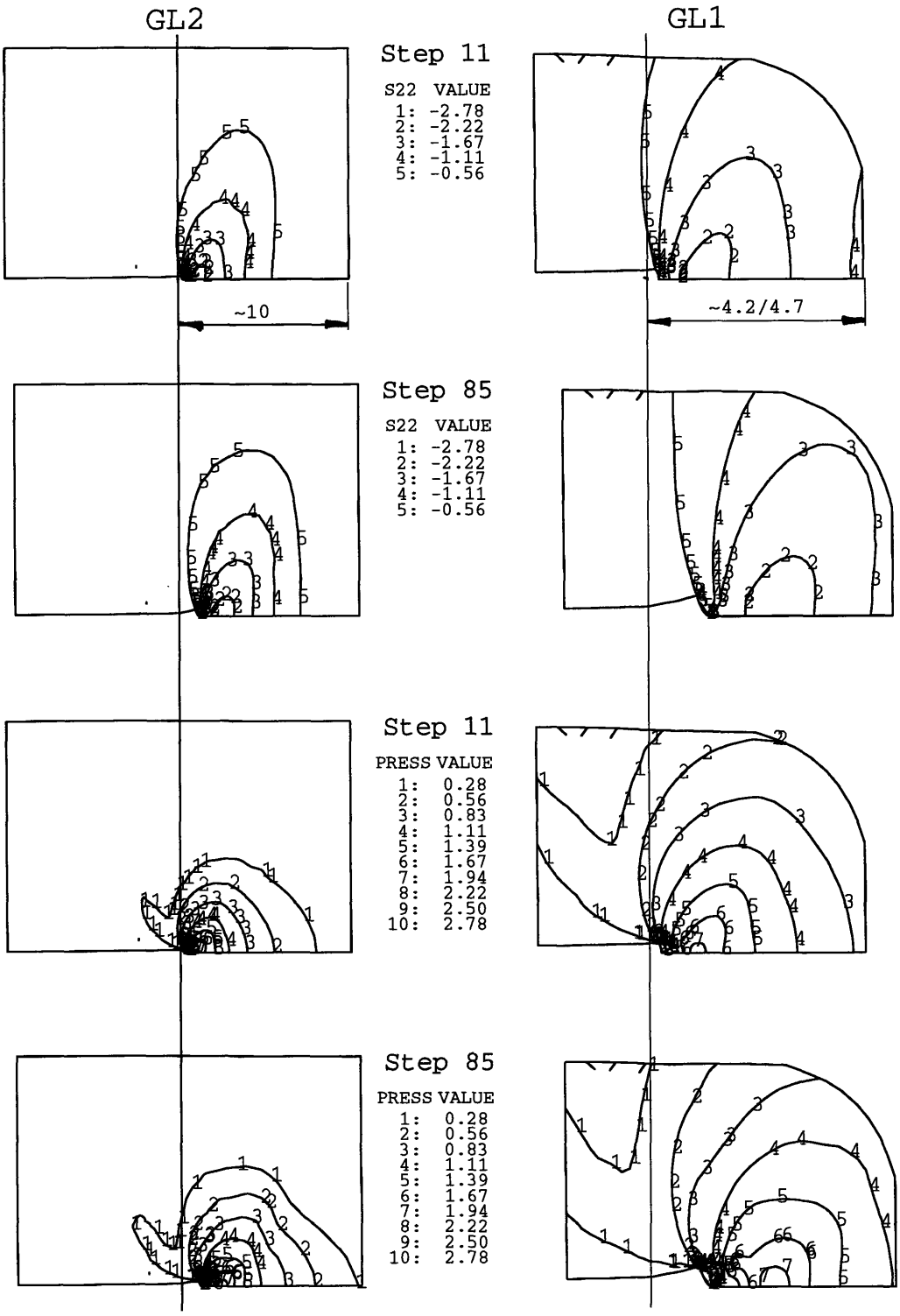

Figure A.24: Contour curves showing $\hat{\sigma}_{22}$ (S22) and the hydostatic pressure $-\frac{1}{3}\hat{\sigma}_{kk}$ (PRESS) for *minimum* load in (end of) cycle 1 (step 11) and cycle 10 (step 85).

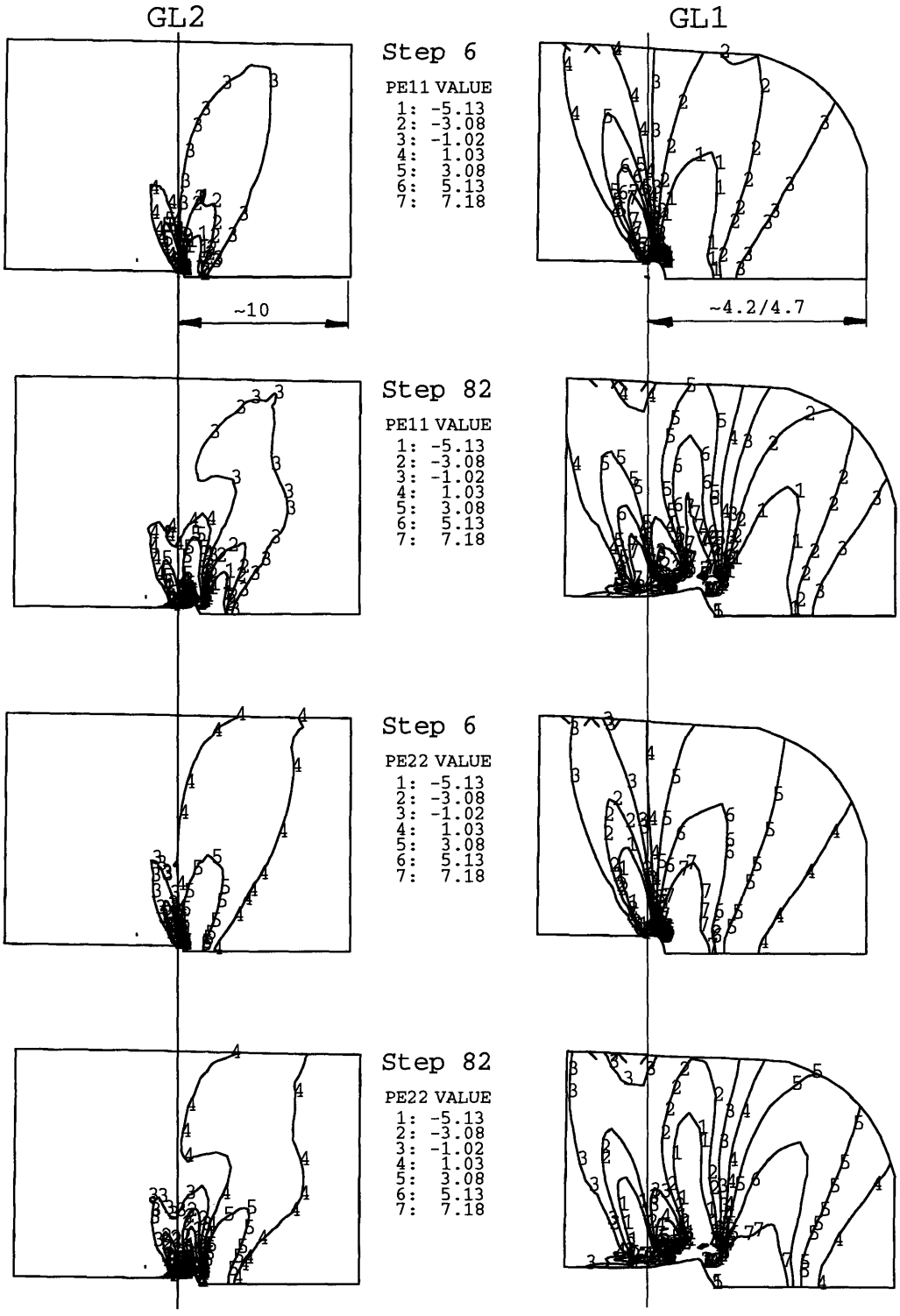

Figure A.25: Contour curves showing the plastic strain components $\hat{\varepsilon}^p_{11}$ (PE11) and $\hat{\varepsilon}^p_{22}$ (PE22) for *maximum* load in cycle 1 (step 6) and cycle 10 (step 82).

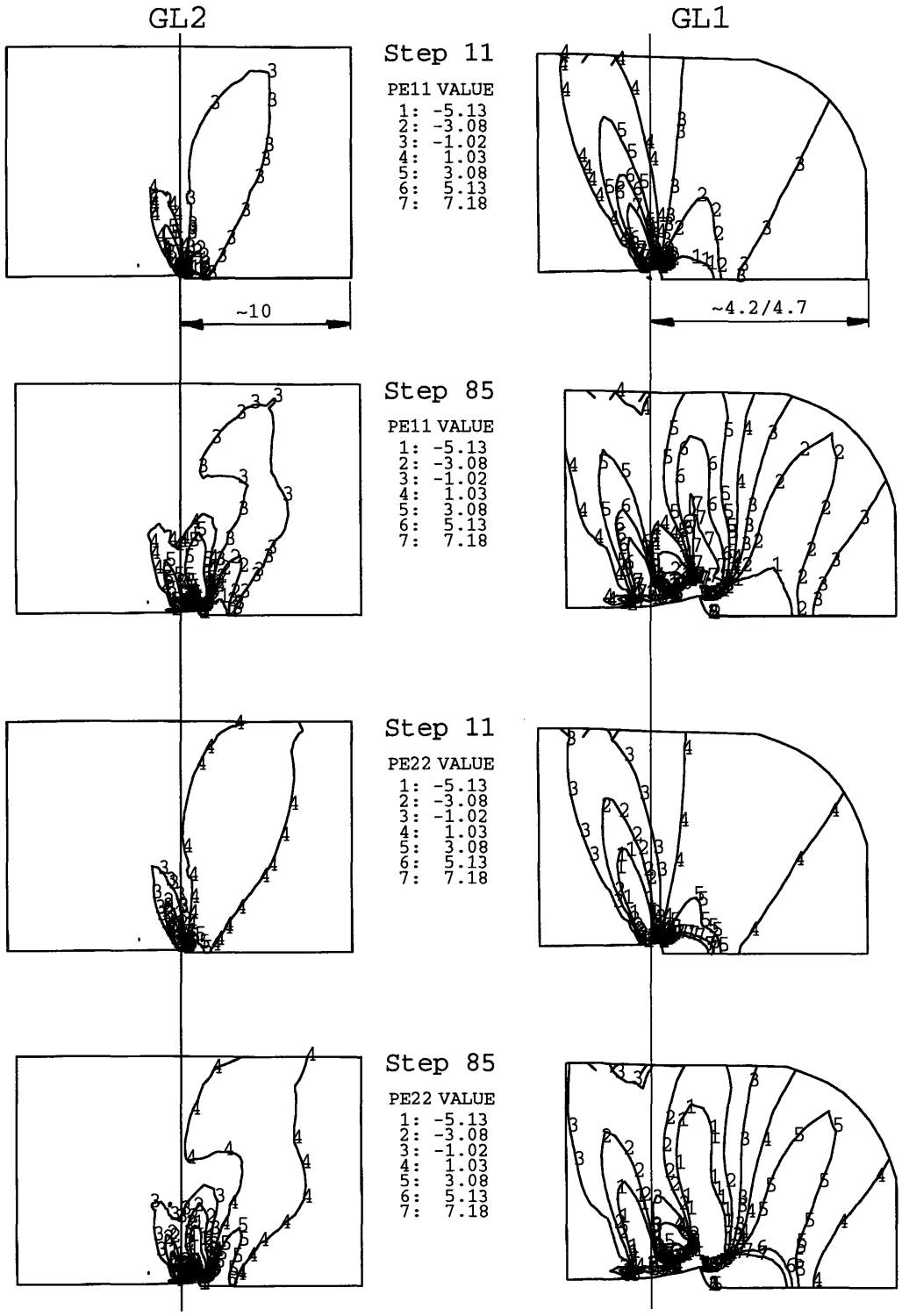

Figure A.26: Contour curves showing the plastic strain components $\hat{\varepsilon}^p_{11}$ (PE11) and $\hat{\varepsilon}^p_{22}$ (PE22) for *minimum* load in (end of) cycle 1 (step 11) and cycle 10 (step 85).

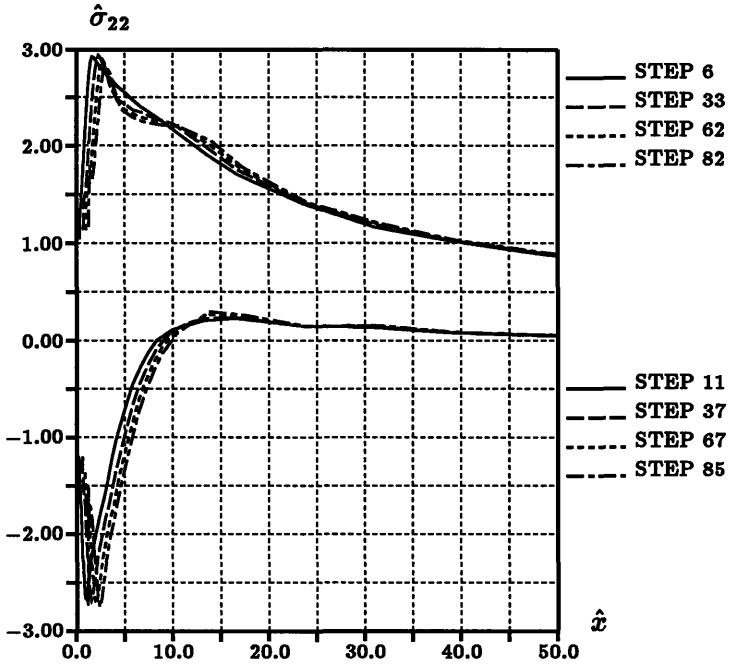

Figure A.27: $\hat{\sigma}_{22}$ as function of position in front of the crack-tip for eight different steps.

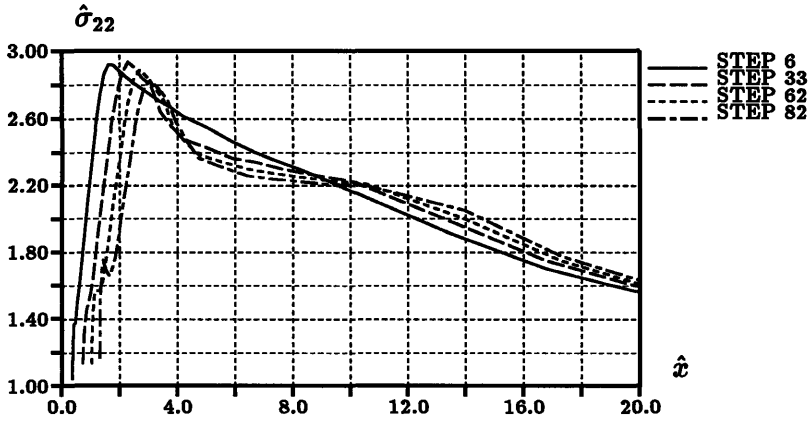

Figure A.28: $\hat{\sigma}_{22}$ as function of position in front of the crack-tip for four different steps corresponding to maximum load.

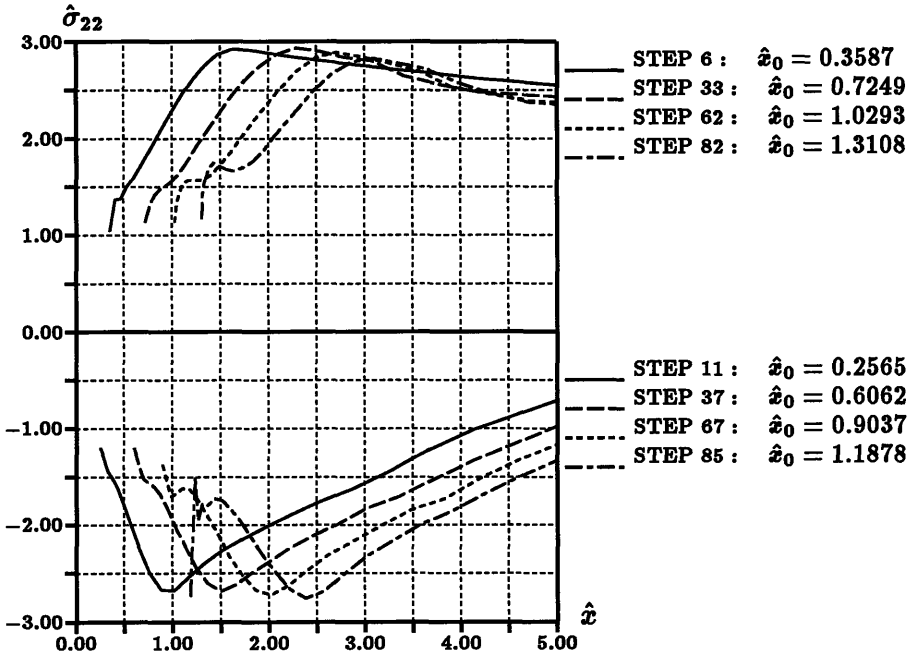

Figure A.29: $\hat{\sigma}_{22}$ as function of position in front of the crack for eight different steps. $\hat{x}_0$ is the current position of the crack front.

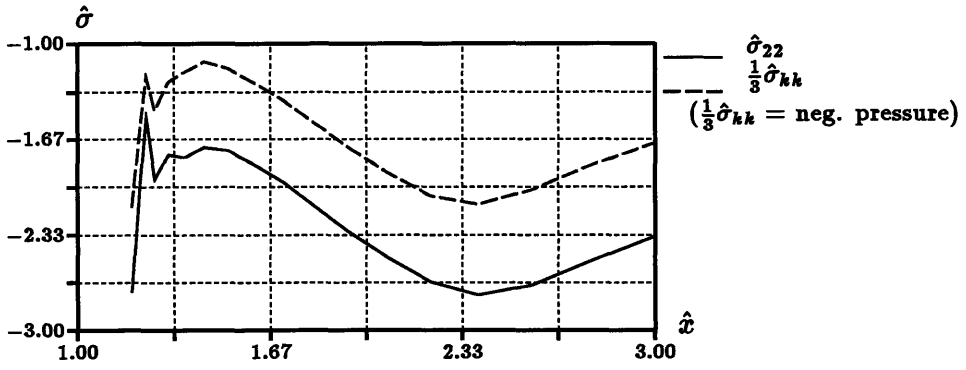

Figure A.30: Magnification of the above curve for step 85 plotted together with the negative of the hydrostatic pressure.

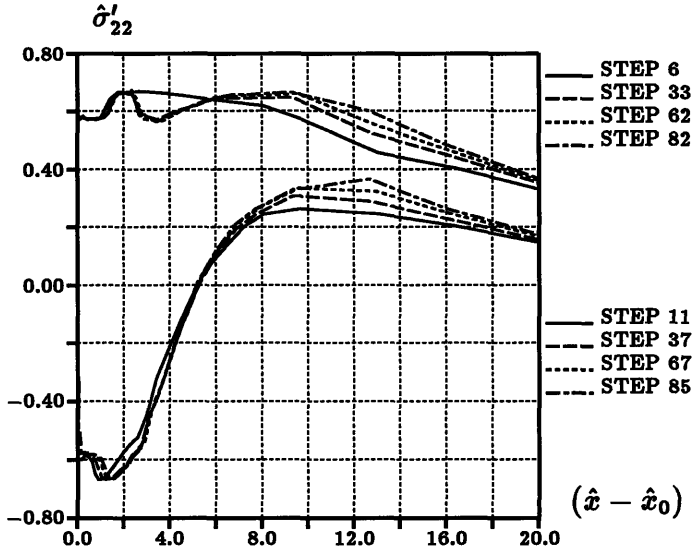

Figure A.31: $\hat{\sigma}'_{22}$, the deviatoric part of $\hat{\sigma}_{22}$, as function of the distance from the current crack front.

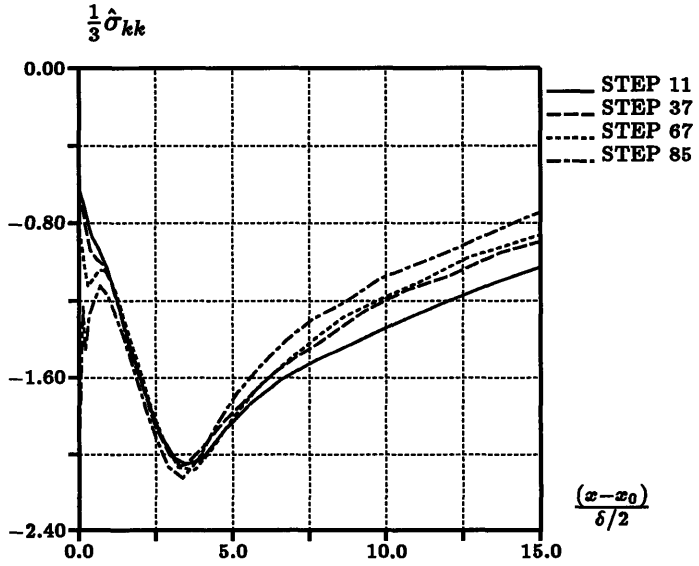

Figure A.32: The mean stress, $\frac{1}{3}\hat{\sigma}_{kk}$ (the negative of the hydrostatic pressure), as function of a scaled distance from the current crack front. The distance is scaled with $\delta/2$ for the current step. The range shown correspond to $\hat{x} - \hat{x}_0 = 2.9$ for step 11, and 5.2 for step85.

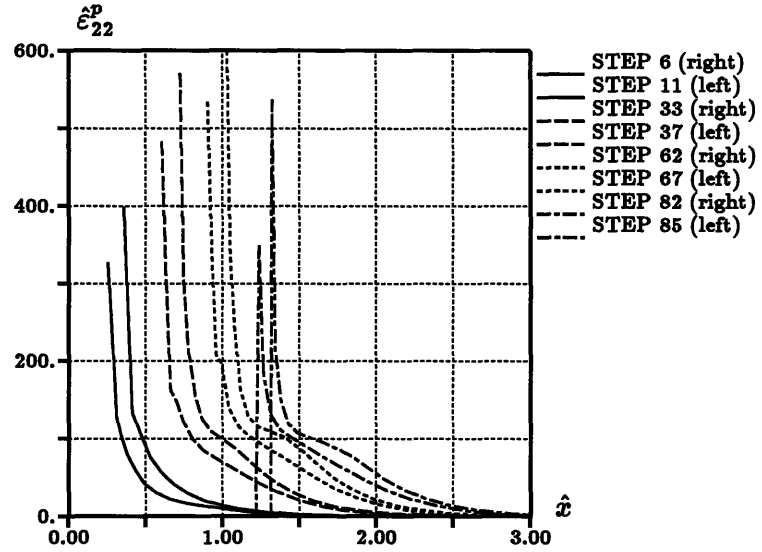

Figure A.33: $\hat{\varepsilon}^p_{22}$ as function of position in front of the crack-tip for eight different steps.

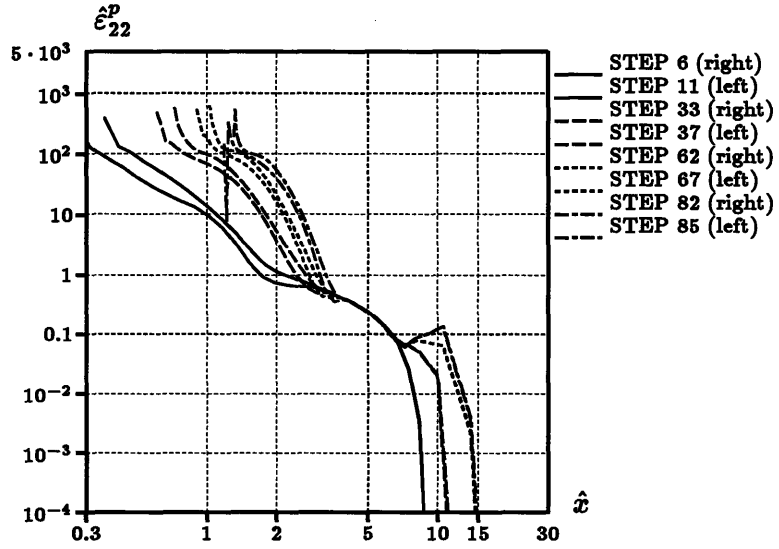

Figure A.34: $\hat{\varepsilon}^p_{22}$ as function of position in front of the crack-tip for eight different steps (Log-Log).